University of Naples "Federico II"

Faculty of Engineering

Electrical Engineering Department

PhD School in Industrial Engineering

PhD in Electrical Engineering

XXV course

New Approaches to Calculation of Lightning Induced Voltages on Overhead Lines for Power Quality Improvement

PhD Thesis of Antonio Pierno

Tutors:

Prof. Amedeo Andreotti
Prof. Giovanni Lupò
Prof. Luigi Verolino

PhD Coordinator:

Prof. Guglielmo Rubinacci

April 2013

... to my Father, my Mother and my Sister

Acknowledgements

First of all, I would like to give my special thanks to my tutors (Profs. Amedeo Andreotti, Giovanni Lupò, Luigi Verolino) for the all things which they have taught me in many aspects of my life, especially in the academic research work. All the results achieved in this thesis derive from their precious teachings and their patience.

I would like to acknowledge Prof. Guglielmo Rubinacci, for his kindness, availability, and support. He has taken on the role of coordinator of the PhD in Electrical Engineering, providing a stimulating educational environment with many interdisciplinary courses and seminars.

I can't forget to thanks my colleagues and friends, Fabio Mottola, Flavio Ciccarelli, Giacomo Ianniello, Cosimo Pisani, Shahab Khormali, and Gianni Clemente, who shared with me this wonderful experience, and their time (and even the coffee breaks), providing help and support when needed.

Finally, I would like to thanks my parents and my sister, who have always sustained, encouraged and helped me to overcome all the difficulties encountered in these years, and my great friend Giuseppe, a person that I can always count on.

Contents

Abstract

Lightning is one of the most visually impressive, powerful and dangerous natural phenomena on Earth. For its spectacular appearance and its effects on life and structures, lightning has always had a significant impact on humans and their societies.

Lightning discharges considered in this work are the so called "cloud-to-ground" lightning discharges, i.e., those that take place between cloud and ground. The high destructive power of this kind of lightning arises from the high energy generated by the cloud-to-ground discharge channel and the lightning stroke current. These discharges can cause damage when they strike directly or strike nearby to a structure.

For low and medium voltage power distribution networks, the height of lines is small compared to the near structures, then indirect lightning events are more frequent than direct strikes. For this reason we shall focus on such a type of lightning discharges, which may cause power outages, disturbances on the network, or failure of electronic and electrical equipment, due to overvoltages produced.

Since it is impossible to avoid a lightning strike, in order to reduce the effects of lightning flashes, it is necessary to provide suitable protection measures, which allow to reduce the risk, defined as the probable annual loss in a system [1], improving the Power Quality of the system.

In this context, an accurate evaluation of lightning induced voltages is therefore essential.

Recent progress in the area of lightning induced voltages is significant, both from numerical and analytical points of view. Numerical approaches have shown excellent development over the years (e.g., [2]-[6]). They are able to accurately model the phenomenon (actual return-stroke current waveshape, finite ground conductivity effects, non-linearities due to surge arresters, and so on). Nevertheless, analytical solutions (e.g., [7]-[12]) still deserve attention, since they are important in the design phase [13], in parametric evaluation and sensitivity analysis (e.g., [14]); they are also implemented in

computer codes for lightning induced effects [15]. Analytical solutions, moreover, provide considerable insight into the phenomenon, which is often obscured in numerical approaches, and do not suffer from numerical instabilities or convergence problems, which could affect accuracy of numerical algorithms [16].

Most of the analytical models proposed so far in literature are approximated and/or incomplete, as will be shown in the thesis.

The aim of this work is to present *new analytical approaches* to the evaluation of lightning induced voltages on overhead power lines, that allow to overcome errors and/or approximations present in the solutions available in the literature. Predictions of the proposed solutions will be also compared to those based on the other approaches found in the literature in order to check their validity and accuracy.

The thesis is organized as follows:

Chapter 1. In this introductory chapter, a brief overview and a description of the lightning phenomenon is given.

Chapter 2. In this chapter, the models proposed in the literature for the evaluation of the lightning induced voltages are summarized. In particular, the most used lightning return-stroke current models are presented, together with the techniques for the calculation of the electromagnetic fields generated by the lightning current. Furthermore, the most important models of field-to-line coupling are discussed.

Chapter 3. This is the main chapter of the thesis. New analytical approaches to the evaluation of lightning induced voltages on overhead power lines are here presented. Most of the proposed analytical solutions are derived in an *exact way*, that is, without introducing approximations.

The cases of an infinitely long, lossless, single-conductor located at a given height above both an infinite-conductivity and a lossy ground plane, and excited by an external EM field due to both a step and a linearly rising current wave moving along a vertical lightning channel are analyzed. Furthermore, some of these solutions are extended to more practical line configurations, such as terminated single-conductor line and multi-conductor line (including grounded conductors).

Finally, the results obtained using the proposed solutions are compared with those given by other formulas or solutions available in the literature.

Chapter 4. This final chapter, is devoted to the conclusions.

References

[1] Z. Flisowski, C. Mazzetti, "A new approach to the complex assessment of the lightning hazard impeding over buildings", *Bulletin of Polish Academy of Sciences*, vol. 32, no. 9-10, pp. 571-581, 1984.

[2] F. Rachidi, C. A. Nucci, and M. Ianoz, "Transient analysis of multiconductor lines above a lossy ground," *IEEE Trans. Power Del.*, vol. 14, no.1, pp. 294–302, Jan. 1999.

[3] G. Diendorfer, "Induced voltage on an overhead line due to nearby lightning", *IEEE Trans. Electromagn. Compat.*, vol. 32, no. 4, pp. 292–299, Nov. 1990.

[4] H. K. Høidalen, J. Slebtak, and T. Henriksen, "Ground effects on induced voltages from nearby lightning," *IEEE Trans. Electromagn. Compat.*, vol. 39, no. 4, pp. 269–278, Nov. 1997.

[5] A. Andreotti, C. Petrarca, V. A. Rakov, L. Verolino, "Calculation of voltages induced on overhead conductors by nonvertical lightning Channels," *IEEE Trans. Electromagn. Compat.*, vol. 54, no. 4, pp. 860-870, Aug. 2012.

[6] A. Andreotti, U. De Martinis, C. Petrarca, V. A. Rakov, L. Verolino, "Lightning electromagnetic fields and induced voltages: Influence of channel tortuosity," *XXXth URSI General Assembly and Scientific Symposium*, 2011, pp.1-4, Istanbul, Turkey, Aug. 2011.

[7] J. O. S. Paulino, C. F. Barbosa, and W. C. Boaventura, "Effect of the surface impedance on the induced voltages in overhead lines from nearby lightning," *IEEE Trans. Electromagn. Compat.*, vol. 53, no. 3, pp. 749-754, Aug. 2011.

[8] S. Rusck, "Induced lightning overvoltages on power transmission lines with special reference to the overvoltage protection of low-voltage networks," *Trans. Royal Inst. Technol.*, no. 120, pp. 1-118, Jan. 1958.

[9] H. K. Høidalen, "Analytical formulation of lightning-induced voltages on multiconductor overhead lines above lossy ground," *IEEE Trans. Electromagn. Compat.*, vol. 45, no. 1, pp. 92-100, Feb. 2003.

[10] F. Napolitano, "An analytical formulation of the electromagnetic field generated by lightning return strokes," *IEEE Trans. Electromagn. Compat.*, vol. 53, no. 1, pp. 108-113, Feb. 2011.

[11] A. Andreotti, D. Assante, F. Mottola, and L. Verolino, "An exact closed-form solution for lightning-induced overvoltages calculations," *IEEE Trans. Power Del.*, vol. 24, no. 3, pp. 1328-1343, Jul. 2009.

[12] C. F. Barbosa and J. O. S. Paulino, "A time-domain formula for the horizontal electric field at the earth surface in the vicinity of lightning," *IEEE Trans. Electromagn. Compat.*, vol.52, no.3, pp. 640-645, Aug. 2010.

[13] *IEEE Guide for Improving the Lightning Performance of Electric Power Overhead Distribution Lines*, IEEE Standard. 1410, 2010.

[14] P. Chowdhuri, "Parametric effects on the induced voltages on overhead lines by lightning strokes to nearby ground," *IEEE Trans. Power Del.*, vol. 4, no. 2, pp. 1185-1194, Apr. 1989.

[15] H. K. Høidalen, "Calculation of lightning-induced overvoltages using models," in *Proc. Int. Conf. Power Syst. Trans.*, Budapest, Hungary, Jun. 20-24, 2003, pp. 7-12.

[16] N. J. Higham, *Accuracy and Stability of Numerical Algorithms*, 2nd ed. Philadelphia, PA: SIAM, 2002.

List of Symbols

a	Phase conductor of the overhead power line.
b	Overhead ground wire.
$b_y(\cdot)$	Azimuthal magnetic induction line normal component.
b_H	$1 + t_f/[2(t_t - t_f)]$.
c	Speed of light in free space.
d	Horizontal distance between the lightning channel and the line conductor.
d_{ba}	Distance between the conductors b and a.
d'_{ba}	Distance between the conductor b and the mirror image of conductor a.
$e_r(\cdot)$	Electric field radial component.
$e_x(\cdot)$	Electric field line axial component.
$e_z(\cdot)$	Electric field vertical component.
$e_{xi}(\cdot)$	Ideal electric field line axial component (calculated as if the ground were a perfect conductor).
$e_{zi}(\cdot)$	Ideal electric field vertical component (calculated as if the ground were a perfect conductor).
h	Single-conductor line height above ground.
h_a	Height above ground of the phase conductor a.
h_b	Overhead ground wire height above ground.
h_c	Lightning channel length.
$h_{yi}(\cdot)$	Ideal azimuthal magnetic field line normal component (calculated as if the ground were a perfect conductor).
$h_\varphi(\cdot)$	Azimuthal magnetic field component.
$i(x,t)$	Induced current along the line.
$i(z',t)$	Lightning current along the discharge channel.

r	$\sqrt{x^2 + d^2}$.
r_0	$\sqrt{x^2 + d^2 + h^2}$.
r_b	Overhead ground wire radius.
t	Time (t = 0, return stroke inception).
t_0	r_0/c.
$\tilde{t}_0$	r/c.
t_1	$\left(L + \sqrt{L^2 + d^2 + h^2}\right)/c$.
t_{1l}	$\left(\lvert -L - x\rvert + \sqrt{L^2 + d^2 + h^2}\right)/c$.
t_{1r}	$\left[(L - x) + \sqrt{L^2 + d^2 + h^2}\right]/c$.
t_2	$\sqrt{d^2 + h^2}/c$.
$\tilde{t}_2$	d/c.
t_f	Front time of the lightning current.
t_h	Time needed for current to fall from the peak value to the half peak value.
t_t	Tail time of the lightning current.
$u(\cdot)$	Heaviside function.
v	Return-stroke current wave propagation speed.
v^*	$v_f/\left(1 + v_f/c\right)$.
v_a	Induced voltage on the phase conductor a in absence of the ground wire.
v_a'	Induced voltage on the phase conductor a.
v_b	Induced voltage on the ground wire b.
v_f	Return-stroke wavefront propagation speed.
$v(\cdot)$	Induced voltage along the line.
x	Position along the line (x = 0, center of the line).
x_l	$[(c \cdot t + x)^2 - d^2 - h^2]/[2(c \cdot t + x)]$.
x_p	Position of the grounding pole along the line.
I_0	Return-stroke peak current.
I_m	Linearly rising current peak value.
J_0	Modified Bessel function of first type and order 0.
J_1	Modified Bessel function of first type and order 1.
L	X-coordinate of the right end-point of the line.

$P(\cdot)$	Attenuation function of the return-stroke current along the channel.
$Q(\cdot)$	Total charge transferred from the ground to the lightning channel.
R_b	Ground resistance of the overhead ground wire b.
S_b	Overhead ground wire cross section b.
T	L/c.
T_l	$\lvert -L - x \rvert / c$.
T_r	$(L - x)/c$.
Z_{ba}	Mutual surge impedance of ground wire b and phase conductor a.
Z_{bb}	Self-surge impedance of overhead ground wire b.
Z_C	Characteristic impedance of the line.
α	I_o/t_f.
β	Ratio of the return stroke speed to c.
γ	$1/\sqrt{1-\beta^2}$.
δ	r/γ.
δ_0	d/γ.
δ_l	$\sqrt{x_l^2 + d^2}/\gamma$.
δ_L	$\sqrt{L^2 + d^2}/\gamma$.
ε	Ground permittivity.
ε_0	Permittivity of free space.
ε_r	Relative ground permittivity.
ζ_0	Free-space wave impedance.
λ	$\beta \cdot c \cdot t - h$.
λ'	$\beta \cdot c \cdot t + h$.
$\hat{\lambda}$	$\beta \cdot (c \cdot t + x)$.
λ_0	$\beta \cdot c \cdot t_0 - h$.
λ_1	$\beta \cdot c \cdot t_2 - h$.
λ_1'	$\beta \cdot c \cdot t_2 + h$.
λ_m	$\beta \cdot (c \cdot t + x) - h$.
λ_p	$\beta \cdot (c \cdot t + x) + h$.
μ_0	Permeability of free space.
ξ	$\sqrt{(\beta \cdot c \cdot t)^2 + \delta^2}$.

ξ_0	$\sqrt{(\beta \cdot c \cdot t_0)^2 + \delta^2}$.
ξ_1	$\sqrt{(\beta \cdot c \cdot t)^2 + \delta_0^2}$.
ξ_l	$\sqrt{\left(\beta \cdot x_l - \hat{\lambda}\right)^2 + \delta_l^2}$.
$\rho(z', t)$	Charge density distribution along the discharge channel.
σ	Ground conductivity.
Λ	Decay constant of the MTLE model.

List of Figures

List of Tables

Chapter 1

An Overview on the Lightning Phenomenon

1.1 Introduction

Experimental observations of the optical and electromagnetic fields generated by lightning flashes during the last years have significantly advanced the knowledge on the mechanism of the lightning discharges. Nevertheless, this knowledge is not as exhaustive as that of long laboratory sparks due to the inability to observe lightning events under controlled conditions. Thus, the mathematical description of the mechanism of a lightning flash is actually relatively poor even though the main features of lightning flashes themselves are well known [1].

In this chapter, and elsewhere in the thesis, a positive discharge is defined as a discharge on which the direction of motion of electrons is opposite to that of the discharge itself; a negative discharge is defined as one in the opposite sense. According to this definition a negative return stroke is a positive discharge and a positive return stroke is a negative discharge.

A positive field is defined as a negative charge being lowered to ground or as a positive charge being raised. According to this definition a lightning flash that transports negative charge to ground produces a positive field change.

1.2 Clouds and lightnings

The source of lightning is usually a thundercloud. A thundercloud generally presents a tripolar electrostatic structure; it contains, in fact, two main regions of charge, one positive

near the top and the other negative at midlevel (both containing a charge of 10÷100 C), and a small positive charge located at the base of the cloud, as shown in Figure 1.1 [2]. Actually, the charge structure in a thunderstorm is more complex than shown in Figure 1.1, it varies from storm to storm, and is occasionally very much different from the structure illustrated, even upside-down with the main positive charge on the bottom and the main negative charge on top [3].

The majority of all lightning discharges are the "cloud discharges". The most common cloud discharges (that are also the most common of all the forms of lighting) occur totally within a single cloud, between the upper positive charge and the main negative charge, where a strong electric field is present, and are called *intracloud* flashes; those that occur between clouds are called *intercloud* lightnings (less common than intracloud flashes); those that occur between one of the cloud charge region and the surrounding air are called *cloud-to-air* lightnings.

A second kind of lightning discharges is represented by the "cloud-to-ground discharges", that take place between the charge centers of the cloud and the ground. There are four types of lightning flashes that occur between the cloud and ground, illustrated in Figure 1.2, classified on the basis of the polarity of the electrical charge carried in the initiation process and the direction of propagation of the initiation process. Figures 1.2a and c show flashes referred to as *downward* lightnings; Figures 1.2b and d depict *upward* lightnings. The most common ground flashes (about 90% of cloud-to-ground lightning events) bring negative charge from the main negative charge region of the cloud down to ground, as shown in Figure 1.2a. The positive ground flashes, which occur about one tenth as frequently as does the negative ground discharges, are instead depicted in Figure 1.2c, and bring positive charge from the cloud, either from the upper or lower positive charge region, down to earth. The remaining two types of cloud-to-ground lightning discharges (actually ground-to-cloud discharges), shown in Figures 1.2b and d, are less common and are upward initiated from an object on the Earth's surface (mountain-tops, tall towers or other tall objects), toward and often into one of the cloud charge regions [2], [3].

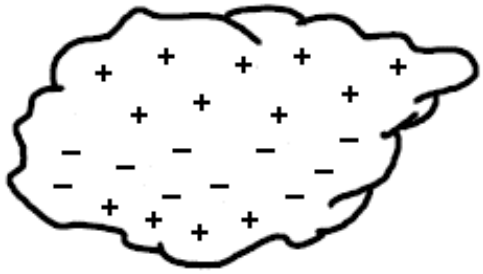

Figure 1.1 – The tripole structure of the thundercloud. Adapted from [2].

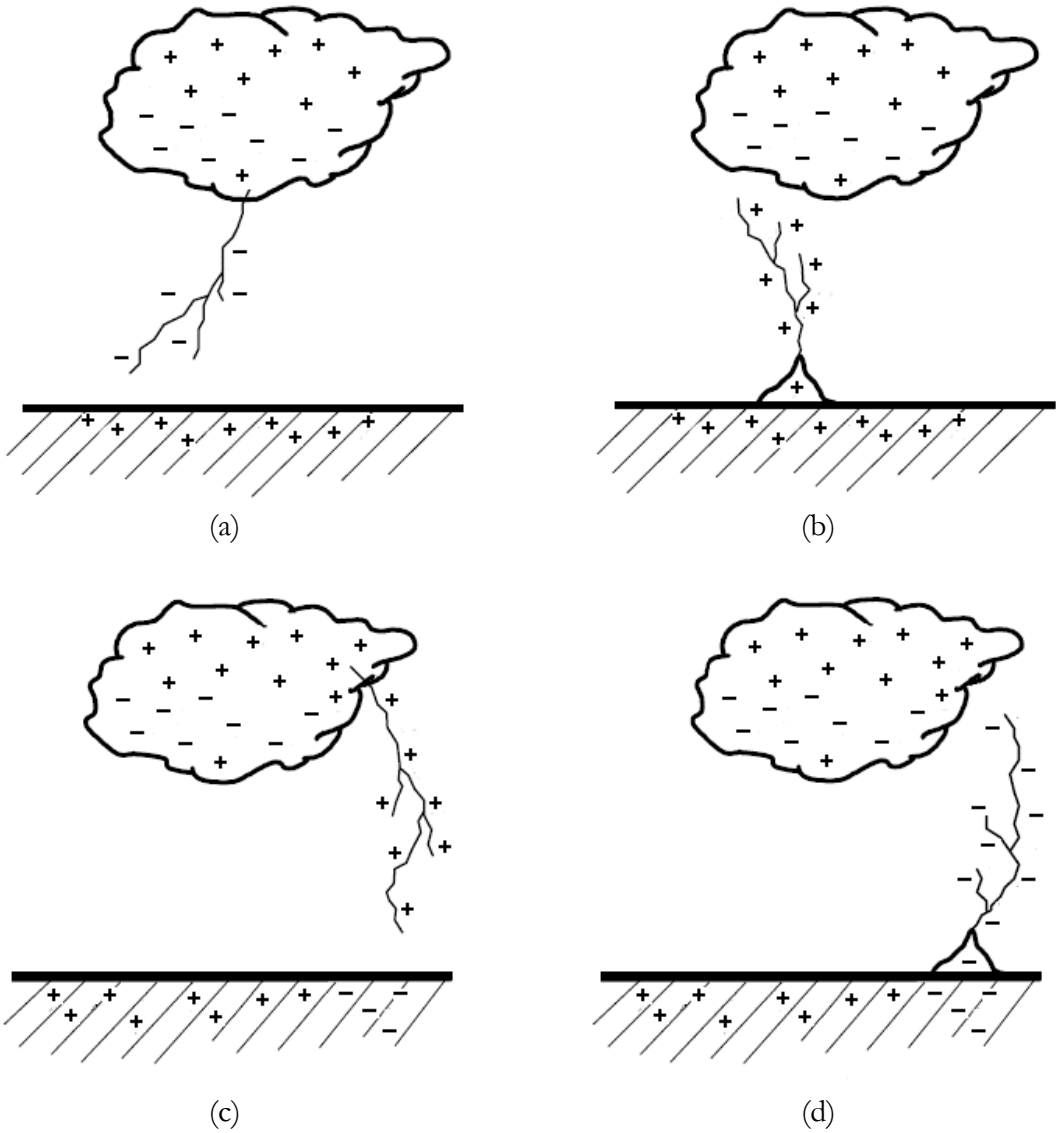

Figure 1.2 – Types of cloud-to-ground lightning discharges as defined from the direction of leader propagation and charge of the initiating leader: a) downward lightning, negatively charged leader; b) upward lightning, positively charged leader; c) downward lightning, positively charged leader; d) upward lightning, negatively charged leader. Adapted from [4].

1.3 The cloud-to-ground lightnings

As outlined in the previous paragraph, the most common cloud-to-ground flashes are the downward lightnings that carries negative charge. This kind of lightning flash may well initiate as a local discharge between the bottom of the main negative charge region and the small positive charge region located at the base of the cloud (see Figure 1.1). This local discharge, also known as "preliminary breakdown" or "initial breakdown", is able to

provide free mobile electrons, those electrons that were previously attached to hail and other heavy particles, and thus immobile. These free electrons represent the main contributor to the lightning current. In negative ground flashes, the free electrons cross the lower positive charge region, neutralizing most of its positive charge, and then continue their travel from cloud to ground in a stepped manner. This process, called "stepped leader", and other main phases of the negative ground flashes are illustrated in Figure 1.3 [1], [3].

The stepped leader moves downward in discrete and subsequent luminous segments of about 50 m length, each of which is called "step". In Figure 1.3, the luminous steps appear as darkened tips on the less-luminous leader channel extending downward from the cloud. Each leader step appears in a microsecond or less, and the time between two luminous steps is of few tens of microseconds (typically 20÷50 μs). Usually, the downward-propagating stepped leader give rise to several branches. The average speed of the bottom of the stepped leader during its travel toward ground is about 2×10^5 m/s, and then the travel between the cloud and the ground takes few tens of milliseconds [5]. A typical stepped leader has about 5 coulombs of negative charge distributed over its length. To establish this charge, on the leader channel, an average current of about 100 to 200 amperes must flow during the whole leader process. However, the pulsed currents which flow in generating the leader steps can have a peak current of the order of 1000 amperes [3]. The stepped-leader channel is likely to consist of a thin core that carries the longitudinal channel current, surrounded by a corona sheath whose diameter is typically several meters [6].

When the stepped leader is near the ground, due to its relatively large negative charge, it attracts concentrated positive charges on the conducting Earth beneath it and, mainly, on objects projecting above the Earth's surface. If this attraction is strong enough, the positive charge (on the Earth or on the objects) will attempt to join and neutralize the negative charge. For doing so, upward-going electrical discharges start from the ground or from grounded objects, as illustrated in Figure 1.3 at 20.00 ms. When one of these upward-moving positively charged leader contacts a branch of the downward-moving leader, it determines the lightning strike-point and the primary lightning channel between cloud and ground. This is the "attachment process" of Figure 1.3, also known as "break-through phase" or "final jump". Then, the negative charge near the bottom of the leader channel moves violently downward to the Earth, originating large currents to flow at ground and making the lightning channel near ground very luminous. The luminosity of the channel and the current, in a process named the "first return stroke", propagate continuously up

the channel and down the branches of the leader channel at a speed typically between one-third and one-half the speed of light (e.g., [7]), as shown in Figure 1.3 at 20.10 and 20.20 ms. Even if the return-stroke's current and high luminosity move upward on the main channel, electrons in the channel always move downward and represent the primary components of the current. Electrons flow up the branches toward the main channel while the return stoke traverses the branches in the outward and downward direction. Some milliseconds after the return stroke starting time, the negative electric charge which were resident on the stepped leader all flow into the ground. Additional current may also flow to ground directly from the cloud once the return stroke has reached the cloud [3]. The high-current return-stroke wave (typically with a peak current of about 30 kA) rapidly heats the channel to a peak temperature near or above 30.000 K and creates a channel pressure of 10 atm or more (e.g., [5]), which results in channel expansion, intense optical radiation, and an outward propagating shock wave that eventually becomes the thunder [6].

It is worth noting that the human eye cannot respond quickly enough to resolve the time between the formation of the leader and the illumination of the leader channel by the return stroke, or to resolve the upward propagation of the return stroke itself. For this reason we do not see the stepped leader before the first return stroke, and for the same reason the return stroke we appears as if all points on the lightning channel were lighted simultaneously.

When the first-stroke current ceases, the lightning discharge may end. In this case, the discharge is termed a "single-stroke" flash. However, more often the cloud-to-ground flashes contain more than one stroke (three or more strokes are common), each one typically separated by 40 or 50 ms from the others. These "subsequent strokes" may occur only if additional negative charge is made available to the upper portion of the previous stroke channel immediately after the end of the previous stroke (normally in a time less than 100 ms). When this additional charge is available, a continuously propagating leader, named "dart leader", moves downward along the previous return-stroke channel, again depositing negative charge along the channel length, as illustrated in Figure 1.3 at 60.00 and 61.00 ms. During the time interval between the end of the first return stroke and the initiation of a dart leader, J- and K-processes occur in the cloud. The J-process can be viewed as a relatively slow positive leader extending from the flash origin into the negative charge region. The K-process then being a relatively fast "recoil streamer" that begins at the tip of the positive leader and propagates toward the flash origin. Both the J-processes and the K-processes in cloud-to-ground flashes serve to transport additional negative charge into and along the existing channel, although not all the way to ground. In this

respect, K-processes may be viewed as attempted dart leaders [6]. The dart leader's trip from cloud to ground takes only a few milliseconds, since, in general, dart leaders travel along the residual channel of the first return strokes at a typical speed of 10^7 m/s. Nevertheless, is not uncommon for the dart leader to take a different path than the first stroke; in this case it ceases to be a dart leader and travel towards the ground as a stepped leader. Furthermore, some dart leaders exhibit stepping near ground while propagating along the path of the preceding return stroke; these leaders being termed dart-stepped leaders.

The dart leader generally deposits less charge, a tenth as much, along its path than does the stepped leader, and hence the subsequent return strokes generally lower less charge to ground and have smaller peak currents than first strokes [3].

Subsequent stroke peak currents range typically from 10 to 15 kA, while first stroke peak currents are typically near 30 kA. The rise times (usually measured between 10% and 90% of peak value) of subsequent stroke currents are generally less than 1 μs, often tenths of a microsecond, whereas the rise times of first strokes currents are usually of some microseconds [8], [9]. The average propagation speed of the return stroke is also different for first strokes and subsequent strokes; in particular, the average velocity of subsequent return strokes over the first few hundred meters close to ground is greater than that of the first return strokes, [10], [11].

As stated above, about 10% of cloud-to-ground lightning flashes are initiated by downward-moving stepped leader that lower positive charge (see Figure 1.2c). The mechanism of positive ground flashes is qualitatively similar to the negative flashes, with differences in the details. For example, the steps of positive stepped leaders are less distinct than the steps of negative stepped leaders. Furthermore, positive return strokes can exhibit currents at the ground whose peak value can exceed 300 kA, considerably larger than for negative strokes whose peak currents rarely exceed 100 kA. Nevertheless, typical positive peak currents are similar to typical negative peak currents (about 30 kA). Positive discharges usually exhibit only one return stroke, and that stroke is almost always followed by a relatively long period of continuing current. The overall charge transfer in positive flashes can considerably exceed that in negative flashes [3].

In upward lightning, see Figure 1.2b and d, the first leader propagates from ground to cloud but does not initiate an observable return stroke or return-stroke-like process when it reaches the cloud charge. Rather, the upward leader primarily provides a connection between the cloud charge region and the ground. After this connection is made and the initial current has ceased to flow, subsequent strokes initiated by downward-moving dart

leaders from the cloud charge, having the same characteristics as strokes following the first stroke in cloud-to-ground lightning, may occur. About half of all upward flashes exhibit such subsequent return strokes [3].

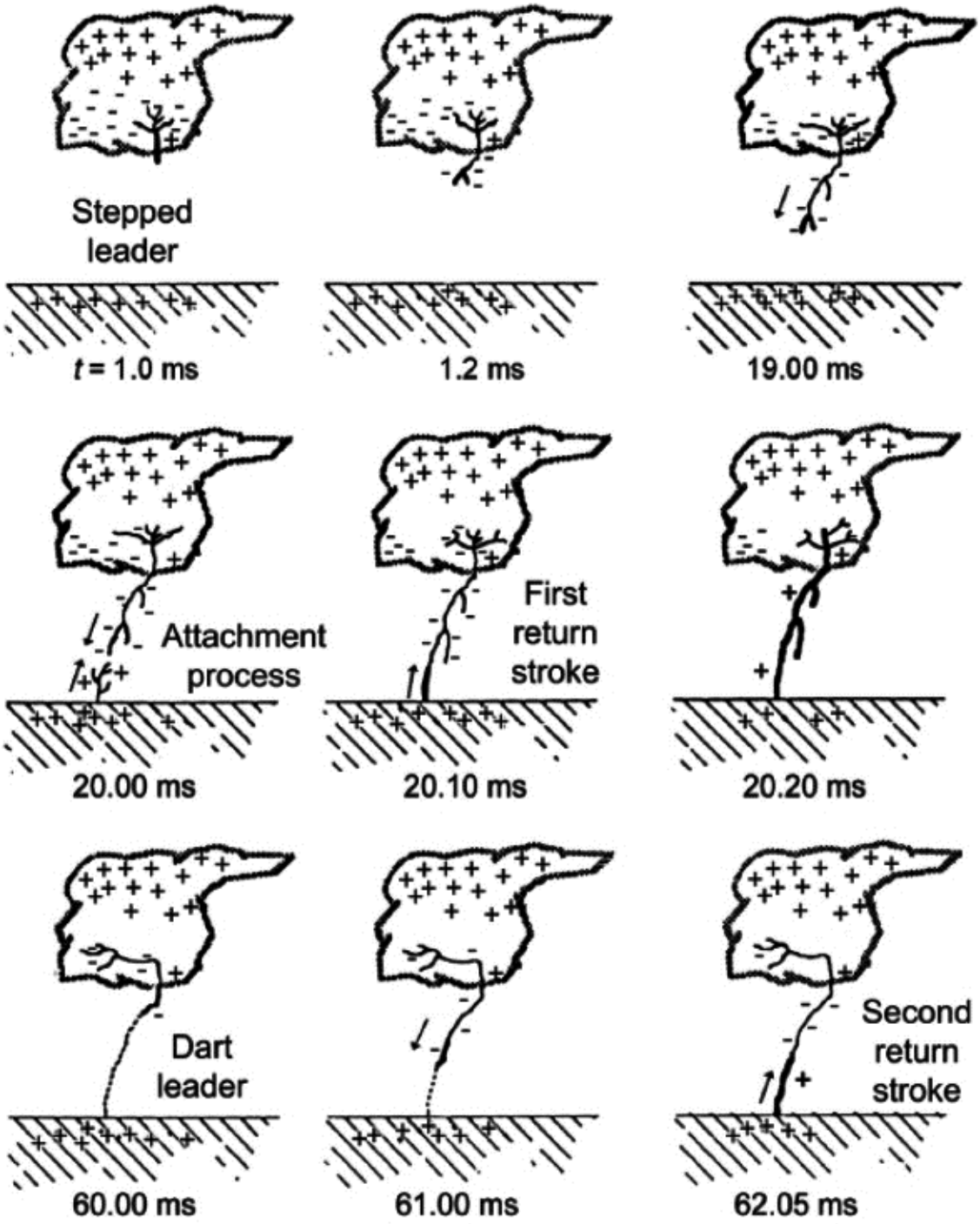

Figure 1.3 – Development of a negative cloud-to-ground lightning discharge. Adapted from [12].

References

[1] V. Cooray, "The mechanism of the lightning flash," in *The Lightning Flash*, 1st ed., Ed. V. Corray, IEE Power Engineering Series vol. 34, London, UK, Ed. The Institution of Engineering and Technology, 2003, ch. 4, pp. 127-240.

[2] E. Williams, "Charge structure and geographical variation of thunderclouds," in *The Lightning Flash*, 1st ed., Ed. V. Corray, IEE Power Engineering Series vol. 34, London, UK, Ed. The Institution of Engineering and Technology, 2003, ch. 1, pp. 1-16.

[3] M.A. Uman, *The art and science of lightning protection*, Cambridge, UK: Cambridge Univ. Press, 2008.

[4] K. Berger, "Blitzstrom-Parameter von Aufwärtsblitzen," *Bull. Schweiz. Elektrotech.*, vol. 69, pp 353-360, 1978.

[5] V. A. Rakov, and M. A. Uman, *Lightning: Physics ad Effects*, Cambridge, UK: Cambridge Univ. Press, 2003.

[6] Y. Baba, and V. A. Rakov, "Present understanding of the lightning return stroke," in *Lightning: Principles, Instruments and Applications*, Eds. H. D. Betz, U. Schumann, and P. Laroche, Springer, 2008.

[7] V. A. Rakov, "Lightning return stroke speed," *J. Lightning Res.*, vol. 1, pp. 1-80, 2007.

[8] K. Berger, R. B. Anderson, and H. Kroninger, "Parameters of lightning flashes," *Electra*, vol. 41, pp. 23-37, Jul. 1975.

[9] R. B. Andersson, A. J. Eriksson, "Lightning parameters for engineering application," *Electra*, vol. 69, pp. 65-102, Mar. 1980.

[10] V. P. Idone, and R. E. Orville, "Lightning return stroke velocities in the thunderstorm research international program (TRIP)," *J. Geophys. Res.*, vol. 87, no. C7, pp. 4903-4915, Jun. 1982.

[11] D. M. Mach, and W. D. Rust, "Photoelectric return stroke velocity and peak current estimates in natural and triggered lightning," *J. Geophys. Res.*, vol. 94, no. D11, pp. 13237-13247, Sep. 1989.

[12] M. A. Uman, *The lightning discharges*, London, UK: Academic Press, 1987 (Revised paperback edition, 2001, New York: Dover Publications, Inc.).

Chapter 2

A Survey on the Evaluation of Lightning-Induced Voltages on Overhead Power Lines

2.1 Introduction

Since the early years of the past century, many researchers activities have been focused on the evaluation of lightning induced voltages on overhead power lines.

The first significant studies on this subject, carried out by K. W. Wagner [1] in 1908, Bewley [2] in 1929, and Norinder [3] in 1936, considered the induced voltages due to indirect lightning as being produced essentially by the electrostatic induction from charged thunderclouds. Wagner [1], stated that, when the lightning discharge occurs, the charge bound to the line is released in form of travelling waves of voltage and current, and it did not consider the electromagnetic field generated by the lightning discharge current.

Afterwards, C. F. Wagner and McCann [4], on the basis of the work of Schonland and Collens [5] on the nature of the lightning flash, stated for the first time that the induced voltages can be considered as due, basically, to the return-stroke current (see Chapter 1). Most of all subsequent studies, including this work, are based on this assumption, that is particularly useful when the lightning stroke is not very close to the distribution line. In fact, as observed by Rachidi *et al.* [6], for distances less than 30 m, some significant overvoltages can be induced also during the leader propagation process (described in detail in Chapter 1) preceding the return stroke.

We remark that, in this thesis, we shall consider only the voltages induced by the electromagnetic field produced by the return-stroke current, as we are not interested in the

study of the effects of lightning discharges very close to the line: for distances less than 30 m, direct lightning flashes are more frequently than indirect ones.

Also in recent years, in literature many efforts have been directed to improve the knowledge of the lightning phenomenon and its effects on power circuits. In particular, many analytical and numerical approaches have been proposed in order to evaluate the induced voltages on an overhead line due to an indirect lightning event. In all these approaches, the calculation of the induced voltages is carried out by following a general procedure, involving the lightning phenomenon and its effects, which can be divided into three main stages:

1. adoption of a return stroke model. To evaluate the electromagnetic field radiated by a lightning discharge, a suitable spatial and temporal model for the description of the return-stroke current distribution and its propagation along the lightning channel is needed;
2. calculation of the electromagnetic field. The electromagnetic field generated by the return-stroke current is calculated by employing the model adopted in the previous step. The effects of the field propagation are also considered;
3. adoption of a coupling model. To evaluate the voltages induced on an overhead line, an appropriate coupling model which describes the interaction between the electromagnetic field and the line conductors must be considered.

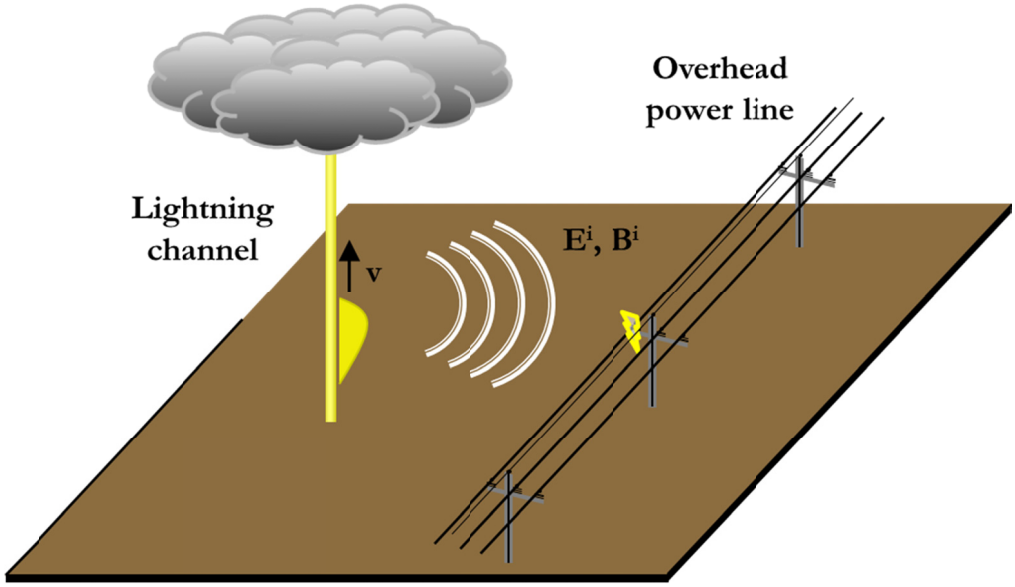

Figure 2.1 – A representation of the three main stages of the lightning induced voltages calculation.

In Figure 2.1 is represented a downward lightning that carries negative charge from the cloud to the ground, whose return-stroke current, as detailed in Chapter 1, propagates up the channel. The lightning channel is here assumed to be perfectly vertical, and this is the only case examined in this thesis work. The electromagnetic "incident" field generated by the return-stroke current propagates toward the line and, by means of coupling phenomena, may cause, for example, a flashover on the insulator surface due to the overvoltage produced.

In the next paragraph, the most common engineering return-stroke current models will be presented and discussed. Paragraph 2.3 will be devoted to the evaluation of the electromagnetic field radiated by a return-stroke current. Finally, in paragraph 2.4, the most important field-to-line coupling models proposed in the literature will be discussed.

2.2 Engineering return-stroke current models

The lightning electromagnetic field is generally calculated making use of a return-stroke current model, that is a mathematical formulae that is capable of predicting the spatial and temporal variation of the lightning current along the channel, the variation of return stroke speed, the temporal spatial characteristics of optical radiation, and the signature of thunder. For the point of view of an engineer, the lightning parameters of particular interest are the return stroke current and its electromagnetic field. Most of the return-stroke models available today are constructed to predict either one or both of these features.

A comprehensive review of the return-stroke models is available in the literature (e. g., [7], and [8]). In [7], Rakov and Uman classified the return stroke models into four categories:

1. "gas dynamic" or "physical" models, which are primarily concerned with the radial evolution of a short segment of the lightning channel and its associated shock wave;
2. "electromagnetic" models, that are usually based on a lossy, thin-wire antenna approximation of the lightning channel. These models involve a numerical solution of Maxwell's equations in order to find the current distribution along the channel from which the remote electric and magnetic fields can be computed;
3. "distributed-circuit" models, that can be viewed as an approximation of the electromagnetic models described above, and that represent the lightning

discharge as a transient process on a vertical transmission line characterized by resistance (R), inductance (L), and capacitance (C), all per unit length;

4. "engineering" models, in which a spatial and temporal distribution of the channel current (or of the channel-charge density) is specified based on such observed lightning return stroke characteristics, as the current at the channel base, the speed of the upward propagating front, and the channel luminosity profile.

The gas dynamic models are primarily used to reproduce physical parameters of the return stroke. The other models are mainly used to reproduce the electromagnetic field radiated from a return-stroke current. In this paragraph, since most of the methods used for the evaluation of the induced voltages are based on engineering models, we shall limit the discussion to this kind of model.

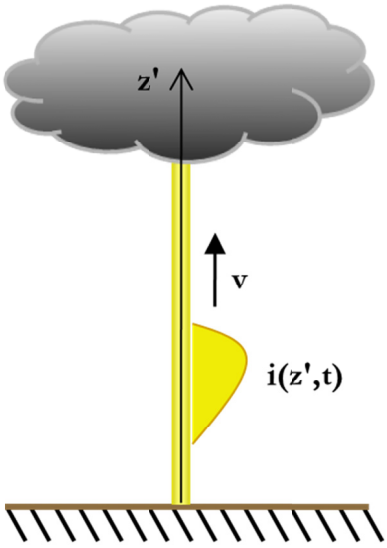

Figure 2.2 – Return stroke channel.

With reference to the Figure 2.2, an engineering model for the return-stroke current is a mathematical specification of the spatial and temporal distribution of the lightning current along the discharge path, $i(z',t)$, or of the channel line charge density, $\rho(z',t)$. Such a mathematical specification includes the return-stroke wavefront velocity, which is generally one of the model inputs [9], the charge distribution along the channel, and a number of adjustable parameters related, to a certain extent, to the discharge phenomenon [8] and which should be inferred by means of model comparison with experimental results [10]. Outputs can be directly used for computation of electromagnetic fields. In these models,

the lightning channel is generally assumed to be straight, vertical and perpendicular to the ground plane, as shown in Figure 2.2.

From an engineering point of view, the models of main interest are those in which the return-stroke current $i(z',t)$ can be related to the channel-base current $i(0,t)$, since it is the only current directly measurable, and for which experimental data are available. For this reason, the most used engineering models presented in the literature give the mathematical specification of the spatial-temporal distribution of the lightning current along the discharge channel as follows [11]:

$$i(z',t) = i\left(0, t - \frac{z'}{v_f}\right) \cdot P(z') \cdot u\left(t - \frac{z'}{v}\right), \tag{2.1}$$

where $u(\cdot)$ is the Heaviside function, v_f is the return-stroke wavefront propagation speed, v is the propagation velocity of the return-stroke current-wave, and $P(\cdot)$ is the attenuation function of the return-stroke current along the channel, which was proposed for the first time by Rakov and Dulzon [12].

The most commonly adopted return stroke models for the lightning induced voltages evaluations are:

- the Bruce and Golde model (BG), described in [13];
- the Travelling Current Source model (TCS), proposed by Heidler [14];
- the Transmission Line model (TL), presented by Uman and McLain [9];
- the Modified Transmission Line model with Linear current decay with height (MTLL), introduced by Rakov and Dulzon [12];
- the Modifiel Transmission Line model with Exponential current decay with height (MTLE), proposed by Nucci *et al.* [15].

These five main models are summarized in Table 2.1, where, according to (2.1), both the propagation velocity and the attenuation function of the return-stroke current along the channel are specified for each model. In the table, h_c is the total channel length, Λ is the current decay constant (assumed in [15] to be 2000 m), and c is the speed of light in the free space.

For sake of completeness, other two return-stroke engineering models will also be presented here: the Master, Uman, Lin, and Standler (MULS) model [16], and the Diendorfer and Uman (DU) model [17].

Model	$P(z')$	v
BG (Bruce and Golde [13]	1	∞
TCS (Heidler [14])	1	$-c$
TL (Uman and McLain [9])	1	v_f
MTLL (Rakov and Dulzon [12])	$1 - z'/h_c$	v_f
MTLE (Nucci *et al.* [15])	$e^{(-z'/\Lambda)}$	v_f

Table 2.1 – Return stroke model summarization, according to [11].

In the following subparagraphs, all these models will be briefly described and discussed. Furthermore, the main models for the channel-base current, $i(0,t)$, proposed in the literature will be presented.

2.2.1 Bruce and Golde (BG) model

Bruce and Golde [13] proposed a simple model of the return-stroke current based on two assumptions: 1) the return stroke front propagates upward with a finite and constant speed which is less than the speed of light, 2) the channel-base current propagates along the lightning channel undistorted and unattenuated. Mathematically, the current at any point on the channel reads:

$$i(z',t) = \begin{cases} i(0,t) & z' \le v_f \cdot t, \\ 0 & z' > v_f \cdot t. \end{cases} \tag{2.2}$$

An equivalent expression in terms of the line charge density on the channel was proposed by Thottappillil *et al.* [18] by means of the continuity equation:

$$\rho(z',t) = \lim_{\Delta z' \to 0} \frac{1}{\Delta z'} \left[\int_0^t i(z' + \Delta z', \tau) d\tau - \int_0^t i(z',\tau) d\tau \right]. \tag{2.3}$$

An initial charge distribution, which takes into account the effects of the charges stored in the corona sheath of the leader, is instantaneously removed by the current. By combining (2.2) and (2.3), the instantaneously removed charged is obtained, and reads [18]:

$$\rho(z',t) = \frac{i\left(0, z'/v_f\right)}{v_f}. \tag{2.4}$$

According with the hypothesis of instantaneous charge removal, the removed charge (2.4) is time independent.

2.2.2 Travelling Current Source (TCS) model

In this model, proposed by Heidler [14], the return-stroke current may be viewed as generated at the upward-moving return-stroke front and propagating downward. In the TCS model, current at a given channel section turns on instantaneously as this section is passed by the front. The channel current expression reads:

$$i(z',t) = \begin{cases} i(0, t + z'/c) & z' \le v_f \cdot t, \\ 0 & z' > v_f \cdot t. \end{cases} \tag{2.5}$$

The equivalent formulation of this model in terms of charge distribution is:

$$\rho(z',t) = -\frac{i(0, z'/v)}{c} + \frac{i(0, z'/v^*)}{v^*}, \tag{2.6}$$

with $v^* = v_f/\left(1 + v_f/c\right)$. As one can see, the TCS model reduces to the BG model if the downward current propagation speed is set equal to infinity instead of the speed of light.

2.2.3 Transmission Line (TL) model

In this model, introduced by Uman and McLain [9], the current is assumed to travel undistorted ad without any attenuation upwards the lightning channel at a constant speed v. The expression of the current at any height z' along the lightning channel is given by:

$$i(z',t) = \begin{cases} i(0, t - z'/v) & z' \le v_f \cdot t, \\ 0 & z' > v_f \cdot t. \end{cases} \tag{2.7}$$

The transfer of charge takes place only from the bottom of the leader channel to the top; thus, no net charge is removed from the channel, i.e., $\rho(z', t) = 0$. This being an unrealistic situation with respect to the present knowledge of lightning physics [19].

The basic hypothesis of this model does not tally with the available experimental data. For example, the results inferred from optical observation show that the current amplitude and current waveshape do change with height. Moreover, return-stroke speed measurements demonstrate that the return stroke speed decreases with increasing height. However, in [20], the authors show that some of the predictions of the TL model are in fairly good agreement with the corresponding measured values, and also that the early time field prediction of the TL model is very similar to that of the more physically reasonable models.

Finally, one can note that the TL model also reduces to the BG model when $v = \infty$.

2.2.4 Modified Transmission Line Linear (MTLL) model

The Transmission Line model with Linear current decay with height was proposed by Rakov and Dulzon [12]. This model can be viewed as incorporating a current source at the channel base, which injects a specified current wave into the channel; that wave propagating upward without distortion but with specified linear attenuation, as seen from the corresponding current expression at a given height z', which reads:

$$i(z', t) = \begin{cases} i(0, t - z'/v) \cdot (1 - z'/h_c) & z' \leq v_f \cdot t, \\ 0 & z' > v_f \cdot t, \end{cases} \tag{2.8}$$

where h_c is the channel length.

This model removed the problem of charge neutralization from the TL model. In fact, the equivalent formulation of this model in terms of charge distribution is:

$$\rho(z', t) = \frac{1 - z'/h_c}{h_c} \cdot \frac{i\left(0, t - z'/v_f\right)}{v_f} + \frac{1}{h_c} \cdot Q(t), \tag{2.9}$$

where $Q(t)$ is the total charge transferred from the ground to the channel at the time t. It is given by:

$$Q(t) = \int_{z'/v}^{t} i(0, \tau - z'/v) d\tau. \tag{2.10}$$

2.2.5 Modified Transmission Line Exponential (MTLE) model

This model was proposed by Nucci *et al.* [15], and it is similar to the MTLL one. It can be viewed as incorporating a current source at the channel base, which injects a specified current wave into the channel; that wave propagating upward without distortion but with exponential attenuation. The current equation reads:

$$i(z', t) = \begin{cases} i(0, t - z'/v) \cdot e^{-z'/\Lambda} & z' \leq v_f \cdot t, \\ 0 & z' > v_f \cdot t, \end{cases} \tag{2.11}$$

where Λ is the constant describing the current decay with height, and it is assumed to be equal to 2000 meters.

The equivalent formulation of this model in terms of charge distribution is:

$$\rho(z', t) = e^{-z'/\Lambda} \cdot \frac{i\left(0, t - z'/v_f\right)}{v_f} + \frac{e^{-z'/\Lambda}}{\Lambda} \cdot Q(t), \tag{2.12}$$

where $Q(t)$, once again, is the total charge transferred from the ground to the channel at the time t, and is still given by (2.10).

The two transmission line models, MTLL and MTLE, represent a modification of the TL model, that does not consider the current attenuation. This attenuation was introduced in order to take into account for the effect of the charges stored in the corona sheath of the leader, and subsequently discharged during the return stroke phase via the upward current [15]. Thus, the fields predicted by these two models result in a better agreement with the experimental results. However, if one considers that, for lightning induced voltages calculation, the early time region of the field plays the major role in the coupling mechanism [21], it follows that the TL model, for the problem of interest, can be considered a useful and relatively simple engineering tool.

2.2.6 Master, Uman, Lin, and Standler (MULS) model

This model, described in [16], results from both physics considerations and experimental results. Originally proposed by Uman, Lin, and Standler (LUS), it was subsequently modified by Master. According to this model, the return-stroke current is composed by three terms: a uniform current, i_u, which accounts for the leader current; an impulsive upward moving current, i_p, that accounts for the collapse of the return-stroke wavefront; and a current, i_c, due to charges stored in the corona sheath of the leader. For the latter term, the surge current is assumed distributed along the channel with a double exponential mathematical form with an exponential decay with the channel height.

2.2.7 Diendorfer and Uman (DU) model

In the Diendorfer and Uman model [17], the return-stroke current may be viewed as generated at the upward-moving return-stroke front, and propagating downward. The current at a given channel section turns on exponentially as this section is passed by the front. The equation of the model reads:

$$i(z',t) = \begin{cases} i(0,t+z'/c) - i(0,z'/v^*)\cdot e^{-(t-z'/v_f)/\tau_D} & z' \le v_f \cdot t, \\ 0 & z' > v_f \cdot t, \end{cases} \tag{2.13}$$

where $v^* = v_f/\left(1+v_f/c\right)$, and τ_D is the decay time constant of the current. As one can see, this current expression is formed by two terms: the first term is a downward-propagating current, as in the TCS model, that exhibits an inherent discontinuity at the upward-moving front; the second term is an opposite polarity current which rises instantaneously to a value equal in magnitude to the current at the front, and then decays exponentially with a time constant τ_D.

The equivalent formulation of this model in terms of charge distribution reads:

$$\rho(z',t) = -\frac{i(0,t+z'/c)}{c} - \left[\frac{i(0,z'/v^*)}{v_f} + \frac{\tau_D}{v^*}\cdot\frac{\partial i(0,z'/v^*)}{\partial t}\right] \cdot e^{-(t-z'/v_f)/\tau_D} + \frac{i(0,t-z'/v^*)}{v^*} + \frac{\tau_D}{v^*}\cdot\frac{\partial i(0,z'/v^*)}{\partial t}. \tag{2.14}$$

If $\tau_D = 0$, the DU model reduces to the TCS model.

2.2.8 The channel-base current

Channel-base current measurements have been performed by means of instrumented high towers or by using the lightning triggering technique, and statistical elaboration of lightning current data have been presented (e.g., [22], [23]). In the case of instrumented towers, one can exploit the fact that tall structures are struck frequently by lightning flashes. Relatively tall structures, such as high towers, can be equipped with current measuring equipment that can record the current signatures at the channel base of lightning flashes. Since the frequency of lightning strikes to a given object increases with increasing height, a reasonable amount of information can be obtained over a time span of a few years using this technique [24], [25]. As regards the lightning triggered technique, a small rocket, trailing a thin metal wire attached to ground through a coaxial shunt, is launched towards a mature thundercloud. As the rocket travels upwards, the field at its tip increases and, when this field reaches a certain critical value, a connecting leader is initiated and travels towards the cloud. Lightning flashes initiated by this upward moving leader will follow the trailing wire to ground, and the lightning channel intercepts the instrumented launching pad and the current is measured directly (e.g., [26]-[28]). However, the first is the best procedure because the inherent nature of triggering procedure: triggered lightning flashes do not contain the first return stroke, which are mediated by stepped leaders in natural lightning flashes.

As already pointed out in Chapter 1, usually, positive flash occurrences are less frequent than negative ones, and also have a lower peak current-derivative. For these reasons, only lightning that lower negative charge to ground will be considered in this work. In Figure 2.3, typical channel-base current waveshapes for negative first (Fig. 2.3a) and subsequent (Fig. 2.3b) return strokes are shown. The statistics of the most important lightning current parameters for the evaluation of the induced voltages (i.e., peak value and front steepness) are summarized in Tables 2.2 and 2.3. In particular, the International Council on Large Electric Systems (CIGRÉ) study group have recommended that the parameters in Table 2.3, adapted from the work of Anderson and Eriksson [23], be used in engineering applications.

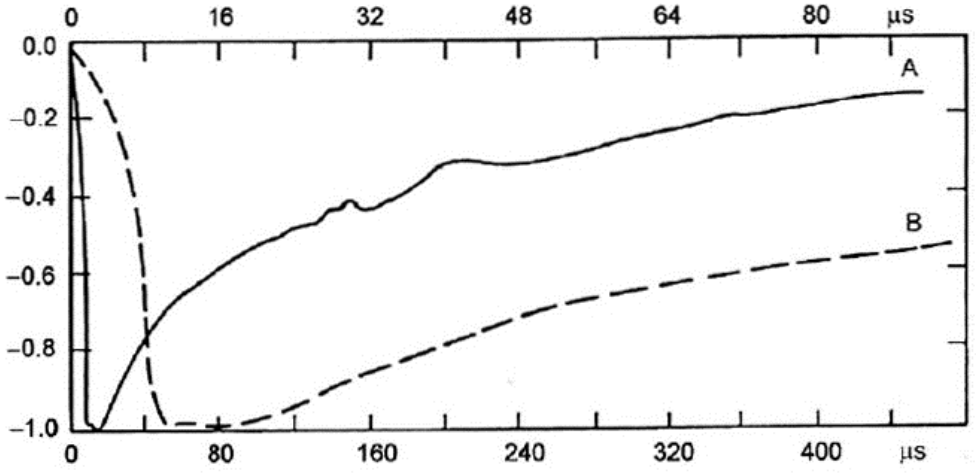

a)

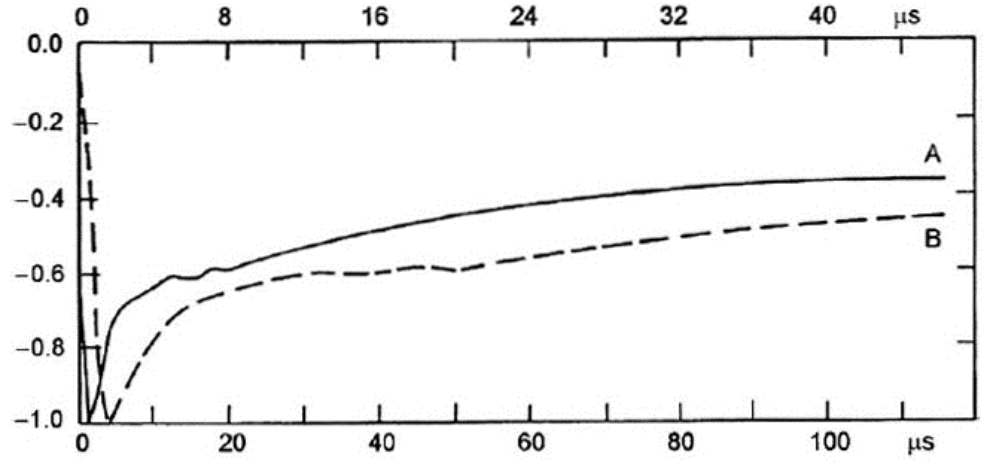

b)

Figure 2.3 – Average negative first- (a) and subsequent-stroke (b) channel-base current each shown on two time scales, A and B. The lover time scales (A) correspond to the solid-line curves, while the upper time scales (B) correspond to the dashed-line curves. The vertical scale is in relative units, the peak values being equal to negative unity. Adapted from [22].

	Percentage exceeding tabulated values					
	95%		**50%**		**5%**	
Stroke	**First**	**Subs**	**First**	**Subs**	**First**	**Subs**
Ipeak [kA]	14	4.6	30	12	80	30
Time to crest [µs]	1.8	0.2	5.5	1.1	18	4.5
$\left(\partial i/\partial t\right)_{max}$ [kA/ms]	5.5	12	12	40	32	120

Table 2.2 – Statistics of peak amplitude, time to crest (or front duration) and maximum front steepness (or rate of rise) for first and subsequent negative return strokes. Adapted from [22].

	Percentage exceeding tabulated values					
	95%		50%		5%	
Stroke	First	Subs	First	Subs	First	Subs
I_{peak} [kA]	14.1	5.2	31.1	12.3	68.5	29.2
Time to crest [μs]	1.8	0.1	4.5	0.6	11.3	2.8
$\left(\partial i/\partial t\right)_{max}$ [kA/ms]	9.1	7.8	24.3	37.8	65	190

Table 2.3 – Statistics of peak amplitude, time to crest and maximum front steepness for first and subsequent negative return strokes. Adapted from [23].

In the literature, several mathematical models for the description of the channel-base current, to use in the return-stroke models discussed above, have been proposed. Some of the most common of these mathematical expressions are described below.

- *Bruce and Golde model*

The channel-base current proposed by Bruce and Golde [13] have a double exponential form. In particular, the authors proposed a channel-base current expression for both the first- and the subsequent-stroke, which reads:

$$i_{first}(0,t) = I_0 \cdot \left(e^{-\alpha t} - e^{-\beta t}\right), \tag{2.15}$$

$$i_{subs}(0,t) = \frac{I_0}{2} \cdot \left(e^{-\alpha t} - e^{-\beta t}\right), \tag{2.16}$$

where I_0 is the peak value of the channel-base current. The value of I_0, and the values of the parameters α and β assumed by Bruce and Golde are reported in Table 2.4. In Figure 2.4, the first- and subsequent-stroke channel-base currents are shown.

- *Pierce and Cianos model*

Pierce [29] proposed a model similar to that of Bruce and Golde, but with different values for the current parameters I_0, α and β, as reported in Table 2.4. Moreover, in [30], Pierce and Cianos introduced a new channel-base current model for the first-stroke, in which a second term is added to the right hand side of (2.15). This new term also have a double exponential form, and leads to a more realistic waveshape, since it adjust the longer time value of the current. The expression proposed by Pierce and Cianos reads:

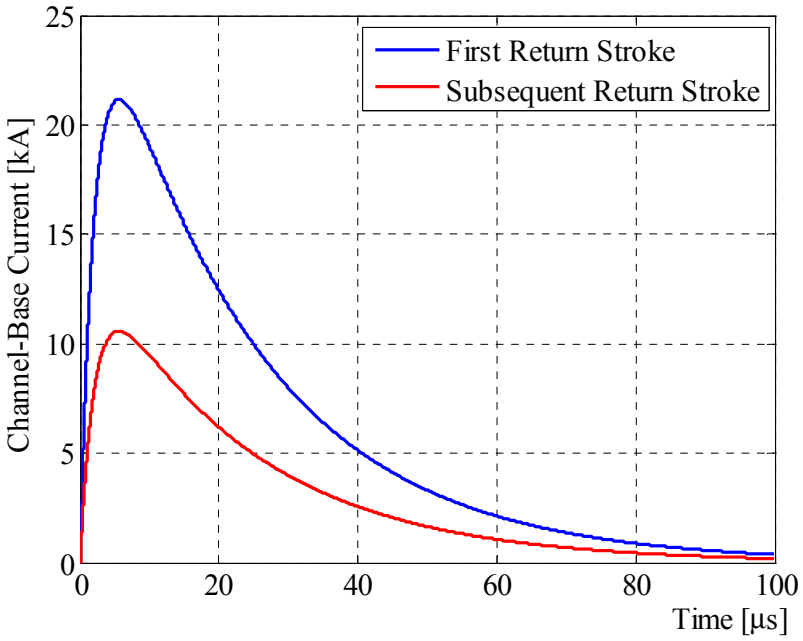

Figure 2.4 – Bruce and Golde channel-base current model.

	First		Subsequents	
Parameters	**Bruce-Golde**	**Pierce-Cianos**	**Bruce-Golde**	**Pierce-Cianos**
I_0 [kA]	30	20	15	10
I_{0i} [kA]	-	2	-	2
α [s^{-1}]	4.4×10^4	2×10^4	4.4×10^4	2×10^4
β [s^{-1}]	4.6×10^5	2×10^6	4.6×10^5	2×10^6
γ [s^{-1}]	-	10^3	-	10^3
δ [s^{-1}]	-	10^4	-	10^4

Table 2.4 – Values of the parameters for the Bruce and Golde, and the Pierce and Cianos channel-base current models [13], [29], [30].

$$i_{first}(0,t) = I_0 \cdot \left(e^{-\alpha t} - e^{-\beta t}\right) + I_{0i} \cdot \left(e^{-\gamma t} - e^{-\delta t}\right). \tag{2.17}$$

The values of all the parameters are given in Table 2.4.

Also for the subsequent return strokes the same adjustments are applied, and the proposed values of the parameters are also reported in Table 2.4. Figure 2.5 shows the channel base current waveshape proposed by Pierce and Cianos, for both first and subsequent return strokes.

It is worth noting that, both the Bruce and Golde model and the Pierce and Cianos one are characterized by an unrealistic convex channel-base current wavefront with a maximum current derivative at $t = 0$.

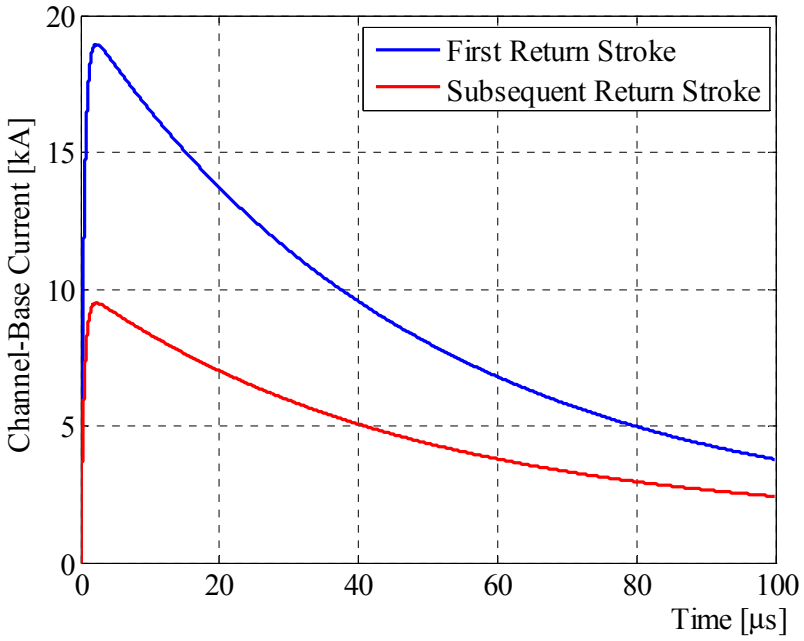

Figure 2.5 – Pierce and Cianos channel-base current model.

- *Heidler model*

The Heidler model [14] reproduces the observed concave rising portion of a typical channel base current waveform, i.e., it does not exhibit a discontinuity in its time derivative, unlike the double-exponential model above presented. The current expression of this model is:

$$i(0,t) = \frac{I_0}{\eta} \cdot \frac{(t/\tau_1)^n}{1+(t/\tau_1)^n} \cdot e^{-\frac{t}{\tau_2}} \cdot u(t), \tag{2.18}$$

where $\eta = e^{[-(\tau_1/\tau_2)\cdot(n\tau_2/\tau_1)^{1/n}]}$ is the correlation factor of the peak current, I_0 is the amplitude of the channel-base current, τ_1 is the rising front time constant, τ_2 is the decay constant of the current waveform, n is the current steepness factor (a number in the range 2÷10). The expression (2.18) allows one to change conveniently the current peak, maximum current derivative, and associated electrical charge transfer nearly independently by changing I_0, τ_1 and τ_2 respectively.

In Table 2.5, typical values for the parameters used to represent a typical subsequent return-stroke current are given [31]. In Figure 2.6, the correspondent channel-base current is plotted. The concave rising portion of the Heidler current can be observed in Figure 2.7, where a magnification of the initial part of the current is shown.

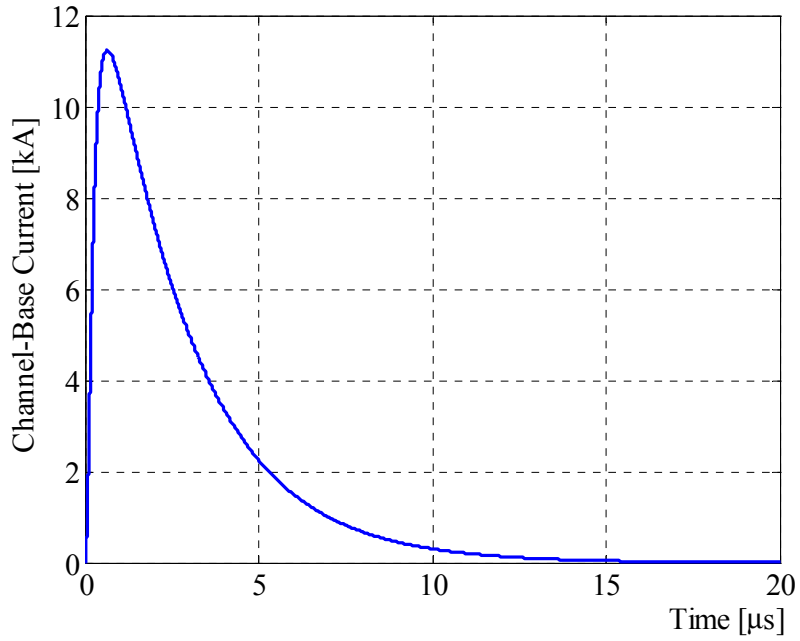

Figure 2.6 – Heidler channel-base current model.

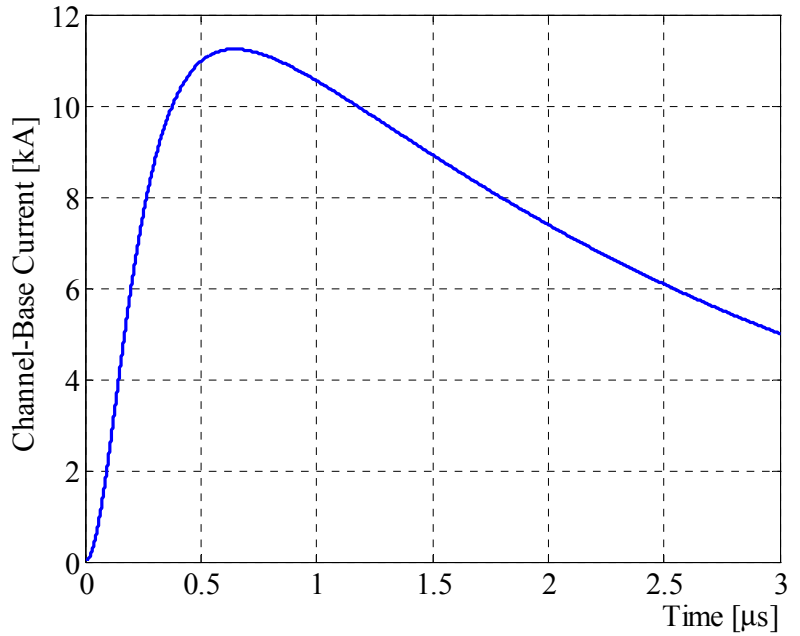

Figure 2.7 – Magnification of the initial part of the current shown in Figure 2.6**.**

I_0 [kA]	τ_1 [μs]	τ_2 [μs]	n
10.7	0.25	2.5	2

Table 2.5 – Typical values for the Heidler channel-base current parameters [31].

Sometimes, a sum of two Heidler functions with different parameters is used to approximate the desired current waveshape. Diendorfer and Uman [17], for example, described the subsequent-stroke current waveform at the channel base by means of the expression:

$$i(0,t) = \left[\frac{I_{01}}{\eta_1}\cdot\frac{(t/\tau_{11})^{n_1}}{1+(t/\tau_{11})^{n_1}}\cdot e^{-\frac{t}{\tau_{12}}} + \frac{I_{02}}{\eta_2}\cdot\frac{(t/\tau_{21})^{n_2}}{1+(t/\tau_{21})^{n_2}}\cdot e^{-\frac{t}{\tau_{22}}}\right]\cdot u(t), \qquad (2.19)$$

with the meaning of the parameters already given for (2.18). In Table 2.6, typical values for the parameters of (2.19) are reported [31].

The correspondent channel-base current is shown in Figure 2.8. One can see that, for longer time bases, the current waveshape predicted by (2.19) is more realistic than the one obtained by using (2.18).

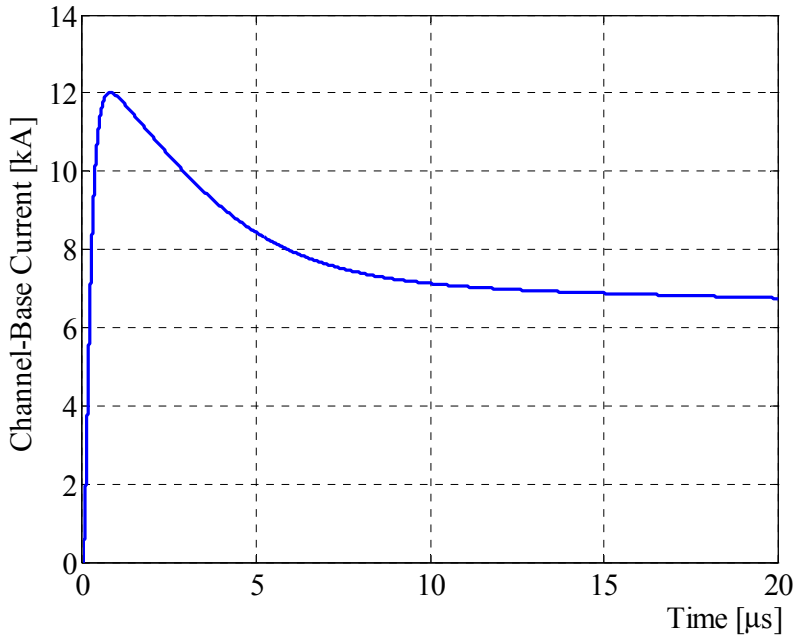

Figure 2.8 – Subsequent-stroke current waveform at the channel base obtained as the sum of two Heidler functions.

I_{01} [kA]	τ_{11} [μs]	τ_{12} [μs]	n_1	I_{02} [kA]	τ_{21} [μs]	τ_{22} [μs]	n_2
10.7	0.25	2.5	2	6.5	2.1	230	2

Table 2.6 – Typical values for the double Heidler channel-base current parameters [31].

Finally, Nucci *et al.* [20] proposed a channel-base current as the sum of a Heidler expression and a double-exponential expression:

$$i(0,t) = \left[\frac{I_{01}}{\eta} \cdot \frac{(t/\tau_1)^n}{1+(t/\tau_1)^n} \cdot e^{-\frac{t}{\tau_2}} + I_{02} \cdot \left(e^{-\frac{t}{\tau_3}} - e^{-\frac{t}{\tau_4}}\right)\right] \cdot u(t). \quad (2.20)$$

Using this equation, we can independently vary the peak current and peak-current derivative by changing I_{01} and τ_1. In Table 2.7, the typical values of the parameters appearing in (2.20) are given [20]. These values are based on the average features of the triggered subsequent return stroke currents. In Figure 2.9, the plot of the current obtained by using (2.20) is shown.

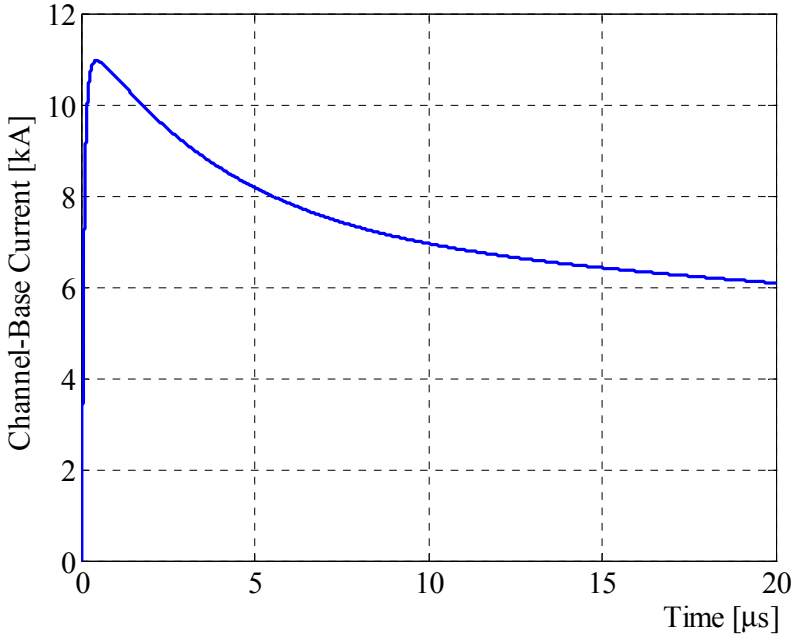

Figure 2.9 – Nucci *et al.* channel-base current model.

I_{01} [kA]	τ_1 [μs]	τ_2 [μs]	n	I_{02} [kA]	τ_3 [μs]	τ_4 [μs]
9.9	0.072	5	2	7.5	100	6

Table 2.7 – Typical values for the channel-base current proposed by Nucci *et al.* [20].

2.2.9 Models validation

Traditional approaches for the validation of the engineering models are based on *direct procedures*. For an assigned return-stroke model, the electromagnetic field is calculated at one or more distances and then compared to the observed one. A return stroke model is then considered suitable if there is a relatively good agreement between calculated and measured

fields. In this view, two main approaches have been used for model validation: the *Typical Return Stroke* approach, and the *Specific Return Stroke* approach [7].

- *Typical Return Stroke Approach*

This approach involves the use of a typical channel-base current waveform and a typical return-stroke propagation speed as model inputs, and then compare the model predicted electromagnetic field with the typical observed fields. This approach has been adopted by Rakov and Dulzon [12], Thottappillil *et al.* [18], and Nucci *et al.* [20]. In particular, Nucci *et al.* [20] identified four characteristic features in the fields at 1-200 km measured by Lin *et al.* [32] and used those features as a benchmark for their validation of the TL, MTLE, BG, TCS, and MULS models. In Figure 2.10, the lightning fields measured by Lin *et al.* for first and subsequent strokes at different distances are shown. The characteristic features include:

a) a sharp initial peak that varies approximately as the inverse distance beyond a kilometer or so in both electric and magnetic fields;
b) a slow ramp following the initial peak and lasting in excess of 100 μs for electric fields measured within a few tens of kilometers;
c) a hump following the initial peak in magnetic fields within a few tens of kilometers, the maximum of which occurs between 10 and 40 μs;
d) a zero crossing within tens of microseconds of the initial peak in both electric and magnetic fields at 50 to 200 km.

For the current and other model characteristics assumed by Nucci *et al.* [20], feature a) is reproduced by all the models examined, feature b) by all the models except for the TL model, feature c) by the BG, TL, and TCS models but not by the MTLE model, and feature d) only by the MTLE model but not by the BG, TL, and TCS models. Diendorfer and Uman [17], showed that the DU model reproduces features a), b), and c). Thottappillil *et al.* [33], demonstrated that a relatively insignificant change in the channel-base current waveform (well within the range of typical waveforms) allows the reproduction of feature d), the zero crossing, by the TCS and DU models. Finally, Rakov and Dulzon [12], showed that the MTLL model reproduces features a), b), and d).

- *Specific Return Stroke Approach*

This second approach involves the use of the channel-base current waveform and the propagation speed measured for the same individual event and compare computed fields

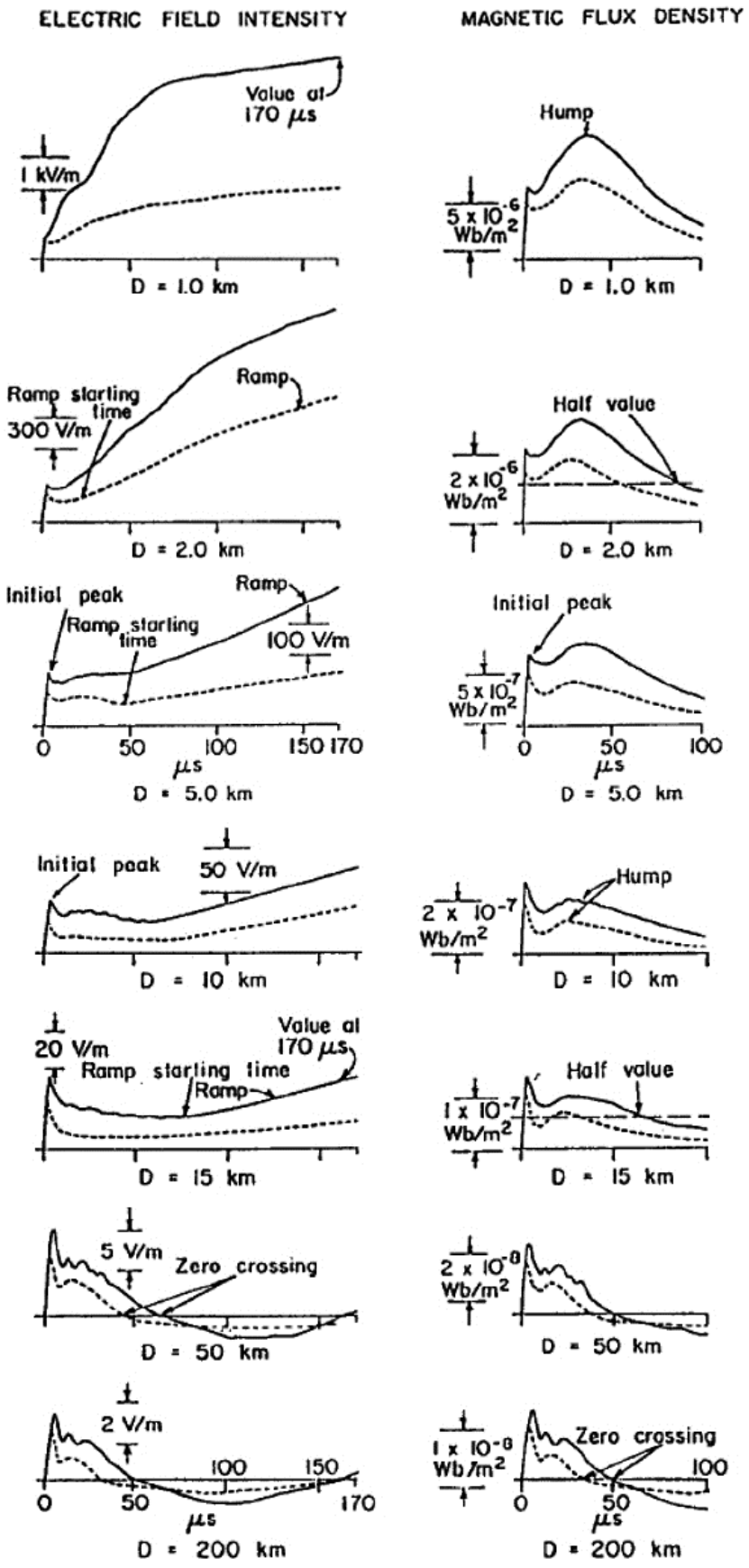

Figure 2.10 – Typical vertical electric field intensity and horizontal magnetic flux density waveforms. The fields are plotted for first (solid line) and subsequent (dashed line) return strokes at distances of 1, 2, 5, 10, 15, 50, and 200 km. Adapted from [32].

with measured fields for that same specific event. This method is able to provide a more definitive answer regarding model validity, but it is feasible only in the case of triggered-lightning return strokes or natural lightning strikes to tall towers where the channel-base current can be measured. In the field calculations, the channel is generally assumed to be straight and vertical, with its origin at ground level $z' = 0$; conditions which are expected to be valid for subsequent strokes, but potentially not for first strokes.

This approach has been adopted by Thottappillil and Uman [34] who compared the TL, TCS, MTLE, and DU models. They used 18 sets of three simultaneously measured features of triggered lightning return strokes: channel-base current, return-stroke propagation speed, and electric field at about 5 km from the channel base. It has been found that the TL, MTLE, and DU models each predict the measured initial electric field peaks with a mean absolute error of about 20%, whereas the TCS model has a mean absolute error of about 40%.

The above presented approaches for the validation of the engineering models are based on direct procedures. A different approach has been proposed by Andreotti *et al.* [35]. They describe the possibility of identifying exactly the attenuation function, $P(z')$, by means of an *inverse procedure*, solving the equations relating the measured field to the channel-base current. Two different procedures to identify the lightning return stroke attenuation, in the frequency domain, were proposed: one for different frequencies, and the other for different distances. Both procedures are able to accurately identify the attenuation function.

2.3 Electromagnetic fields generated by lightning flashes

In the literature, two main methods have been used to obtain the analytical expressions of the electric and magnetic fields radiated from a known distribution of currents and charges. One of these is the *monopole technique* or the continuity equation technique (e.g., [36], [37]), which has been primarily used in the power systems literature for lightning fields calculation, and requires a knowledge of both the current and the charge densities as a function of time and space [38]. The second method, the *dipole technique* or Lorentz condition technique, is described in most electromagnetic books (e.g., [39]-[41]) and is widely used in the study of the antennas.

As demonstrated by Rubinstein and Uman [38], these two techniques are absolutely equivalent, even though their analytical expressions are different.

In the following, we shall briefly describe both the monopole and dipole techniques.

2.3.1 The monopole technique

As well known, Maxwell's equations for a linear, homogeneous, isotropic, time-invariant medium can be written as follows:

$$\boldsymbol{\nabla} \cdot \varepsilon_m \boldsymbol{E} = \rho, \tag{2.21}$$

$$\boldsymbol{\nabla} \cdot \mu_m \boldsymbol{H} = 0, \tag{2.22}$$

$$\boldsymbol{\nabla} \times \boldsymbol{E} = -\frac{\partial \mu_m \boldsymbol{H}}{\partial t}, \tag{2.23}$$

$$\boldsymbol{\nabla} \times \boldsymbol{H} = \boldsymbol{J} + \frac{\partial \varepsilon_m \boldsymbol{E}}{\partial t}. \tag{2.24}$$

Given that (2.22) can be derived from (2.23) by taking the divergence of the latter and integrating over time, with the information that at some times $\mu_m \boldsymbol{H}$ was zero, these equations represent seven independent differential equations in the following unknowns:

- three components of the electric field intensity $\boldsymbol{E}$;
- three components of the magnetic field intensity $\boldsymbol{H}$;
- three components of the current density $\boldsymbol{J}$;
- the charge density ρ.

With ten unknowns and only seven equations, at least three of the unknowns either need to be specified or to be related to other unknowns to solve the Maxwell's equations.

If we know both the charge and all components of the current density, the problem of finding the fields is overspecified since four of the ten unknowns are specified. This overspecification, forming the basis of the monopole technique, allows us to find, in some cases, simpler solutions to otherwise cumbersome problems.

To facilitate the solution of Maxwell's equations for the case of specified or known sources, vector and scalar potentials are used. This approach can be found in many textbooks (e.g., [39]-[41]).

If we define

$$\boldsymbol{E} = -\boldsymbol{\nabla}\phi - \frac{\partial \boldsymbol{A}}{\partial t}, \tag{2.25}$$

and

$$\mu_m \boldsymbol{H} = \boldsymbol{\nabla} \times \boldsymbol{A}, \tag{2.26}$$

and substitute (2.25) and (2.26) into (2.21)-(2.24) with the divergence of $\boldsymbol{A}$ specified by the so-called Lorentz condition:

$$\boldsymbol{\nabla} \cdot \boldsymbol{A} + \mu_m \varepsilon_m \frac{\partial \phi}{\partial t} = 0, \tag{2.27}$$

Maxwell's equations reduce to two equations for $\boldsymbol{A}$ and ϕ, the inhomogeneous solutions of which are

$$\boldsymbol{A}(\boldsymbol{r}_s, t) = \frac{\mu_m}{4\pi} \int_{V'} \frac{\boldsymbol{J}(\boldsymbol{r}'_s, t - |\boldsymbol{r}_s - \boldsymbol{r}'_s|/c)}{|\boldsymbol{r}_s - \boldsymbol{r}'_s|} dV', \tag{2.28}$$

$$\phi(\boldsymbol{r}_s, t) = \frac{1}{4\pi \cdot \varepsilon_m} \int_{V'} \frac{\rho(\boldsymbol{r}'_s, t - |\boldsymbol{r}_s - \boldsymbol{r}'_s|/c)}{|\boldsymbol{r}_s - \boldsymbol{r}'_s|} dV', \tag{2.29}$$

as described, for example, in [39]-[41]. The geometry by which (2.28) and (2.29) are to be interpreted is shown in Figure 2.11.

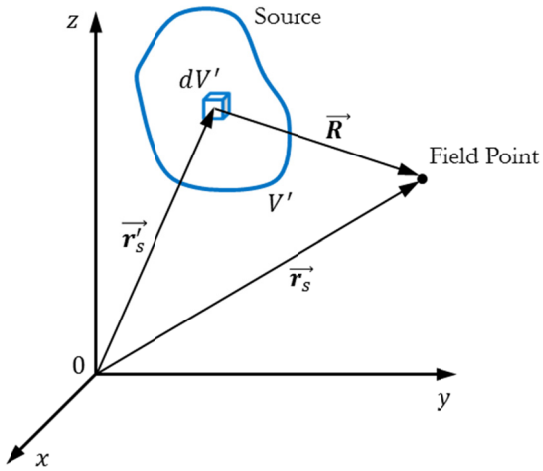

Figure 2.11 – Geometry and coordinate system for source and field points used in solution for vector potential found in (2.28) and scalar potential found in (2.29).

To calculate fields using the monopole technique, (2.25), (2.26), (2.28), (2.29), along with the continuity equation,

$$\nabla \cdot \boldsymbol{J} + \frac{\partial \rho}{\partial t} = 0, \tag{2.30}$$

which follows from taking the divergence of (2.24) and combining the resultant relation with (2.21), have to be used.

In this technique, the source is described in terms of both current density and line charge density, and the field equations are expressed in terms of both charge density and current. The current continuity equation is needed to relate the current density and charge density. There is no need for the explicit use of the Lorentz condition in this technique, although properly specified scalar and vector potentials do satisfy the Lorentz condition.

For example, considering a vertical lightning channel over an infinitely conducting plane, as the one depicted in Figure 2.12, to find the electric and magnetic fields radiated from a return-stroke current which travels up from the channel, and whose specific distributions of charge and current are described by one of the models presented in the previous section, we can use the above equations together with the method of images. In particular, we have to substitute the expressions describing the current and charge distributions for the actual channel, and those for the image channel, into (2.28) and (2.29), respectively. Then, by solving the integrals, we obtain the expressions for the vector and scalar potentials, both for the real and image distribution. Hence, we can calculate the total scalar and vector potentials. Finally, by using (2.25) and (2.26) we can obtain the desired expressions for the electric and magnetic fields.

2.3.2 The dipole technique

Once the source is specified, the radiated fields can always be computed without approximation other than those involved in the computational process. In the problems concerning the lightning induced voltages calculation, the most commonly field equations adopted for the evaluation of return-stroke fields in the time domain have been proposed by Master and Uman [42]. By assuming the ground as a perfect conductor, they have derived the equations for the electric and magnetic fields originated by a vertical dipole of infinitesimal length by solving Maxwell's equations (2.21)-(2.24) in terms of the retarded scalar and vector potentials (2.28), (2.29). The geometry of the problem is shown in Figure 2.12.

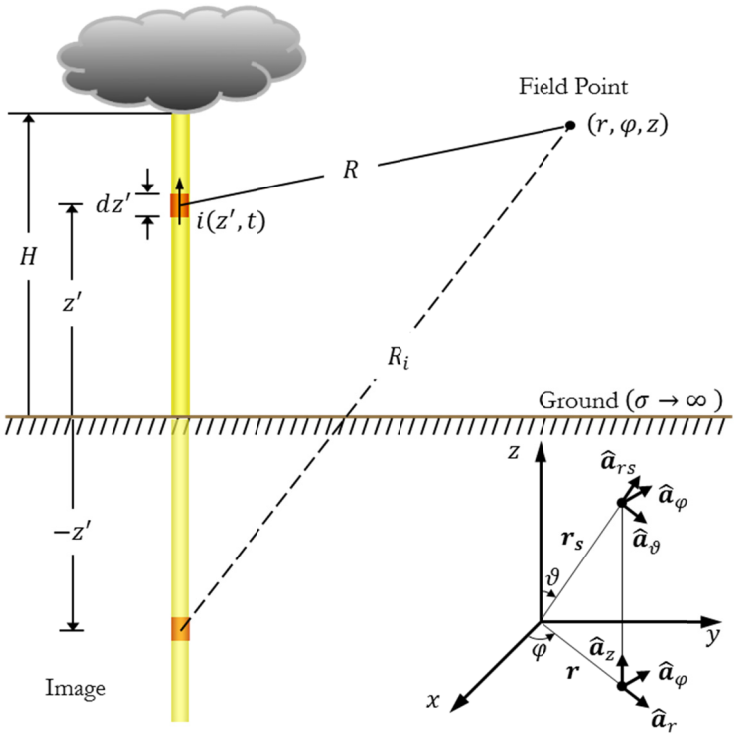

Figure 2.12 – Geometry for the return stroke field evaluation: dipole technique.

The lightning return-stroke channel is modeled as a straight line, and the current on the lightning channel is represented by $i(z', t)$, where z' indicates the position along the z axis with origin at the base of the channel, and t indicates the time. At time $t = 0$ the return stroke starts to propagate from the ground. The field evaluated is originated by a vertical electric dipole of infinitesimal length dz' placed at height z', that is a linear current element whose length is vanishingly small compared with the distance at which the field are to be calculated (the current is assumed to be a constant over the length of the dipole). In the cylindrical coordinate system shown in Figure 2.12, assuming a perfectly conducting ground, the field generated by the dipole is characterized by the vertical and radial electric field components. The equations proposed in [42] are

$$de_r(r,z,t) = \frac{dz'}{4\pi \cdot \varepsilon_0} \cdot \left[\frac{3r \cdot (z-z')}{R^5} \cdot \int_0^t i\left(z', \tau - \frac{R}{c}\right) d\tau + \frac{3r \cdot (z-z')}{c \cdot R^4} \right.$$

$$\left. \cdot\, i\left(z', t - \frac{R}{c}\right) + \frac{r \cdot (z-z')}{c^2 \cdot R^3} \cdot \frac{\partial i(z', t - R/c)}{\partial t} \right], \tag{2.31}$$

$$de_z(r,z,t) = \frac{dz'}{4\pi \cdot \varepsilon_0} \cdot \left[\frac{2 \cdot (z-z')^2 - r^2}{R^5} \cdot \int_0^t i\left(z', \tau - \frac{R}{c}\right) d\tau + \frac{2 \cdot (z-z')^2 - r^2}{c \cdot R^4} \right.$$

$$\left. \cdot\, i\left(z', t - \frac{R}{c}\right) - \frac{r^2}{c^2 \cdot R^3} \cdot \frac{\partial i(z', t - R/c)}{\partial t} \right], \tag{2.32}$$

$$dh_\varphi(r,z,t) = \frac{dz'}{4\pi} \cdot \left[\frac{r}{R^3} \cdot i\left(z', t - \frac{R}{c}\right) + \frac{r}{c \cdot R^2} \frac{\partial i(z', t - R/c)}{\partial t} \right], \tag{2.33}$$

where

- $i(z', t)$ is the current along the lightning channel;
- $R = \sqrt{(z-z')^2 + r^2}$ is the distance between the electric dipole and the observation point;
- r is the projection of R in the xy-plane (see Figure 2.12);
- c is the speed of light.

In (2.31) and (2.32), the three terms are called, respectively, the electrostatic field, the induction or intermediate field, and the radiation or far-zone field. In (2.33), the first term on the right-hand side is the induction field and the second the radiation field.

The total electromagnetic exciting field can be obtained by integrating (2.31)-(2.33), where the current distribution as a function of height and time is given by one of the return-stroke models presented above, along the lightning channel and its image, and is described by the following equations:

$$e_r(r,z,t) = \frac{1}{4\pi \cdot \varepsilon_0} \cdot \left[\int_{-H}^{H} \frac{3r \cdot (z-z')}{R^5} \cdot \int_0^t i\left(z', \tau - \frac{R}{c}\right) d\tau\, dz' + \int_{-H}^{H} \frac{3r \cdot (z-z')}{c \cdot R^4} \right.$$

$$\left. \cdot\, i\left(z', t - \frac{R}{c}\right) dz' + \int_{-H}^{H} \frac{r \cdot (z-z')}{c^2 \cdot R^3} \cdot \frac{\partial i(z', t - R/c)}{\partial t} dz' \right], \tag{2.34}$$

$$e_z(r,z,t) = \frac{1}{4\pi\cdot\varepsilon_0}\cdot\left[\int_{-H}^{H}\frac{2\cdot(z-z')^2-r^2}{R^5}\cdot\int_0^t i\left(z',\tau-\frac{R}{c}\right)d\tau\,dz'\right.$$

$$\left.+\int_{-H}^{H}\frac{2\cdot(z-z')^2-r^2}{c\cdot R^4}\cdot i\left(z',t-\frac{R}{c}\right)dz'-\int_{-H}^{H}\frac{r^2}{c^2\cdot R^3}\cdot\frac{\partial i(z',t-R/c)}{\partial t}dz'\right], \quad (2.35)$$

$$h_\varphi(r,z,t) = \frac{1}{4\pi}\cdot\left[\int_{-H}^{H}\frac{r}{R^3}\cdot i\left(z',t-\frac{R}{c}\right)dz'+\int_{-H}^{H}\frac{r}{c\cdot R^2}\frac{\partial i(z',t-R/c)}{\partial t}dz'\right]. \quad (2.36)$$

Other, different, field expressions in the time domain, with specific application to lightning, can be found in [18], [43]-[45].

It is worth to observe that, in this technique, the source is described only in terms of current density, and that the field equations (2.34)-(2.36) are expressed only in terms of current. Indeed, the use of the Lorentz condition (2.27) eliminates the need for the specification of the line charge density along with the current density and assures that the current continuity equation, which is not explicitly used in this technique, is satisfied.

2.3.3 The effect of the finite ground conductivity

If the observation point, $P(r,\varphi,z)$, of the lightning electromagnetic field is located on the ground surface, and the ground is assumed to be perfectly conducting, only two field components, the vertical electric field and the azimuthal magnetic field, are present. The horizontal electric field component is zero, as required by the boundary condition on the surface of a perfect conductor. At an observation point above a perfectly conducting ground, a nonzero horizontal electric field component exists.

In the case of a finitely conducting ground, a horizontal electric field exists above ground and also both on and below its surface.

For distances not exceeding a few kilometers, the perfect ground conductivity assumption is a reasonable approximation for the vertical component of the electric field and for the horizontal component of the magnetic field, as shown by several authors (e.g, [46]-[47]). In fact, considering for example the dipole technique, the contributions of the source dipole and of its image to these field components add constructively and,

consequently, small variations in the image field due to the finite ground conductivity will have little effect on the total field. On the other hand, the horizontal component of the electric field is appreciably affected by a finite ground conductivity. Indeed, for such a field component, the effects of the two contributions subtract, and small changes in the image field may lead to appreciable changes in the total horizontal field. Although the intensity of the horizontal field component is generally much smaller than that of the vertical one, within the context of certain coupling models it plays an important role in the coupling mechanism [48]-[52] and, hence, an accurate calculation method has to be chosen for it.

Methods for the calculation of the horizontal field using the exact Sommerfeld integrals [53] are not practical because of the limitations on computational time.

Two approximate solutions of the Sommerfeld integrals, both originally proposed in the frequency domain, are then commonly used for the computation of the horizontal electric field in presence of a finitely conducting earth. The first is termed "wave tilt formula" and was proposed by Zenneck [54], whereas the second one is the so-called "Cooray-Rubinstein formula", and was presented by Cooray [55] and by Rubinstein [47].

- *Wave tilt formula*

The term "wave tilt" originates from the fact that when a plane electromagnetic wave propagates over a finitely conducting ground, the total electric field at the ground surface is tilted from the vertical because of the presence of a nonzero horizontal (radial) electric field component. The tilt is in the direction of propagation if the vertical electric field component is directed upward, or in the opposite direction if the vertical electric field component is directed downward, being the vertical component of the Poynting vector directed into the ground in both cases. The magnitude of this tilt, and hence the amplitude of the field, depends on the conductivity and the dielectric constant of the soil.

The wave tilt formula sates that, for a plane wave, the ratio between the horizontal electric field, $E_r(P,\omega)$, and the vertical electric field, $E_z(P,\omega)$, in the frequency domain, is equal to the ratio of the propagation constants in the air and in the ground [54]. Therefore, the horizontal electric field component is given by:

$$E_r(r,z,\omega) = E_z(r,z,\omega) \cdot \frac{1}{\sqrt{\varepsilon_r + \sigma/(j\omega \cdot \varepsilon_0)}}, \tag{2.37}$$

where σ and ε_r are the conductivity and relative permittivity of the ground, respectively, and ω is the angular frequency. This formula is a special case (valid for grazing incidence)

of the theory of the reflection of electromagnetic waves off a conducting surface and, hence, is a reasonable approximation only for relatively distant lightning strikes or for the early microseconds of close lightning when the return stroke is near ground. The vertical electric field, $E_z(r, z, \omega)$, in (2.37) is typically computed assuming the ground as a perfect conductor, or is measured.

In 1988, Thomson *et al.* [56] presented an expression for the magnitude of the horizontal electric field component as a function of the magnitude of the vertical electric field component by using the time domain approach described by Master in 1982 [57]. By using this technique, the vertical electric field can be approximated as a sequence of superposed delayed ramps, since a ramp has an analytical inverse transform expression like equation (2.37). The horizontal electric field is then determined in the time domain as the superposition of the responses to the ramps.

- *Cooray-Rubinstein formula*

The Cooray-Rubinstein formula is expressed as follows [47], [55]:

$$E_r(r, z, \omega) = E_{rp}(r, z, \omega) - H_{\varphi p}(r, 0, \omega) \cdot \frac{c \cdot \mu_0}{\sqrt{\varepsilon_r + \sigma/(j\omega \cdot \varepsilon_0)}}, \tag{2.38}$$

where ε_0 is the free space permeability, $E_{rp}(r, z, \omega)$ is the Fourier transform of the horizontal electric field at height z above ground and $H_{\varphi p}(r, 0, \omega)$ is the azimuthal magnetic field component at ground level, both computed as if the ground were a perfect conductor. The second term on the right-hand side of (2.38) is equal to zero for $\sigma \to \infty$ and becomes increasingly important as σ decreases.

This approach has been shown to produce satisfactory approximation of the horizontal electric field for some significant cases. In particular, it reproduces the positive, bipolar and negative polarities of the field at close (one hundred meters), intermediate (some kilometers), and far (tens of kilometers) distances, respectively, and at all these ranges it predicts results close to those predicted by more accurate expressions [47], [58], [59].

2.4 Field-to-line coupling models

Once the electromagnetic field is calculated making use of a return-stroke current model, it is used to calculate the voltages and currents induced on the conducting system.

To do this, the most general and rigorous approach to use is the one based on Maxwell's equations [60]. However, due to the length of distribution lines, the use of such a theory for the evaluation of lightning induced voltages implies long computation times. Also the simplest approach known as "the quasi-static approximation" [61], according to which the propagation of the field is neglected and coupling between incident fields and the line conductors can be described by means of lumped elements (e.g., inductances and capacitances), is not appropriate. In fact, such an approach requires that the dimensions of the line conductors be smaller than about one tenth of the minimum significant wavelength of the electromagnetic field. This assumption is not valid for power lines excited by lightning electromagnetic fields (above 1MHz frequency, that is below 300 m wave length). Another possible approach, that is the most suitable for the problem of interest, is the "transmission line approximation" [62]. The basic assumptions of this theory are that the transverse dimension of the line is much smaller than the minimum significant wavelength and that the response of the line to the lightning fields is quasi-transverse electromagnetic (quasi-TEM), i.e., the electromagnetic field due to the electric charges and currents along the line is confined in the transverse plane and perpendicular to the line axis. In this way, the line can be represented by a series of elementary sections to which the quasi-static approximation applies. Each section is excited progressively by the incident electromagnetic field so that longitudinal propagation effects are taken into account.

In the literature, the most used coupling models adopted for lighting induced voltages evaluation are based on the transmission line approximation. In this section, we shall briefly present and discuss three of these most popular coupling models:

- the Taylor, Satterwhite, and Harrison model, described in [62];
- the Agrawal, Price, and Gurbaxani model, proposed in [63];
- the Rachidi model, presented in [64].

To do this, we will refer to the geometry shown in Figure 2.13, that is a lossless, single-conductor overhead line located at height h above a perfectly conducting ground, parallel to the x-axis and contained in the xz-plane, terminated on two impedances, Z_0 and Z_L. The line is excited by an *incident* external electromagnetic field (E^i, B^i), shown in Figure 2.13, which is the sum of the field radiated by the lightning return-stroke current and of the field reflected by the ground, determined in absence of the wire. The total field (E, B) is given by the sum of the incident field and the so-called *scattered* field, which represents the field produced by the reaction of the conductor wire to the incident field.

As we shall see, all the above mentioned coupling models lead to a pair of equations involving time and space derivatives of induced voltages and currents along the line, and source terms, that are a function of the incident external electromagnetic field components. These equations are obtained integrating Maxwell's equations along the contour path defined in Figure 2.13 and using the transmission line approximation.

It has been demonstrated by Nucci and Rachidi [65], that the three models considered here are fully equivalent approaches, i.e., they provide identical results in terms of total induced voltage (and total induced current) even if they have different formulations.

It is also worth noting that an earlier field-to-line coupling model was developed by Rusck [36]. It has been shown by Nucci *et al.* [66] and by Cooray [58] that Rusck's equations, expressed in terms of scalar potential, are absolutely equivalent to the above mentioned models, as far as the excited electromagnetic field is originated by a straight vertical channel.

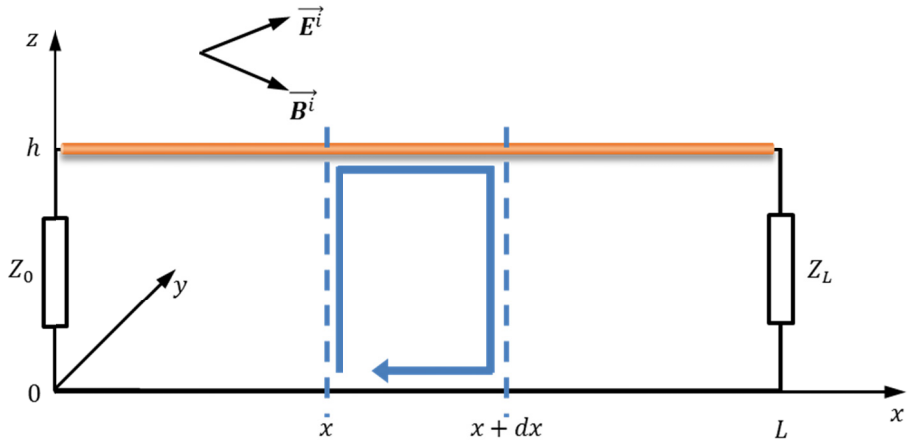

Figure 2.13 – Reference geometry for field-to-line coupling models.

2.4.1 Taylor, Satterwhite and Harrison model

This coupling model, described in [62], refers to a two-wire transmission line excited by a general external electromagnetic field. With respect to the Figure 2.13, the first wire is located at $z = 0$, and the second one at $z = h$. The incident magnetic field, B^i, is taken in the y direction and the incident electric field, E^i, is in the xz-plane. The model is described by two coupling equations in the frequency domain, which reads:

$$\begin{cases} \dfrac{dV(x)}{dx} + j\omega \cdot L' \cdot I(x) = -j\omega \cdot \displaystyle\int_0^h B_y^i(x,z)dz, \\ \dfrac{dI(x)}{dx} + j\omega \cdot C' \cdot V(x) = -j\omega \cdot C' \cdot \displaystyle\int_0^h E_x^i(x,z)dz, \end{cases} \tag{2.39}$$

where $V(x)$ is the total induced voltage along the line, $I(x)$ is the total induced current along the line, C' and L' are the per-unit-length capacitance and inductance of the line, respectively; $E_x^i(x,z)$ is the horizontal component of the incident electric field along the line, and $B_y^i(x,z)$ is the azimuthal component of the incident magnetic induction.

The boundary condition are

$$V(0) = -Z_0 \cdot I(0), \tag{2.40}$$

$$V(L) = Z_L \cdot I(L). \tag{2.41}$$

The second members of (2.39) are the source terms, which are expressed in terms of transverse magnetic induction and vertical electric components of inducing field. In Figure 2.14, the equivalent circuit of this coupling model is shown for a lossless single-conductor overhead line. The forcing functions in (2.39) are included as a set of distributed series voltage and parallel current sources along the line.

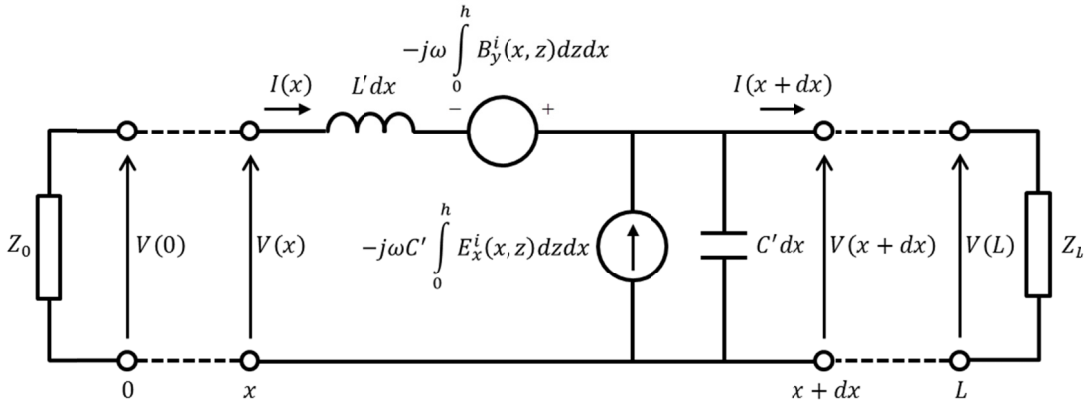

Figure 2.14 – Equivalent coupling circuit according to the Taylor *et al.* formulation for a lossless single-conductor overhead line.

2.4.2 Agrawal, Price, and Gurbaxani model

This coupling model, proposed in [63], refers to the general case of a multi-conductor line plus a reference conductor, excited by a non-uniform electromagnetic field. With reference to the Figure 2.13, we are interested to the case of a single-conductor located at $z = h$, with the reference conductor located at $z = 0$. The incident magnetic field, B^i, is taken in the y direction and the incident electric field, E^i, is in the xz-plane. The model is described by two coupling equations in the frequency domain, which reads:

$$\begin{cases} \dfrac{dV^s(x)}{dx} + j\omega \cdot L' \cdot I(x) = E_x^i(x,h), \\ \dfrac{dI(x)}{dx} + j\omega \cdot C' \cdot V^s(x) = 0, \end{cases} \tag{2.42}$$

where $E_x^i(x,h)$ is the horizontal component of the incident electric field along the line, C' and L' are the per-unit-length capacitance and inductance of the line, respectively, $I(x)$ is the induced current and $V^s(x)$ is the scattered voltage, related to the total voltage $V(x)$ by the following equation

$$V^s(x) = V(x) - V^i(x) = V(x) + \int_0^h E_z^i(x,z)dz. \tag{2.43}$$

The term $V^i(x)$ is called the incident (or exciting) voltage, and $E_z^i(x,z)$ is the vertical component of the incident electric field.

The boundary conditions, written in terms of the scattered voltages and the total current are given by

$$V^s(0) = -Z_0 \cdot I(0) + \int_0^h E_z^i\,(0,z)dz, \tag{2.44}$$

$$V^s(L) = Z_L \cdot I(L) + \int_0^h E_z^i\,(L,z)dz. \tag{2.45}$$

In Figure 2.15, the equivalent circuit of this coupling model is shown. For this model, the forcing function is the exciting electric field tangential to the line conductor and is represented by distributed voltage sources along the line. In agreement with boundary conditions (2.44) and (2.45), two lumped voltage sources are inserted at the line terminations.

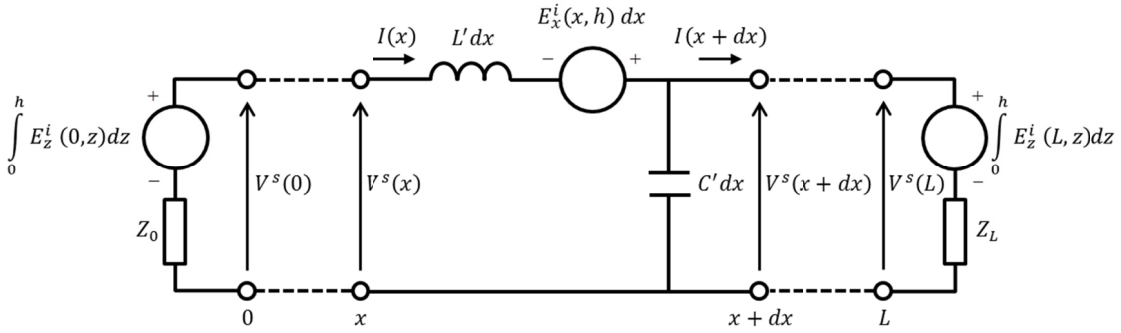

Figure 2.15 – Equivalent coupling circuit according to the Agrawal *et al.* formulation for a lossless single-conductor overhead line.

The difference between the formulation (2.42) and the formulation (2.39) proposed by Taylor *et al.* are lies essentially in the representation of the source terms. In the formulation of Agrawal *et al.*, the source terms are expressed as a function of incident electric field components only, whereas in the formulation of Taylor *et al.*, the source terms are functions of both electric and magnetic incident fields.

2.4.3 Rachidi model

The model proposed by Rachidi [64], also refers to the case of a multi-conductor line plus a reference conductor excited by a non-uniform electromagnetic field. With reference to the Figure 2.13, all the considerations made for the Agrawal *et al.* formulation are still valid. The model is described by the following two coupling equations in the frequency domain:

$$\begin{cases} \dfrac{dV(x)}{dx} + j\omega \cdot L' \cdot I^s(x) = 0, \\ \dfrac{dI^s(x)}{dx} + j\omega \cdot C' \cdot V(x) = \dfrac{1}{L'} \cdot \displaystyle\int_0^h \frac{\partial B_x^i(x,z)}{\partial y} dz, \end{cases} \tag{2.46}$$

where $B_x^i(x,z)$ is the horizontal component of the incident magnetic field along the line, C' and L' are the per-unit-length capacitance and inductance of the line, and $I^s(x)$ is the scattered current, related to the total current by the following equation

$$I^s(x) = I(x) - I^i(x) = I(x) + \frac{1}{L'}\int_0^h B_y^i(x,z)dz. \tag{2.47}$$

The term $I^i(x)$ is called the incident (or exciting) current, and $B_y^i(x,h)$ is the horizontal component of the incident magnetic induction normal to the line.

The boundary conditions, written in terms of the scattered current are

$$I^s(0) = -\frac{V(0)}{Z_0} + \frac{1}{L'}\int_0^h B_y^i\,(0,z)dz, \tag{2.48}$$

$$I^s(L) = \frac{V(L)}{Z_L} + \frac{1}{L'}\int_0^h B_y^i\,(L,z)dz. \tag{2.49}$$

In this formulation, the source terms are expressed in terms of magnetic incident field components. The use of this model is particularly interesting when the exciting field is determined experimentally, since only the measurement of magnetic field (generally much easier than that of electric field) is needed.

In Figure 2.16, the equivalent circuit of this coupling model is shown for a lossless single-conductor overhead line.

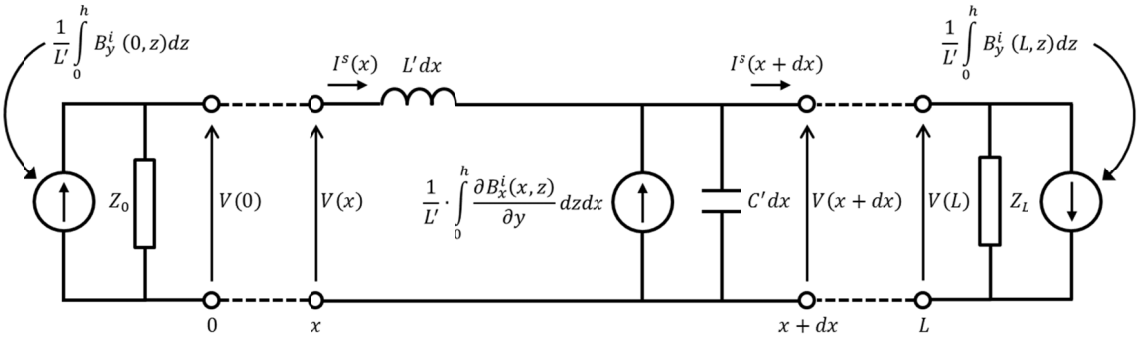

Figure 2.16 – Equivalent coupling circuit according to the Rachidi formulation for a lossless single-conductor overhead line.

References

[1] K. W. Wagner, *Elektromagnetische ausgleichsvorgänge in freileitungen und kabeln*, (German edition), par. 5, Berlin, Germany: Leipzig, 1908.

[2] L. V. Bewley, "Traveling waves due to lightning," in *Trans. A.I.E.E.,* vol. 48, pp. 1050-1064, Jul. 1929.

[3] H. Norinder, "Some recent tests on the investigation of induced surges," *CIGRÉ*, paper 303, Paris, 1936.

[4] C. F. Wagner, and G. D. McCann, "Induced voltages on transmission lines," in *Trans. A.I.E.E.,* vol. 61, pp. 916-930, Dec. 1942.

[5] B. F. J. Schonland, and H. Collens "Progressive lightning," in *Proc. Roy. Soc. London,* series A, vol. 143, pp. 654-674, Feb. 1934.

[6] F. Rachidi, M. Rubinstein, C. A. Nucci, and S. Guerrieri, "Influence of the leader electric field change on voltages induced by very close lightning on overhead lines," in *Proc. of the 22nd Int. Conf. on Lightning Protection,* Budapest, Hungary, Sep. 19-23, 1994.

[7] V. A. Rakov, and M. Uman, "Review and evaluation of lightning return stroke models including some aspects of their application," *IEEE Trans. Electromagn. Compat.,* vol. 40, no. 4, pp. 403-426, Nov. 1998.

[8] C. Gomez, and V. Cooray, "Concepts of lightning return stroke," *IEEE Trans. Electromagn. Compat.,* vol. 42, no. 2, pp. 82-96, Feb. 2000.

[9] M. A. Uman, D. K. McLain, "Magnetic field of lightning return stroke," *J. Geophys. Res.,* vol. 74, no. 28, pp. 6899-6910, Jan. 1969.

[10] C. A. Nucci, and F. Rachidi, "Experimental validation of a modification to the transmission line model for LEMP calculations," in *Proc. of the 8th Int. Symp. on Electromagn. Compat.*, Zurich, Switzerland, Mar. 7-9, 1989, pp. 389-394.

[11] V. A. Rakov, "Lightning electromagnetic fields: Modeling and measurements," in *Proc. of the 12th Int. Symp. on Electromagn. Compat.,* Zurich, Switzerland, Feb. 1997, pp. 59-64.

[12] V. A. Rakov, and A. A. Dulzon, "A modified transmission line model for lighting return stroke field calculations," in *Proc of the 9th Int. Symp. on Electromagn. Compat.,* Zurich, Switzerland, Mar. 1991, pp. 229-235.

[13] C. E. R. Bruce, and R. H. Golde, "The lightning discharge," *J. Inst. Electr. Eng.*, vol. 88, part II, no.6, pp. 487-505, Dec. 1941.

[14] F. Heidler, "Travelling current source model for LEMP calculation," in *Proc of the 6th Symp. on Electromagn. Compat.,* Zurich, Switzerland, Mar. 5-7, 1985, pp. 157-162.

[15] C. A. Nucci, C. Mazzetti, F. Rachidi, and M. Ianoz, "On lightning return stroke models for LEMP calculations," in *Proc. of the 19th Int. Conf. Lightning Protection,* Graz, Austria, Apr. 25-29, 1988, pp. 463-470.

[16] M. J. Master, M. A. Uman, Y. T. Lin, and R. B. Standler, "Calculations of lightning return stroke electric and magnetic fields above ground," *J. Geophys. Res.,* vol. 86, no. C12, pp. 12127-12133, Dec. 1981.

[17] G. Diendorfer, and M. A. Uman, "An improved return stroke model with specified channel-base current," *J. Geophys. Res.,* vol. 95, no. D9, pp. 13621-13644, Aug. 1990.

[18] R. Thottappillil, V. A. Rakov, and M. A. Uman, "Distribution of charge along the lightning channel: Relation to remote electric and magnetic fields and to return stroke models," *J. Geophys. Res.,* vol. 102, no. D6, pp. 6987-7006, Jan. 1997.

[19] M. A. Uman, *The lightning discharges,* London, UK: Academic Press, 1987.

[20] C. A. Nucci, G. Diendorfer, M. A. Uman, F. Rachidi, M. Ianoz, and C. Mazzetti, "Lightning return stroke current models with specified channel-base current: a review and comparison," *J. Geophys. Res.,* vol. 95, no. D12, pp. 20395-20408, Nov. 1990.

[21] C. A. Nucci, F. Rachidi, M. Ianoz, and C. Mazzetti, "Lightning-induced overvoltages on overhead lines," *IEEE Trans. Electromagn. Compat.,* vol. 35, no. 1, pp. 75-86, Feb. 1993.

[22] K. Berger, R. B. Anderson, and H. Kröninger, "Parameters of lightning flashes," *Electra*, no. 41, pp. 23-37, Jul. 1975.

[23] R. B. Anderson, and A. J. Eriksson, "Lightning parameters for engineering application," *Electra*, no. 69, pp. 65-102, Mar. 1980.

[24] K. Berger, "Novel observations on lightning discharges: results of research on mount San Salvatore," *J. Franklin Inst.*, vol. 283, no. 6, pp. 478-525, Jun. 1967.

[25] E. Garbagnati, and G. B. Lo Piparo, "Parameter von blitzströmen," *Elektrotech. Z. ETZ-A,* vol. 103, no. 2, pp. 61-65, 1982.

[26] R. Fieux, C. Gary, and P. Hubert, "Artificially triggered lightning above land," *Nature,* vol. 257, pp. 212-214, Sep. 1975.

[27] R. J. Fisher, G. H. Schnetzer, R. Thottappillil, V. A. Rakov, M. A. Uman, and J. D. Goldberg, "Parameters of triggered-lightning flashes in Florida and Alabama," *J. Geophys. Res.*, vol. 98, no. D12, pp. 22887-22902, Jan. 1993.

[28] V. A. Rakov, "Lightning discharges triggered using rocket- and wire techniques," *Recent Res. Devel. Geophysics,* vol. 2, pp. 141-171, 1999.

[29] E. T. Pierce, "Triggered lightning and some unsuspected lightning hazards," *Naval Research Reviews*, vol. 25, no.3, pp. 14-28, Mar. 1972.

[30] E. T. Pierce, and N. A. Cianos, "Ground-lightning environment for engineering usage," Stanford: Research Institute, Menlo Park, CA, Tech. Report, Aug. 1972.

[31] C. A. Nucci, "Lightning-induced voltages on overhead power lines. Part I: Return-stroke current models with specified channel-base current for the evaluation of return stroke electromagnetic fields," *Electra*, vol. 161, pp. 74-102, Aug. 1995.

[32] Y. T. Lin, M. A. Uman, J. A. Tiller, R. D. Brantley, W. H. Beasley, E. P. Krinder, and C. D. Weidman, "Characterization of lightning return stroke electric and magnetic fields from simultaneous two-station measurements," *J. Geophys. Res.*, vol. 84, no. C10, pp. 6307-6314, Jan. 1979.

[33] R. Thottappillil, M. A. Uman, and G. Diendorfer, "Influence of channel base current and varying return stroke speed on the calculated fields of three important return stroke models," in *Proc. 1991 Int. Conf. Lightning Static Electricity*, Cocoa Beach, FL, pp. 1182-1189, Apr. 1991.

[34] R. Thottappillil, and M. A. Uman, "Comparison of lightning return stroke models," *J. Geophys. Res.,* vol. 98, no. D12, pp. 22903-22914, Jan. 1993.

[35] A. Andreotti, U. De Martinis, and L. Verolino, "An inverse procedure for the return stroke current identification," *IEEE Trans. Electromagn. Compat.*, vol. 43, no. 2, pp. 155-160, May 2001.

[36] S. Rusck, "Induced lightning over-voltages on power transmission lines with special reference to the overvoltage protection of low-voltage networks," *Trans. Royal Inst. of Tech.,* no. 120, pp. 1-118, 1958.

[37] P. Chowdhuri, and E. T. B. Gross, "Voltage surges induced on overhead lines by lightning strokes," in *Proc. Inst. Elect. Eng.*, vol. 114, no.12, pp. 1899-1907, Dec. 1967.

[38] M. Rubinstein, and M. A. Uman, "Methods for calculating the electromagnetic fields from a known source distribution: application to lightning," *IEEE Trans. Electromagn. Compat.*, vol. 31, no. 2, pp. 183-189, May 1989.

[39] J. A. Stratton, *Electromagnetic Theory*, New York: McGraw-Hill, 1941.

[40] J. D. Jackson, *Classical Electrodynamics*, New York: Wiley, 1962.

[41] J. R. Reitz, F. J. Milford, and R. W. Christy, *Foundations of Electromagnetic Theory*, 3rd ed., Reading, MA: Addison-Wesley, 1980.

[42] M. J. Master, and M. A. Uman, "Transient electric and magnetic fields associated with establishing a finite electrostatic dipole," *American J. Phys.*, vol. 51, no. 2, pp. 118-126, Feb. 1983.

[43] R. Thottappillil, and V. A. Rakov, "On different approaches to calculating lightning electric fields," *J. Geophys. Res.*, vol. 106, no. D13, pp. 14191-14205, Jul. 2001.

[44] M. Rubinstein, and M. A. Uman, "On the radiation field turn-on term associated with travelling current discontinuities in lightning," *J. Geophys. Res.*, vol. 95, no. D4, pp. 3711-3713, Jan. 1990.

[45] E. M. Thomson, "Exact expressions for the electric and magnetic fields from a propagating lightning channel with arbitrary orientation," *J. Geophys. Res.*, vol. 104, no. D18, pp. 22293-22300, Sep. 1999.

[46] B. Djebari, J. Hamelin, C. Leteinturier, and J. Fontaine, "Comparison between experimental measurements of the electromagnetic field emitted by lightning and different theoretical models. Influence of the upward velocity of the return stroke," in *Proc. of the 4th Int. Symp. on Electromagn. Compat,* Zurich, Switzerland, Mar. 1981.

[47] M. Rubinstein, "An approximate formula for the calculation of the horizontal electric field from lightning at close, intermediate, and long range," *IEEE Trans. Electromagn. Compat.*, vol. 38, no. 3, pp. 531-535, Aug. 1996.

[48] M. J. Master, and M. A. Uman, "Lightning induced voltages on power lines: Theory," *IEEE Trans. Power Appar. Syst.,* vol. 103, no. 9, pp. 2502-2518, Sep. 1984.

[49] M. Rubinstein, A. Y. Tzeng, M. A. Uman, P. J. Medelius, and E. M. Thomson, "an experimental test of a theory of lightning-induced voltages on an overhead wire," *IEEE Trans. Electromagn. Compat.*, vol. 31, no. 4, pp. 376-383, Nov. 1989.

[50] G. Diendorfer, "Induced voltage on an overhead line to nearby lightning," *IEEE Trans. Electromagn. Compat.*, vol. 32, no. 4, pp. 292-299, Nov. 1990.

[51] C. A. Nucci, F. Rachidi, M. Ianoz, and C. Mazzetti, "Lightning-induced overvoltages on overhead lines," *IEEE Trans. Electromagn. Compat.*, vol. 35, no. 1, pp. 75-86, Feb. 1993.

[52] M. Ishii, K. Michishita, Y. Hongo, and S. Ogume, "Lightning-induced voltage on an overhead wire dependent on ground conductivity," *IEEE Trans. Power Del.*, vol. 9, no. 1, pp. 109-118, Jan. 1994.

[53] A. Sommerfeld, "On the propagation of waves in wireless telegraphy," *Ann. Phys.*, vol. 81, no.25, pp. 1135-1153, Dec. 1926.

[54] J. Zenneck, *Wireless Telegraphy*, New York: McGraw-Hill, 1915 (English translation, A. E. Seelig).

[55] V. Cooray, "Horizontal fields generated by return strokes," *Radio Science,* vol. 27, no. 4, pp. 529-537, Aug. 1992.

[56] E. M. Thomson, P. J. Medelius, M. Rubinstein, M. A. Uman, J. Johnson, and J. W. Stone, "Horizontal electric fields from lightning strokes," *J. Geophys. Res.,* vol. 93, no. D3, pp. 2429-2441, Mar. 1998.

[57] M. J. Master, "Lightning induced voltages on power lines: Theory and experiment," *Ph.D. dissertation*, University of Florida, Gainesville, 1982.

[58] V. Cooray, "Calculating lightning-induced overvoltages in power lines: a comparison of two coupling models," *IEEE Trans. Electromagn. Compat.*, vol. 36, pp. 179-182, 1994.

[59] F. Rachidi, C. A. Nucci, M. Ianoz, and C. Mazzetti, "Influence of a lossy ground on lightning-induced voltages on overhead lines," *IEEE Trans. Electromagn. Compat.*, vol. 38, no. 3, pp. 250-264, Aug. 1996.

[60] F. M. Tesche, "Comparison of the transmission line and scattering models for computing the HEMP response of overhead cables," *IEEE Trans. Electromagn. Compat.*, vol. 34, no.2, pp. 93-99, May 1992.

[61] C. T. A. Johnk, *Engineering electromagnetic field and waves*, New York: John Wiley and Sons, 1975.

[62] C. D. Taylor, R. S. Satterwhite, and C. W. Harrison, "The response of a terminated two-wire transmission line excited by a non-uniform electromagnetic field," *IEEE Trans. Antennas Propagat.*, vol. 13, no. 6, pp. 987-989, Nov. 1965.

[63] A. K. Agrawal, H. J. Price, and S. H. Gurbaxani, "Transient response of multiconductor transmission lines excited by a nonuniform electromagnetic field," *IEEE Trans. Electromagn. Compat.*, vol. 22, no. 2, pp. 119-129, May. 1980.

[64] F. Rachidi, "Formulation of the field-to-transmission line coupling equations in terms of magnetic excitation field," *IEEE Trans. Electromagn. Compat.*, vol. 35, no. 3, pp. 404-407, Aug. 1993.

[65] C. A. Nucci, and F. Rachidi, "On the contribution of the electromagnetic field components in field-to-transmission line interaction," *IEEE Trans. Electromagn. Compat.*, vol. 37, no. 4, pp. 505-508, Nov. 1995.

[66] C. A. Nucci, F. Rachidi, M. Ianoz, and C. Mazzetti, "Comparison of two coupling models for lightning induced overvoltage calculations," *IEEE Transactions on Power Delivery,* vol. 10, pp. 330-338, 1995.

Chapter 3

New Approaches to Calculation of Lightning Induced Voltages

3.1 Introduction

Power quality issues are nowadays fundamental. In particular, Medium Voltage (MV) distribution lines are very sensitive to nearby lightning strike effects. Accurate evaluation of lightning induced voltages is therefore essential to address those issues.

Lightning induced voltages have been the subject of many textbooks (e.g., [1], [2]) and papers. Recent progress in this area is significant, both from numerical and analytical point of view. Numerical approaches have shown excellent development over the years (e.g., [3]-[7]). They are able to accurately model the phenomenon (realistic return-stroke current waveshape, finite ground conductivity effects, non-linearities due to surge arresters and so on). Nevertheless, analytical solutions (e.g., [8]-[13]) still deserve attention, since they are important in the design phase [14], in parametric evaluation, and sensitivity analysis (e.g., [15]); they are also implemented in computer codes for lightning induced effects [16]. Analytical solutions, moreover, do not suffer from numerical instabilities or convergence problems, which could affect accuracy of numerical algorithms [17].

Among analytical expressions, exact solutions, i.e. solutions that, for the considered model, are derived with no approximations, are particularly useful, since they can be used as a test bench for approximate analytical solutions, in order to analyze their limits of applicability [8]; they can be used also for testing the validity of numerical approaches.

Exact solutions, unfortunately, can be obtained only for very simple configurations.

The most basic case for lightning induced voltage calculations is concerned with the evaluation of the analytical functions expressing the waveform of the voltage induced on a lossless, single conductor located over an infinite-conductivity ground plane and excited by

an external field due to a step current moving at constant speed along a vertical lightning channel, unattenuated and without distortion (i.e., according to the TL model, described in Chapter 2). The configuration is depicted in Figure 3.1, case (a).

This simple and practically unrealistic configuration, has been solved, in chronological order, by Rusck [9], Chowdhuri and Gross [18], [19], Liew and Mar [20], Høidalen [10], and Andreotti *et al.* [8]. In particular, Rusck and Høidalen evaluated approximate solutions [8], by using different coupling models (Rusck [9] and Agrawal *et al.* [21] coupling models, respectively) and different models for computing lightning electromagnetic field (monopole and dipole techniques, respectively, both discussed in Chapter 2). The two solutions were found to be the same [10], showing the important result that the solution is model-independent. A further step was made by Andreotti *et al.* who, by using the monopole approach for the lightning electromagnetic field evaluation and the Taylor *et al.* coupling model (described in Chapter 2), found the *exact* solution, i.e., the solution that, for the described model, was obtained with no approximations. Furthermore, Andreotti *et al.* demonstrated [8] that the Rusck-Høidalen solution represents the first-order approximation to their solution, and it is an excellent approximation for distribution lines, where indirect lightning effects are more important; differences were found between exact and Rusck-Høidalen approach for transmission lines.

A more realistic situation is the calculation of the induced voltage waveshape based on the model described before, but for the case of a linearly rising current (followed by a constant or drooping tail) instead of a step current: the configuration is the one in Figure 3.1, case (b). Approximate analytical solutions for this problem have been proposed by Chowdhuri-Gross [18], [19], Liew-Mar [20], Høidalen [10], Sekioka [23], and will be discussed later in this section.

A further step to consider in the analytical models is the consideration of the lossy ground effects. Several authors have presented simple formulas or more complex analytical developments for the model described by both case (a) and case (b) of Figure 3.1. For case (a), formulas have been proposed by Barker *et al.* [24], Darveniza [25], and Paulino *et al.* [26]. In particular, Barker *et al.* proposed a correction factor to be applied to the Rusck's formula for the induced voltage peak value (and not for the overall waveshape) calculated at the point closest to the lightning channel ($x = 0$). Darveniza presented an empirical formula, deduced from theoretical considerations and experimental data, which represents an extension of the Rusck's formula for the induced voltage peak value again at $x = 0$, by replacing the actual height of the line with an effective height, which is a function of ground conductivity. Paulino *et al.*, based on the studies [27], [28], proposed an extension of

the Rusck's formula, again for the peak value at $x = 0$, by considering an additional term which is a function of ground conductivity to account for lossy ground effects. For case (b), a formula has been proposed by Paulino *et al.* [29], which can be used to evaluate the induced voltage peak value at $x = 0$, whereas Høidalen [10] proposed an analytical approach for the overall waveshape at any position x along the line.

The first purpose of this chapter is to extend the work started in [8] by solving in an exact way the case of a terminated single-conductor line and other more realistic configurations in presence of a perfectly conducting ground, that is, long multi-conductor line with grounded conductors (ground wires) and single- and multi-conductor lines (including grounded conductors) excited by a linearly rising current (instead of a step current).

The second purpose is to take into account lossy ground effects. It should be noted that lossy ground affects the lightning electromagnetic fields, in particular, the horizontal electric field at line height (as detailed in Chapter 2). The propagation of the induced voltage along the line is affected too. In this work, we will only consider the lossy-ground effects on the horizontal field at line height.

The results obtained using the models developed here, for both perfectly conducting and lossy ground, will be compared with those given by other formulas/solutions found in the literature.

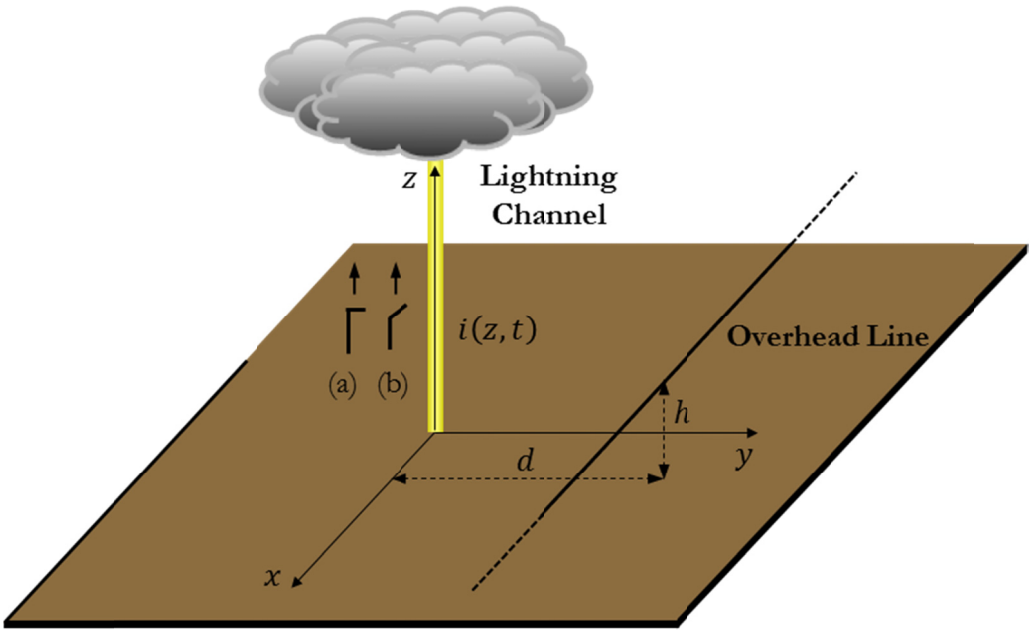

Figure 3.1 – Lightning channel and infinitely long overhead line: (a) step current, and (b) linearly rising current.

3.2 Perfectly conducting ground case

As previously anticipated, in this section, results obtained by Andreotti *et al.* in [8] will be extended to different line configurations.

Specifically, the solution proposed in [8] will be firstly reviewed and reformulated. Then we will present the exact solution for the evaluation of the induced voltages produced by a step current on a terminated (matched and unmatched) single-conductor line located above a perfectly conducting ground. Furthermore, other more realistic configurations, still in the presence of an ideal ground, as the cases of a long multi-conductor line with grounded conductors (ground wires) and single- and multi-conductor lines (including grounded conductors) excited by a linearly rising current (instead of a step current), will be analyzed.

3.2.1 Step channel-base current

3.2.1.1 Infinitely long, single-conductor line

In [8], the authors presented the *exact analytical* solution for the evaluation of the induced voltage induced on a long, lossless, single conductor located over an infinite-conductivity ground plane, and excited by an external field due to a step channel-base current moving along a vertical lightning channel according to the TL model. The configuration is depicted in Figure 3.1.

The expression for the induced voltage along the line was obtained by analytically solving the following expression [8]:

$$v(x,t) = \left[-\int_0^h e_z(x,d,z,t)dz \right. \\ \left. -\frac{1}{2}\cdot\int_{-\infty}^{+\infty} e_x\left(\eta,d,h,t-\frac{|\eta-x|}{c}\right)\cdot sign(\eta-x)d\eta \right]\cdot u(t-t_0), \qquad (3.1)$$

where $e_z(\cdot)$ and $e_x(\cdot)$ are the vertical and the line axial component of the electric field radiated by the return-stroke step current, respectively, c is the speed of light in free space, $u(\cdot)$ is the Heaviside function, t_0 is the arrival time of the field to the observation point, given by

$$t_0 = \frac{r_0}{c} = \frac{\sqrt{x^2 + d^2 + h^2}}{c}. \tag{3.2}$$

The meaning of the other symbols is the same as in Figure 3.1.

For the purposes of this work, we need to rewrite the solution of (3.1), keeping separate the two contributions on the right-hand side, due, respectively, to the vertical and horizontal components of the electric field (in [8], the two contributions were directly simplified in the summation). It is important to keep the two contributions separate since, when taking into account lossy ground effects [30], the vertical contribution can be directly used, because it can be considered practically unaffected by the ground effects [31], [32], whereas one has to modify the horizontal contribution to consider such effects [33], [34] (see Chapter 2 for a detailed discussion of the finite ground conductivity effects). Making reference to the first term on the right-hand side of (3.1) as $v^z(x,t)$ and the second one as $v^x(x,t)$, we rewrite the induced voltage as

$$v(x,t) = v^z(x,t) + v^x(x,t). \tag{3.3}$$

The vertical-field contribution $v^z(x,t)$ is written here as in [8]

$$v^z(x,t) = -\int_0^h e_z(x,d,z,t) \cdot u(t - t_0)dz = \frac{\zeta_0 \cdot I_0}{4\pi \cdot \beta} \cdot \left[2\, ln\left(\frac{h + r_0}{r}\right) + \frac{1}{\gamma^2} \cdot ln\left(\frac{\lambda + \sqrt{\lambda^2 + \delta^2}}{\lambda' + \sqrt{\lambda'^2 + \delta^2}}\right)\right] \cdot u(t - t_0), \tag{3.4}$$

where

- ζ_0 is the free space wave impedance;
- I_0 is the return-stroke peak current;
- β is the ratio between the return-stroke speed v and c;
- $r_0 = \sqrt{x^2 + d^2 + h^2}$;
- $r = \sqrt{x^2 + d^2}$;
- $\gamma = 1/\sqrt{1 - \beta^2}$;
- $\lambda = \beta \cdot c \cdot t - h, \lambda' = \beta \cdot c \cdot t + h$;
- $\delta = r/\gamma$.

As noted earlier, this expression can be directly applied also in the case of lossy ground, since it is practically unaffected by ground losses.

As to the horizontal-field contribution, $v^x(x,t)$, it is made up of two parts

$$v^x(x,t) = v_1^x(x,t) + v_2^x(x,t), \tag{3.5a}$$

with

$$v_1^x(x,t) = -\frac{1}{2}\cdot\int_x^{+\infty} e_x\left(\eta, d, h, t - \frac{\eta - x}{c}\right)\cdot u(t-t_0)d\eta \tag{3.5b}$$

and

$$v_2^x(x,t) = \frac{1}{2}\cdot\int_{-\infty}^{x} e_x\left(\eta, d, h, t + \frac{\eta - x}{c}\right)\cdot u(t-t_0)d\eta. \tag{3.5c}$$

The solution of (3.5b), by using a procedure analogous to the one in [8], can be expressed as

$$v_1^x(x,t) = \frac{\zeta_0\cdot I_0}{8\pi\cdot\beta}\cdot\left\{ln\left(\frac{\lambda_m - \beta x_l + \sqrt{(\beta x_l - \lambda_m)^2 + \delta_l^2}}{\lambda_p - \beta x_l + \sqrt{(\beta x_l - \lambda_p)^2 + \delta_l^2}}\right) + ln\left(\frac{\lambda' + \sqrt{\lambda'^2 + \delta^2}}{\lambda + \sqrt{\lambda^2 + \delta^2}}\right)\right.$$

$$+\beta\left[ln\left(\frac{x_l - \beta\lambda_m + \sqrt{(\beta x_l - \lambda_m)^2 + \delta_l^2}}{x_l - \beta\lambda_p + \sqrt{(\beta x_l - \lambda_p)^2 + \delta_l^2}}\right) + ln\left(\frac{x - \beta\lambda_p + \sqrt{(\beta x - \lambda_p)^2 + \delta^2}}{x - \beta\lambda_m + \sqrt{(\beta x - \lambda_m)^2 + \delta^2}}\right)\right]$$

$$\left.+ln\left(\frac{h + \sqrt{x_l^2 + d^2 + h^2}}{-h + \sqrt{x_l^2 + d^2 + h^2}}\right) - 2\,ln\left(\frac{h + r_0}{r}\right)\right\}\cdot u(t-t_0), \tag{3.5d}$$

where

- $\lambda_m = \beta\cdot(c\cdot t + x) - h$;
- $\lambda_p = \beta\cdot(c\cdot t + x) + h$;
- $x_l = [(c\cdot t + x)^2 - d^2 - h^2]/[2(c\cdot t + x)]$;
- $\delta_l = \sqrt{x_l^2 + d^2}/\gamma$.

The solution of (3.5c) can be obtained from (3.5d), by replacing x with $-x$. Solution (3.5) represents the exact expression for the perfectly-conducting ground case. In presence of lossy ground, as we will see later on, the solution needs a modification, for example by using the Cooray-Rubinstein formula (2.38) in the time domain [35].

Finally, by adding the vertical (3.4) and the horizontal (3.5) contributions, one obtains the desired expression of the total induced voltage. Figure 3.2 shows, as an example, a 3-D plot of the induced voltages on a 10 m high single conductor located above perfectly-conducting ground at a distance d = 100 m from the lightning channel, with I_0 = 10 kA and β = 0.4.

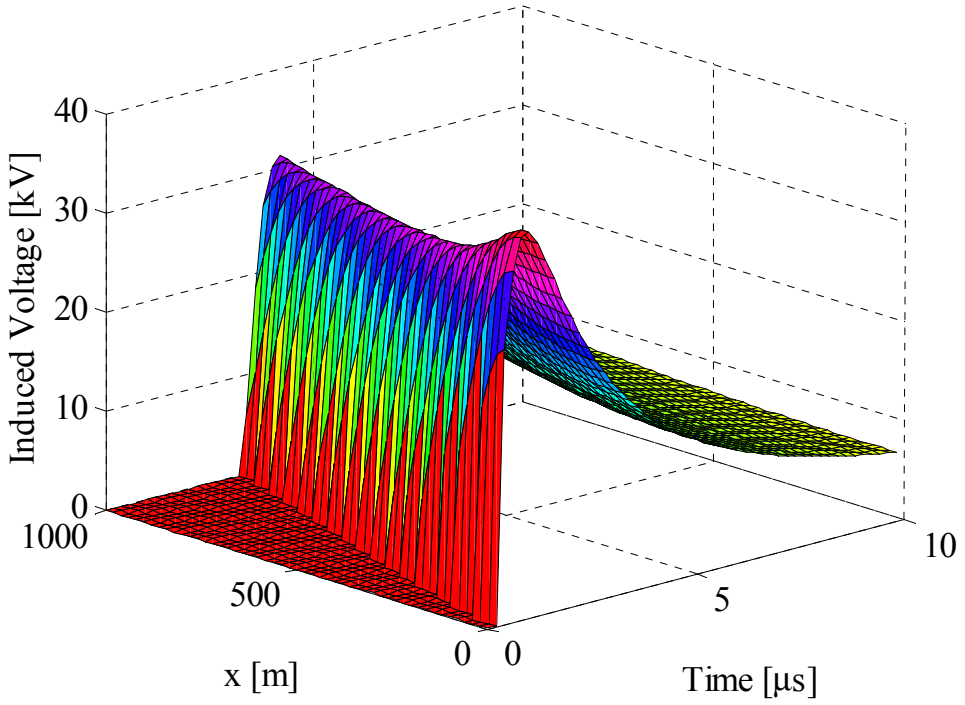

Figure 3.2 – 3-D plot of the induced voltages (h =10 m, d = 100 m, I_0 = 10 kA, β = 0.4).

3.2.1.2 Matched single-conductor line

In this case, we make reference to Figure 3.3. We will consider a finite length single-conductor line terminated at both ends in its characteristic impedance.

The induced voltage evaluated at the line center (x = 0) is given by [8], [36]

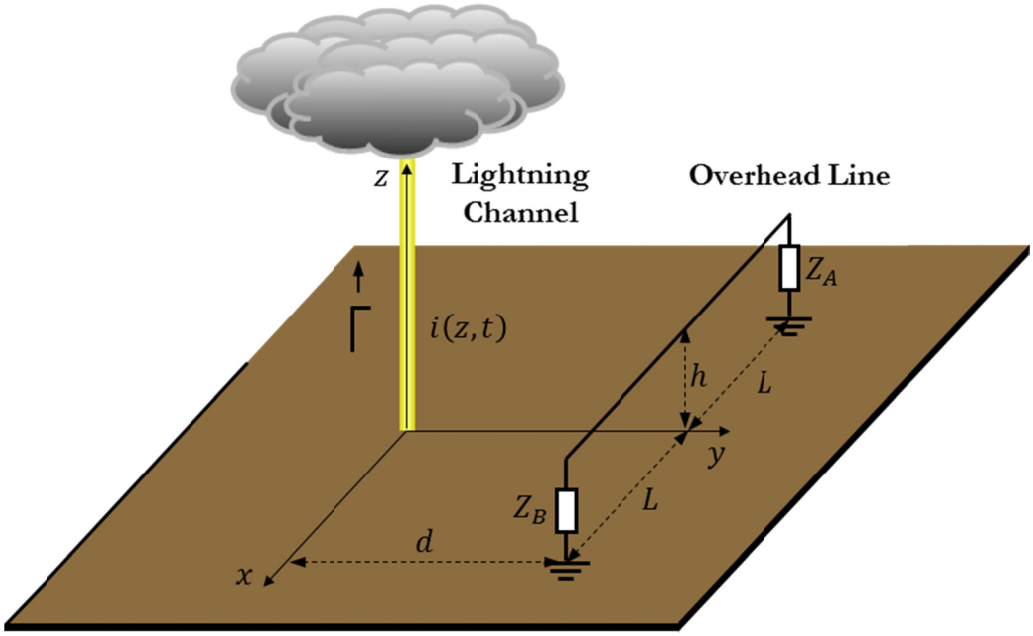

Figure 3.3 – Terminated line case.

$$v_L(0,t) = -\int_0^h e_z(0,d,z,t)\cdot u(t-t_0)dz + \frac{1}{2}\cdot\int_0^h e_z(L,d,z,t-T)\cdot u(t-t_1)dz$$
$$+\frac{1}{2}\cdot\int_0^h e_z(-L,d,z,t-T)\cdot u(t-t_1)dz$$
$$-\frac{1}{2}\cdot\int_{-L}^{L} e_x\left(\eta,d,h,t-\frac{|\eta|}{c}\right)\cdot sign(\eta)\cdot u(t-t_0)d\eta, \qquad (3.6)$$

where

- L is the x-coordinate of the right end point of the line (due to the symmetry, the x-coordinate of the left end point is $-L$);
- $T = L/c$ is the one-way delay of the line, i.e., the amount of time it takes for the field to travel along the line from both ends to the observation point;
- $t_1 = \left(L + \sqrt{L^2 + d^2 + h^2}\right)/c$ is the amount of time it takes for the lightning field to reach the both ends and then to move along the line until the observation point.

The subscript L has been added to distinguish it from the result for an infinite-length line given in the previous section. One can readily identify the difference by the presence of two more contributions due to the vertical "risers". Analogous result applies to the induced voltage evaluated at an arbitrary value of the abscissa along the line, x:

$$v_L(x,t) = -\int_0^h e_z(x,d,z,t)\cdot u(t-t_0)dz + \frac{1}{2}\cdot\int_0^h e_z(L,d,z,t-T_r)\cdot u(t-t_{1r})dz$$
$$+\frac{1}{2}\cdot\int_0^h e_z(-L,d,z,t-T_l)\cdot u(t-t_{1l})dz$$
$$-\frac{1}{2}\cdot\int_{-L}^{L} e_x\left(\eta,d,h,t-\frac{|\eta-x|}{c}\right)\cdot sign(\eta-x)\cdot u(t-t_0)d\eta\,, \qquad (3.7)$$

where

- $T_r = (L-x)/c$ is the amount of time it takes for the field to travel along the line from the right end to the observation point;
- $T_l = |-L-x|/c$ is the amount of time it takes for the field to travel along the line from the left end to the observation point;
- $t_{1r} = \left[(L-x)+\sqrt{L^2+d^2+h^2}\right]/c$ is the amount of time it takes for the lightning field to reach the right end and then to move along the line until the observation point;
- $t_{1l} = \left[|-L-x|+\sqrt{L^2+d^2+h^2}\right]/c$ is the amount of time it takes for the lightning field to reach the left end and then to move along the line until the observation point.

For the first three terms on the right-hand side of (3.7), the solution can be simply obtained from the expression (3.4), whereas for the last term, the horizontal contribution, we need to make further considerations.

By referring to this term as $v_L^x(x,t)$, we have

$$v_L^x(x,t) = -\frac{1}{2}\cdot\int_{-L}^{L} e_x\left(\eta,d,h,t-\frac{|\eta-x|}{c}\right)\cdot sign(\eta-x)\cdot u(t-t_0)d\eta$$
$$= -\frac{1}{2}\cdot\left[\int_x^L e_x\left(\eta,d,h,t-\frac{\eta-x}{c}\right)d\eta\right.$$
$$\left.-\int_{-L}^{x} e_x\left(\eta,d,h,t+\frac{\eta-x}{c}\right)d\eta\right]\cdot u(t-t_0). \qquad (3.8)$$

The first integral can be rewritten as

$$\int_x^L e_x\left(\eta, d, h, t-\frac{\eta-x}{c}\right)\cdot u(t-t_0)d\eta = \int_x^{\tilde{x}_l} e_x\left(\eta, d, h, t-\frac{\eta-x}{c}\right)\cdot u(t-t_0)d\eta, \tag{3.9}$$

with $\tilde{x}_l$ given by

$$\tilde{x}_l = \begin{cases} x_l(t) & x \le x_l(t) < L \iff t_0 \le t < t_{1r}, \\ L & x_l(t) \ge L \iff t \ge t_{1r}, \end{cases} \tag{3.10}$$

where $x_l(t)$ is a "dynamic" integration limit, which takes into account for the propagation effects toward and along the line (see Appendix and [8] for details).

According to (3.10), the solution, for times such that $x_l(t) < L$, that is $t < t_{1r}$, is the same as in [8, (50)]. For longer times ($t \ge t_{1r}$), the solution is given by

$$\begin{aligned} \int_x^L e_x\left(\eta, d, h, t-\frac{\eta-x}{c}\right)u(t-t_{1r})d\eta = \frac{\zeta_0\cdot I_0}{4\pi\cdot\beta}\Bigg\{ & ln\left(\frac{\lambda+\sqrt{\lambda^2+\delta^2}}{\lambda'+\sqrt{\lambda'^2+\delta^2}}\right) - 2ln\left(\frac{r}{h+r_0}\right) \\ & + ln\left(\frac{\lambda_p-\beta L+\sqrt{(\beta L-\lambda_p)^2+\delta_L^2}}{\lambda_m-\beta L+\sqrt{(\beta L-\lambda_m)^2+\delta_L^2}}\right) + ln\left(\frac{-h+\sqrt{L^2+d^2+h^2}}{h+\sqrt{L^2+d^2+h^2}}\right) + \beta \\ & \cdot\left[ln\left(\frac{L-\beta\lambda_p+\sqrt{(\beta L-\lambda_p)^2+\delta_L^2}}{L-\beta\lambda_m+\sqrt{(\beta L-\lambda_m)^2+\delta_L^2}}\right) + ln\left(\frac{x-\beta\lambda_m+\sqrt{(\beta x-\lambda_m)^2+\delta^2}}{x-\beta\lambda_p+\sqrt{(\beta x-\lambda_p)^2+\delta^2}}\right)\right]\Bigg\} \\ & \cdot u(t-t_{1r}), \end{aligned} \tag{3.11}$$

with $\delta_L = \sqrt{L^2+d^2}/\gamma$. All other symbols are as defined above.

Similarly, the second integral on the right-hand side of (3.8) can be rewritten as

$$\int_{-L}^x e_x\left(\eta, d, h, t+\frac{\eta-x}{c}\right)\cdot u(t-t_0)d\eta = \int_{\tilde{x}_l'}^x e_x\left(\eta, d, h, t+\frac{\eta-x}{c}\right)\cdot u(t-t_0)d\eta, \tag{3.12}$$

where $\tilde{x}_l'$ is

$$\tilde{x}_l' = \begin{cases} x_l'(t) & -L < x_l'(t) \le x \quad \Leftrightarrow \; t_0 \le t < t_{1l}, \\ -L & x_l'(t) \le -L \quad \Leftrightarrow \quad t \ge t_{1l}, \end{cases} \tag{3.13}$$

and where $x_l'(t)$, like as $x_l(t)$, is a "dynamic" integration limit, which account for the propagation effects toward and along the line (see Appendix and [8] for details).

The solution of (3.12) can be obtained from the solution of (3.9) replacing x with $-x$ and negating the whole expression.

In this way, we obtain the expression of the induced voltage at an arbitrary value of x along the line.

The exact solution for the point closest to the lightning channel (x = 0) assumes a simpler form: for times such that $x_l(t) < L$, or, equivalently, $x_l'(t) > -L$ (note that for x = 0, $x_l(t) = -x_l'(t)$) the solution is the one found in [8]:

$$v_L(0,t) = v_{L1}(0,t) - v_{L2}(0,t), \tag{3.14a}$$

with

$$v_{L1}(0,t) = -\frac{\zeta_0 \cdot I_0}{4\pi} \cdot \left[ln\left(-\beta\lambda + \sqrt{\lambda^2 + \delta_0^2} \right) + \beta \cdot ln\left(\lambda + \sqrt{\lambda^2 + \delta_0^2} \right) \right] u(t - t_2), \tag{3.14b}$$

where $\delta_0 = d/\gamma$, $t_2 = \sqrt{d^2 + h^2}/c$. The expression of $v_{L2}(0,t)$ can be obtained by replacing λ with λ' in (3.14b).

For longer times, we have

$$v_L(0,t) = v_{L3}(0,t) - v_{L4}(0,t), \tag{3.15a}$$

with

$$v_{L3}(0,t) = -\frac{\zeta_0 \cdot I_0}{4\pi} \cdot \left\{ ln\left(-\beta\lambda + \sqrt{\lambda^2 + \delta_0^2} \right) - ln\left(L - \beta\lambda + \sqrt{(\beta L - \lambda)^2 + \delta_L^2} \right) \right.$$
$$\left. \beta \cdot \left[ln\left(\lambda + \sqrt{\lambda^2 + \delta_0^2} \right) - ln\left(\lambda - \beta L + \sqrt{(\beta L - \lambda)^2 + \delta_L^2} \right) \right] \right\} \cdot u(t - t_1), \tag{3.15b}$$

and $v_{L4}(0,t)$ obtained by replacing λ with λ' in (3.15b).

To summarize, (3.14) represents the exact solution for a finite length line, for times such that $x_l(t) < L$, whereas (3.15) represents the exact analytical solution for longer times.

In Figure 3.4, the induced voltage at $x = 0$ for a 10-m height line, located at a distance d = 100 m, is shown. The line is matched at both ends. Plots are obtained for various line lengths, ranging from 400 m to 3 km with a 200 m step. One can note, in contrast to the infinite-length line, the "jump" due to the vertical risers; clearly, increasing L delays the "jump". In Figure 3.5, the induced voltage is evaluated at $x = L$ (the same as at $x = -L$). In this case, apart from the "jump", one more effect is noticed: the induced voltage varies as the line length increases. This effect allows one to make the following observation: in principle, the lightning electromagnetic field illuminates the line for its entire length; in order to reduce the computational burden in computer codes used for lightning-induced voltages calculations (e.g., [16] and [37]), one has to choose a shorter length of the line which is able to mimic the line for its whole length (e.g., a line 20-km long, which in principle is illuminated over all the 20 km of its length, could be acceptably represented by an illuminated segment of 2 km, considering the rest of the line as passive). Now, if the considered illuminated portion is too short, the corresponding induced voltage is not accurate: for example, as noted above, in Figure 3.5 the induced voltage becomes more or less constant when the line is 2-km long or more, i.e., a selected portion of 2 km or more will be able to mimic a longer illuminated line. It is clear that if the segment selected for the illuminated portion of the line is not sufficiently long, one could get an underestimation of the induced voltages. The proposed solution could be used as a means for addressing this issue. For example, as noted above, in the case analyzed in Figure 3.5 (h = 10 m, d = 100 m) a length of 2 km can be considered suitable.

Finally, in Figure 3.6 a comparison of the results obtained by using (3.14) and (3.15), and those obtained by using Rusck's formula [9], the latter adapted to a finite length line, is shown for a line of length 2 km, a height of 10 m, located at a distance d = 100 m from the lightning channel. As in the case of an infinite length line [8], no differences can be spotted on the graph: the maximum relative error was found to be 0.58%. Differences can be found for typical heights of transmission lines [8].

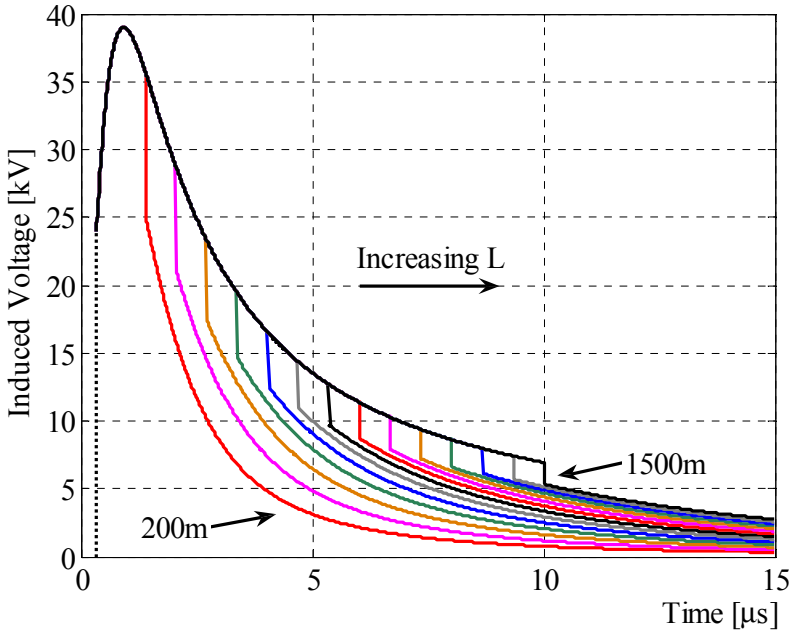

Figure 3.4 – Plot of the induced voltage at the center of a line whose length ($2L$) varies from 400 to 3000 m with a step of 200 m (h = 10 m, d = 100 m, I_0 = 10 kA, β = 0.4).

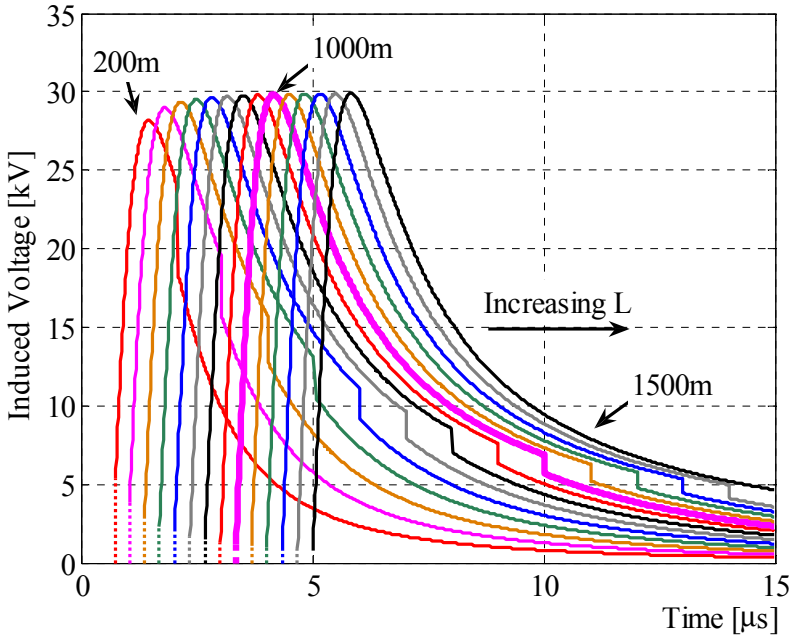

Figure 3.5 – Plot of the induced voltage at both ends of a line whose length ($2L$) varies from 400 to 3000 m with a step of 200 m (h = 10 m, d = 100 m, I_0 = 10 kA, β = 0.4).

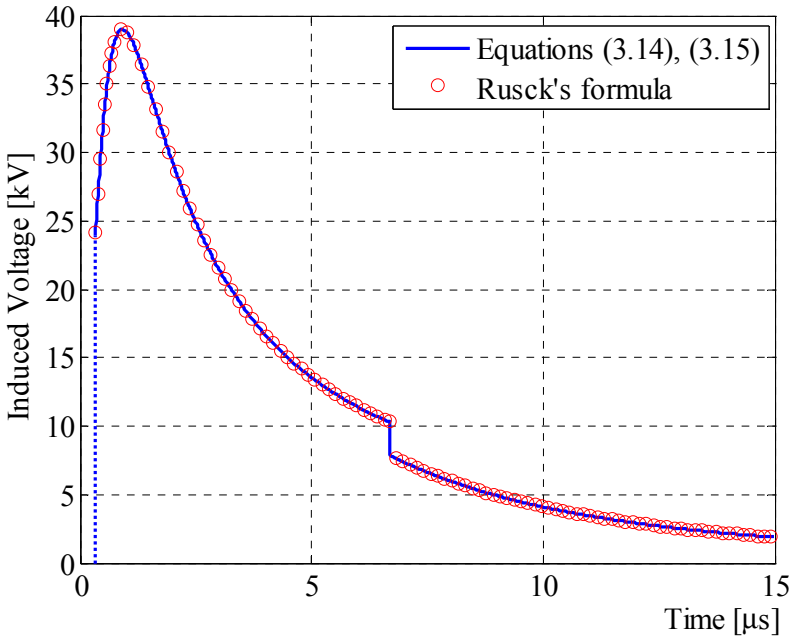

Figure 3.6 – Comparison between exact equations (3.14), (3.15) and Rusck's expression at the center of a 2-km length line (h = 10 m, d = 100 m, I_0 = 10 kA, β = 0.4).

3.2.1.3 Unmatched single-conductor line

In this case, we still make reference to Figure 3.3, but the two terminating impedances can be arbitrary. Under the assumption of a lossless line, it is possible to obtain an analytical solution for the transient response of this line excited by the lightning external field. In particular, the voltage at the left termination as viewed from the lightning channel reads [2]

$$\tilde{v}_L(-L,t) = (1+\rho_1)\cdot\sum_{n=0}^{\infty}(\rho_1\cdot\rho_2)^n\cdot\frac{1}{2} \cdot\left[\rho_2\cdot v^s\left(t-\frac{4(n+1)\cdot L - x_s}{c}\right) - v^s\left(t-\frac{4n\cdot L + x_s}{c}\right)\right], \tag{3.16}$$

where x_s is the x-coordinate of the source (in our case, the lightning channel is located at x_s = 0), ρ_1 and ρ_1 are the voltage reflection coefficients at the load of the line, given by

$$\rho_1 = \frac{Z_A - Z_C}{Z_A + Z_C}, \qquad \rho_2 = \frac{Z_B - Z_C}{Z_B + Z_C}. \tag{3.17}$$

Here, Z_A and Z_B are the termination impedances, whereas Z_C is the line characteristic impedance. The exciting source $v^s(t)$ is given by [2]

$$v^s(t) = \int_{-L}^{L} e_x(x,d,h,t)dx + \int_{0}^{h} e_z(-L,d,z,t)dz - \int_{0}^{h} e_z(L,d,z,t)dz\,. \tag{3.18}$$

In our case, one can verify that

$$v^s\left(t - \frac{4(n+1)\cdot L - x_s}{c}\right) = 2\cdot v_L\left(L, t - \frac{4(n+2)\cdot L}{c}\right), \tag{3.19}$$

and that

$$v^s\left(t - \frac{4n\cdot L + x_s}{c}\right) = -2\cdot v_L\left(-L, t - \frac{4n\cdot L}{c}\right). \tag{3.20}$$

The expression of $v_L(x,t)$ can be obtained by solving (3.7) as explained in the previous paragraph.

Hence, we can evaluate the voltage induced at the left termination as

$$\tilde{v}_L(-L,t) = (1+\rho_1)\cdot\sum_{n=0}^{\infty}(\rho_1\cdot\rho_2)^n \cdot\left[\rho_2\cdot v_L\left(L, t - \frac{4(n+2)\cdot L}{c}\right) + v_L\left(-L, t - \frac{4n\cdot L}{c}\right)\right]. \tag{3.21}$$

We set $n = 5$, which is sufficient to show all the waveshapes and reflections on the time scale chosen. In Figure 3.7 the induced voltage (at the left end) for a line which is terminated in two impedances smaller than the matching impedance is shown ($Z_A = Z_B = 0.1 \times Z_C$). In Figure 3.8, the induced voltage is shown for two impedances greater than the matching one ($Z_A = Z_B = 10 \times Z_C$). Finally, in Figure 3.9 the line is terminated in two impedances with one greater and the other smaller than the matching impedance ($Z_A = 0.1 \times Z_C$ and $Z_B = 10 \times Z_C$).

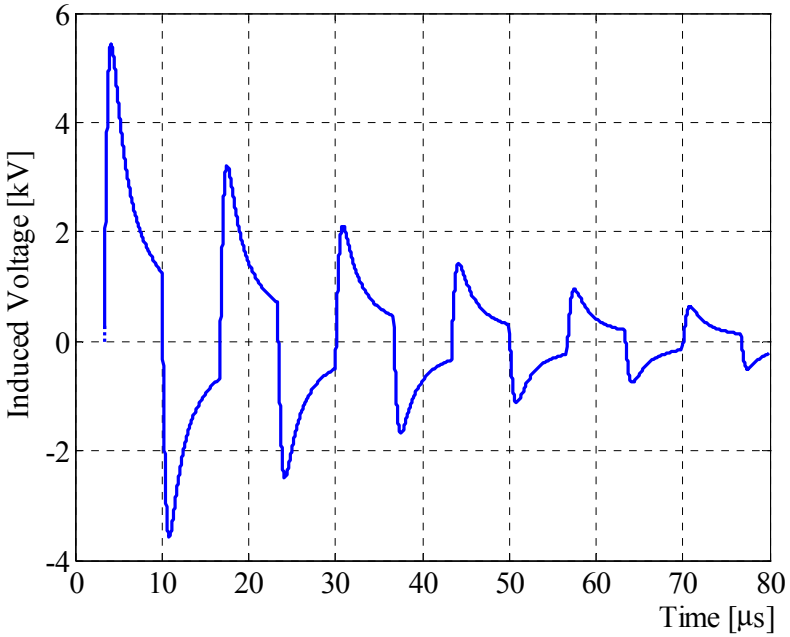

Figure 3.7 – Induced voltage at the left end of a 2-km line terminated in $Z_A = Z_B = 0.1 \times Z_C$ (h = 10 m, d = 100 m, I_0 = 10 kA, β = 0.4).

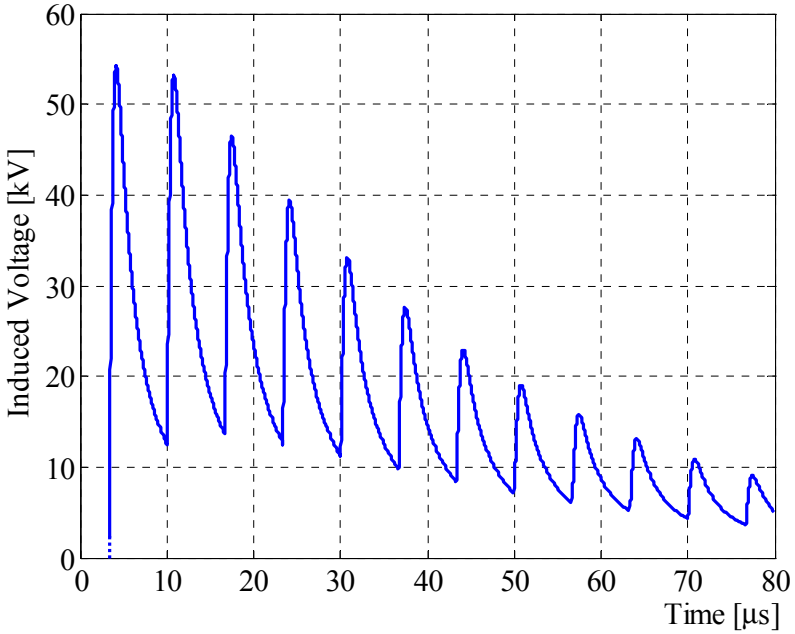

Figure 3.8 – Induced voltage at the left end of a 2-km line terminated in $Z_A = Z_B = 10 \times Z_C$ (h = 10 m, d = 100 m, I_0 = 10 kA, β = 0.4).

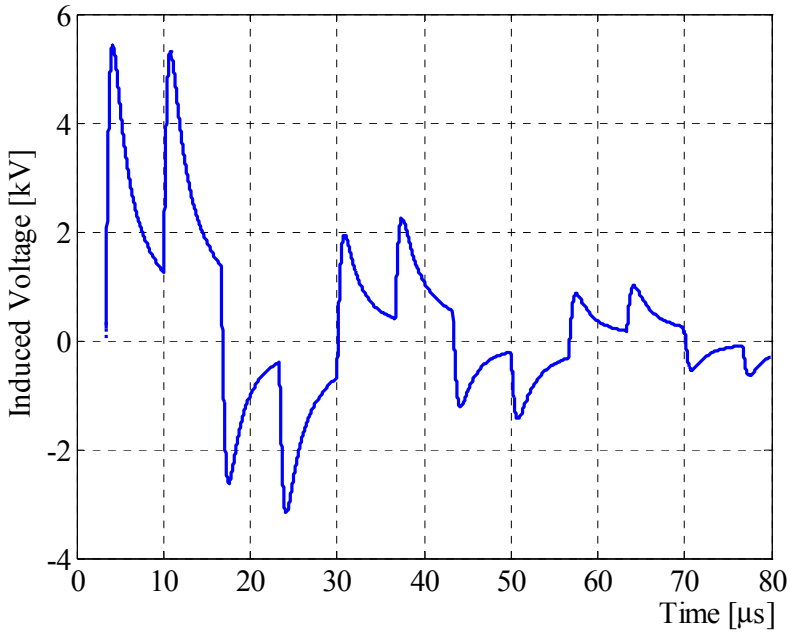

Figure 3.9 – Induced voltage at the left end of a 2-km line terminated in $Z_A = 0.1 \times Z_C$ and $Z_B = 10 \times Z_C$ ($h = 10$ m, $d = 100$ m, $I_0 = 10$ kA, $\beta = 0.4$).

3.2.1.4 Multi-conductor line

In this section, we will consider a lossless multi-conductor line. As an example, we will consider a three-phase line with an overhead ground wire, shown in case (a) of Figure 3.10.

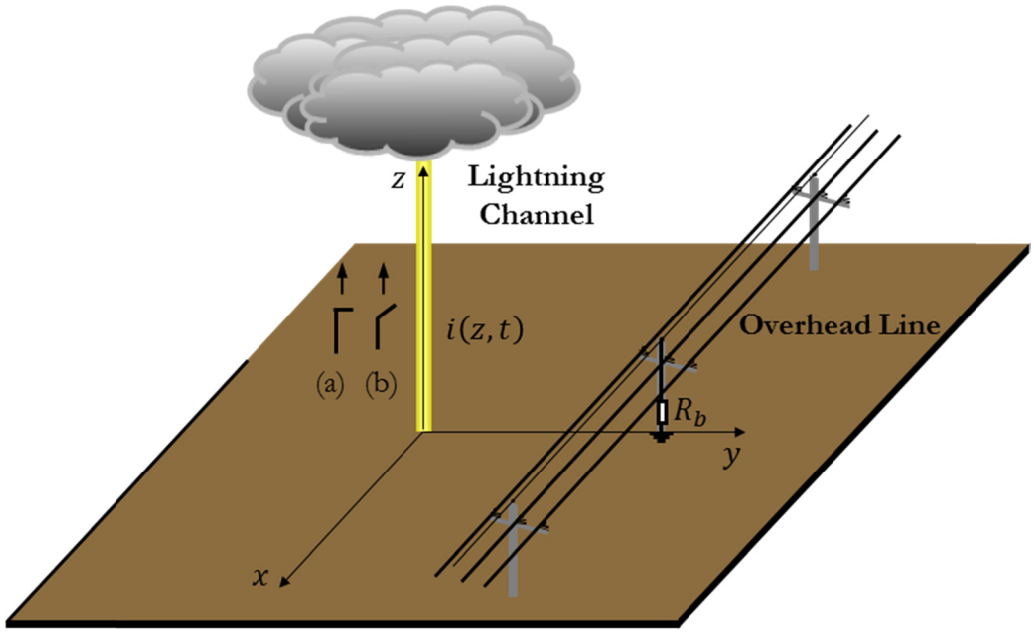

Figure 3.10 – Infinitely long, lossless, multi-conductor line: (a) step current, and (b) linearly rising current.

One of the general approaches to electromagnetic coupling to overhead line is the Taylor *et al.*'s model. Two different, but equivalent models are the Agrawal *et al.*'s model and the model proposed by Rachidi. All these models have been presented in Chapter 2 for a single-conductor line. According to Taylor *et al.*'s model, the coupling equations for a multi-conductor line, in the time domain, are

$$\begin{cases} \dfrac{\partial}{\partial x}[v(x,t)] + [l'] \cdot \dfrac{\partial}{\partial t}[i(x,t)] = \dfrac{\partial}{\partial t}\left[\displaystyle\int_0^h b_y(x,d,z,t)dz\right], \\ \dfrac{\partial}{\partial x}[i(x,t)] + [c'] \cdot \dfrac{\partial}{\partial t}[v(x,t)] = -[c'] \cdot \dfrac{\partial}{\partial t}\left[\displaystyle\int_0^h e_z(x,d,z,t)dz\right], \end{cases} \tag{3.22}$$

where

- $[v(x,t)]$ is the induced voltage vector;
- $[i(x,t)]$ is the induced current vector;
- $[l']$ and $[c']$ are, respectively, the inductance and the capacitance matrices per unit length of the line;
- $b_y(\cdot)$ is the y-component of the magnetic field.

Another different coupling model was proposed by Rusck [9]. It is equivalent to the three models referred to above when the lightning channel is vertical [38], which is the case in this work.

Rusck's model is described by the following coupling equations:

$$\begin{cases} \dfrac{\partial}{\partial x}\left[v^{\phi}(x,t)\right] + [l'] \cdot \dfrac{\partial}{\partial t}[i(x,t)] = 0, \\ \dfrac{\partial}{\partial x}[i(x,t)] + [c'] \cdot \dfrac{\partial}{\partial t}\left[v^{\phi}(x,t)\right] = [c'] \cdot \dfrac{\partial}{\partial t}\left[\phi^{i}(x,d,h,t)\right], \end{cases} \tag{3.23}$$

where $\left[\phi^{i}(\cdot)\right]$ is the vector of the inducing scalar potentials of the incident field. These expressions give $\left[v^{\phi}(\cdot)\right]$, the vector of the induced voltages due to the inducing scalar potentials of the incident field. To obtain the total induced voltage, the following expression can be used [9]:

$$[v(x,t)] = \left[v^{\phi}(x,t)\right] + \int_0^h \frac{\partial}{\partial t}\left[A_z^i(x,d,h,t)\right]dz, \tag{3.24}$$

where $\left[A_z^i(\cdot)\right]$ is the vector of the vertical components of the vector potentials of the incident field.

It is well known that, for an infinitely long line, the solution of the multi-conductor coupling equations (3.22) or (3.23) in terms of induced voltage on a given conductor is not affected by the presence of the other conductors [9], [39]. A coupling can occur at transition points, e.g., ground wire earthing (grounding) points, or at termination impedances [40]. In this case, the induced voltage on a given conductor is affected by the other conductors. An important case is that of the induced voltage on a phase wire, which is reduced by the presence of ground wire(s) [9], [39], [40].

For a power line equipped with ground wire(s), it is important to quantify this shielding effect. The effect can be quantified by the ratio between the voltage induced on the considered conductor (here denoted a), v_a', and the voltage that would be induced on the same conductor by removing the ground wire(s), v_a. In the following, we will focus on the case of a line equipped with a ground wire which is earthed at only one point, as the one shown in Figure 3.10. The extension to the case of multiple earthings (e.g., earthing at every pole), which is fundamental when evaluating the lightning performance of the line, requires a more complex treatment due to the reflections caused by the earthing points, as shown for the case of the unmatched single-conductor line, and will be developed in future studies. We also note that analytical models, as the one developed here, can be applied only to linear devices such as grounding connections; for nonlinear devices such as surge arresters, numerical approaches are to be used (e.g., [41] and [42]).

The ratio v_a'/v_a has been referred to as Shielding Factor (SF) [9], [40] or Protective Ratio (PR) [39], [43].

In the case of power lines equipped with a ground wire connected at only one grounding point, the general formulation for the induced voltage v_a' at the grounding connection is [44], [45]

$$v_a' = v_a - \frac{Z_{ba}}{Z_{bb} + 2R_b} \cdot v_b, \tag{3.25}$$

where

- $Z_{ba} = 1/2\pi\sqrt{\mu_0/\varepsilon_0} \cdot ln(d'_{ba}/d_{ba})$ is the mutual surge impedance of ground wire b and phase conductor a;
- $Z_{bb} = 1/2\pi\sqrt{\mu_0/\varepsilon_0} \cdot ln(2h_b/r_b)$ is the self-surge impedance of the overhead ground wire b;

- R_b is the ground resistance of the overhead ground wire;
- v_b is the voltage induced on the ground wire;
- d'_{ba} is the distance between the ground wire and the mirror image of conductor a;
- d_{ba} is the distance between the ground wire b and the conductor a;
- h_b is the height of the overhead ground wire;
- r_b is the radius of the ground wire, whose cross section is S_b.

Hence, the SF (PR) is given by

$$\frac{v'_a}{v_a} = 1 - \frac{Z_{ba}}{Z_{bb} + 2R_b} \cdot \frac{v_b}{v_a}. \tag{3.26}$$

In our case of exact formulation for the step current, the ratio v_b/v_a is the ratio between the expressions obtained by applying (3.3) to conductors a and b. In this case, the SF (PR) depends on the line geometry through Z_{ba} and Z_{bb}, on the grounding resistance R_b, and, through the ratio v_b/v_a, on the specific position of the earthing pole x_p, and it is also a function of time. Other authors, including Rusck [9], found instead that the ratio was simply a function of the line geometry and grounding resistance. We will use our exact approach to check Rusck's result [9]. Rusck, starting from the coupling model (3.23), (3.24), investigated the shielding effect and found that, for one ground wire earthed at only one pole, it is given by

$$\frac{v'_a}{v_a} = 1 - \frac{Z_{ba}}{Z_{bb} + 2R_b} \cdot \frac{h_b}{h_a}, \tag{3.27}$$

where h_a is the height of the phase conductor a.

In this case, the SF (PR) is a function only of the line geometry (i.e., the conductors' placement in the line section, as in the example shown in Figure 3.11 [46]), through Z_{ba}, Z_{bb}, h_a, h_b, and of the grounding resistance R_b. It does not depend on the position x_p of the grounding pole along the line nor is it a function of time. This approach greatly simplifies the problem, but it is necessary to check its validity.

For this purpose, we recall [8] that Rusck's formula was the first-order approximation of the exact solution proposed by Andreotti *et al.*, based on approximating the horizontal electric field by the first term of its series expansion around $z = 0$ and considering the vertical component to be constant between 0 and h (equal to the value obtained for $z = 0$), i.e.,

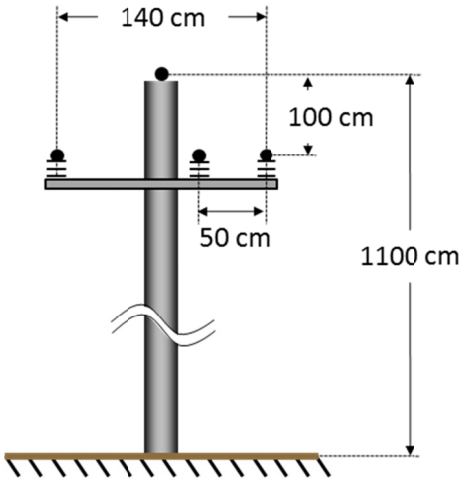

Figure 3.11 – Geometry of a three-phase distribution line with an overhead ground wire [46].

$$e_x(x,y,z,t) \cong \left.\frac{\partial e_x(x,y,z,t)}{\partial z}\right|_{z=0} \cdot z, \tag{3.28}$$

$$e_z(x,y,z,t) \cong e_z(x,y,0,t). \tag{3.29}$$

This approximation makes the ratio v_b/v_a, which in general is given by applying (3.3) to conductors a and b, to become simply h_b/h_a, as shown in (3.27). We now show that for typical distribution line geometries such the one shown in Figure 3.11, the simplifying hypothesis introduced by Rusck is fully acceptable, as illustrated by Figures 3.12 and 3.13, where the dependence of the shielding effect on time and x_p is shown for the typical distribution line geometry given in Figure 3.11, by assuming R_b = 0 Ω, and an overhead ground wire cross section, S_b, of 16 mm^2. The values used for all other parameters are reported in the figure captions. One can see that the variations are of no practical importance and the values are very close to the SF (PR) value of 0.63538 calculated by means of (3.27).

For completeness, in order to show how the SF (PR) depends on the position of the ground wire, we apply (3.27) to the distribution line of Figure 3.11 by moving the ground wire to different positions. Considering a perfectly grounded shielding wire, the loci shown in Figure 3.14 are obtained. One can see that some shielding effects can be obtained even via ground wires belonging to different power lines; for example, a power line, parallel to and 7.5 m away from the considered one, and equipped with a ground wire located at a height of 14 m above the ground, produces a SF between 0.80 and 0.85. In Figure 3.15, we show, also for the typical distribution-line geometry of Figure 3.11, the SF (PR) as a

function of height of the ground wire, considering its possible locations both above and below the phase conductors. The evaluation is carried out both for the inner phase conductor (the conductor closest to the ground wire) and for the outer ones for the case of zero-resistance grounding. In Figure 3.16, the effect of the earthing resistance for the inner phase conductor is shown. The plots refer to different values of grounding resistance, varying from 0 Ω (perfect grounding) to 200 Ω, with a 20 Ω step.

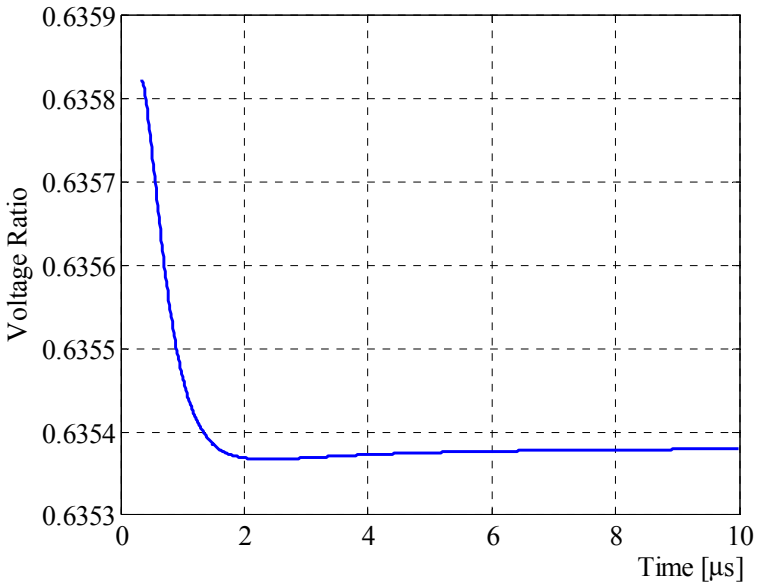

Figure 3.12 – Voltage ratio for the central phase conductor with x_p = 0 m, h_a= 10 m, h_b= 11 m, S_b= 16 mm^2, R_b = 0 Ω, d = 100 m, I_0 = 10 kA, β = 0.4.

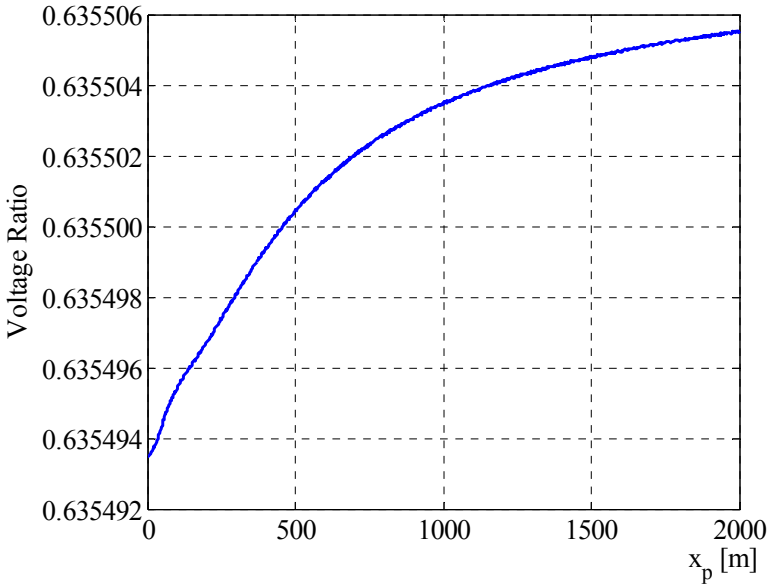

Figure 3.13 – Voltage ratio (peak values) for the central phase conductor with x_p varying from 0 to 2 km, h_a= 10 m, h_b= 11 m, S_b= 16 mm^2, R_b = 0 Ω, d = 100 m, I_0 = 10 kA, β = 0.4.

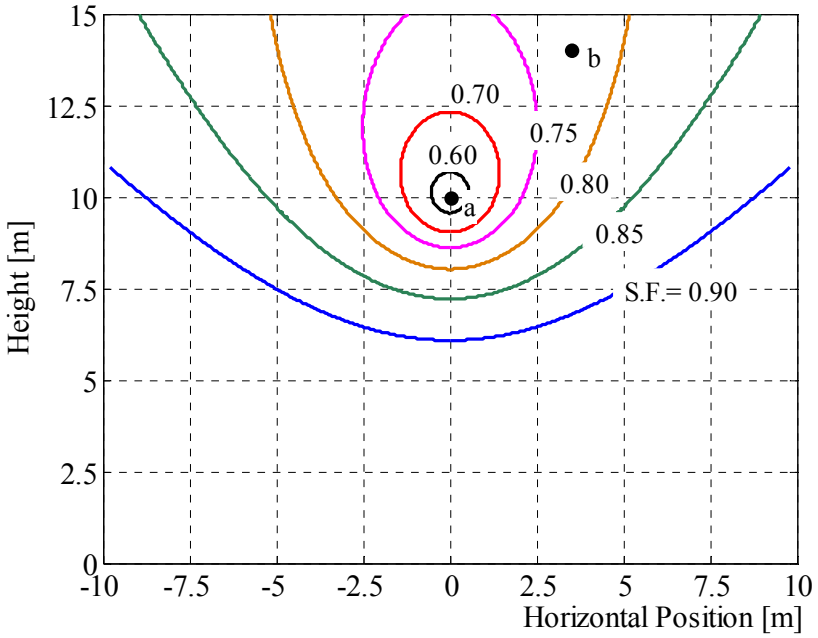

Figure 3.14 – Loci of the SF relevant to conductor a, in fixed position and isolated from the ground, for various locations of a perfectly grounded shielding wire, b.

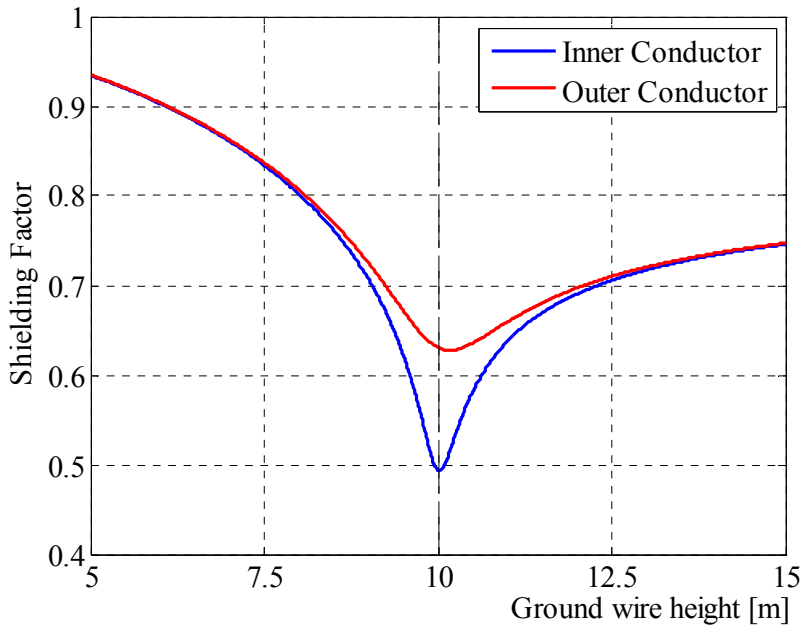

Figure 3.15 – Plot of the SF versus ground wire height for the line geometry shown in Figure 3.11 in the case of perfect (zero-resistance) grounding. Due to symmetry, the SF is the same for both outer conductors.

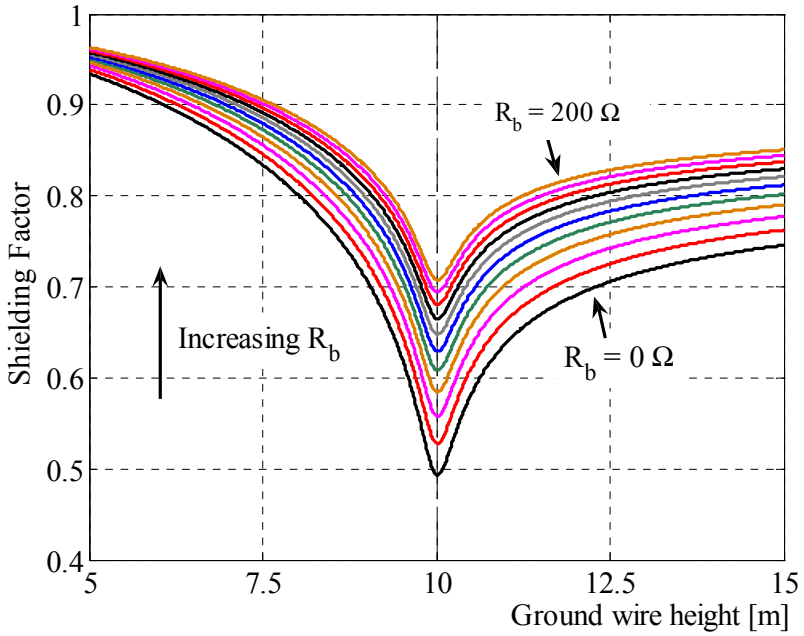

Figure 3.16 – Plot of the SF for the inner conductor of Figure 3.11 versus ground wire height and various grounding resistance (R_b) values.

3.2.2 Linearly rising channel-base current

3.2.2.1 Infinitely long, single-conductor line

A linearly rising current wave propagating along the channel is more consistent with the actual rising behavior of the lightning current. Figure 3.17 shows a linearly rising current approximating a typical recorded channel-base current [47].

Here, we will start from the exact solution for the induced voltage due to a lightning step current, in order to derive the exact solution for the case of a linearly rising current by means of Duhamel's integral, which allows one to obtain the response of a system, $y(t)$, to an arbitrary time-varying excitation, $f(t)$, using the unit step response of the system, $s(t)$:

$$y(t) = \int_0^t s(\tau)\, f'(t-\tau) d\tau. \tag{3.30}$$

We will consider both constant-level (i.e., a current with "tail time" $t_t = \infty$) and drooping current tails (see Figure 3.18), following the linearly rising front.

We will first calculate the induced voltage at the point closest to the lightning channel and then the induced voltage for an arbitrary value of x along the line.

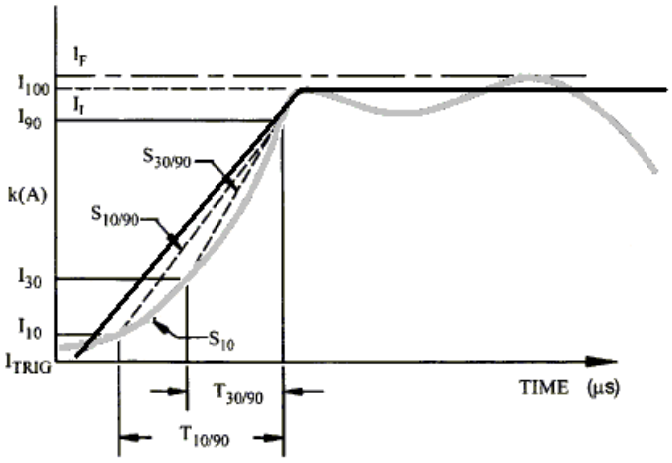

Figure 3.17 – Linearly rising lightning current with constant tail superimposed on a typical recorded lightning channel-base current (adapted from [47]).

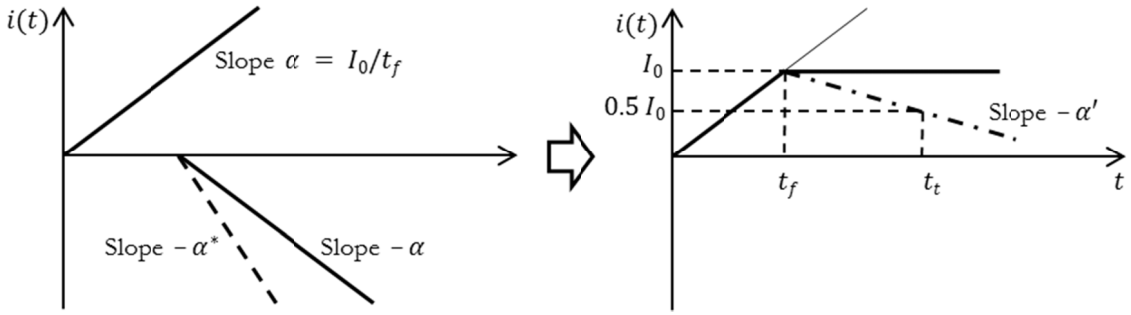

Figure 3.18 – Linearly rising current waveshapes with constant-level and drooping tails.

In the case of a step current, the exact solution for the point closest to the lightning channel is given by (3.14). Let us consider the convolution integral (3.30) when the input $f(t)$ is a ramp of constant slope $\alpha = I_0/t_f$

$$f(t) = \alpha \cdot t \cdot u(t), \tag{3.31}$$

where the "front time" t_f is assumed here to be the time needed for the current to rise from 0 to its peak value I_0, and where the unit-step response $s(t)$ is the one given by expression (3.14). Using (3.14) and (3.31) in (3.30), we obtain

$$v_r(0,t) = v_{r1}(0,t) - v_{r2}(0,t), \tag{3.32a}$$

where

$$v_{r1}(0,t) = -\frac{\mu_0}{4\pi}\alpha \cdot \int_{\lambda_1}^{\lambda} \left[ln\left(\vartheta + \sqrt{\vartheta^2 + \delta_0^2}\right) + \frac{1}{\beta} \cdot ln\left(-\beta\vartheta + \sqrt{\vartheta^2 + \delta_0^2}\right)\right] d\vartheta, \quad (3.32b)$$

and

$$v_{r2}(0,t) = -\frac{\mu_0}{4\pi}\alpha \cdot \int_{\lambda_1'}^{\lambda'} \left[ln\left(\vartheta + \sqrt{\vartheta^2 + \delta_0^2}\right) + \frac{1}{\beta} \cdot ln\left(-\beta\vartheta + \sqrt{\vartheta^2 + \delta_0^2}\right)\right] d\vartheta, \quad (3.32c)$$

with $\lambda_1 = \beta \cdot \mathrm{c} \cdot t_2 - h$ and $\lambda_1' = \beta \cdot \mathrm{c} \cdot t_2 + h$. The subscript r has been added to refer to a linearly rising current.

Solutions of the integrals (3.32b) and (3.32c) are given in the Appendix. By using (A.1) and (A.2), we obtain

$$v_{r1}(0,t) = v_{r1}'(0,t) - v_{r1}''(0,t), \quad (3.32d)$$

with $v_{r1}'(0,t)$ given by

$$v_{r1}'(0,t) = -\frac{\mu_0}{4\pi}\alpha \cdot \left\{ \lambda \cdot \left\{ ln\left(\lambda + \sqrt{\lambda^2 + \delta_0^2}\right) + \frac{1}{\beta} \cdot \left[ln\left(-\beta\lambda + \sqrt{\lambda^2 + \delta_0^2}\right) - 1\right]\right\} + \frac{d}{\beta} \cdot \left[arctan\left(\frac{\lambda}{d}\right) - arctan\left(\frac{\beta \cdot d}{\sqrt{\lambda^2 + \delta_0^2}}\right)\right] - \sqrt{\lambda^2 + \delta_0^2}\right\} \cdot u(t - t_2), \quad (3.32e)$$

and $v_{r1}''(0,t)$ obtained replacing λ with λ_1 in $v_{r1}'(0,t)$.

Analogously, for $v_{r2}(0,t)$, we obtain

$$v_{r2}(0,t) = v_{r2}'(0,t) - v_{r2}''(0,t), \quad (3.32f)$$

where $v_{r2}'(0,t)$ and $v_{r2}''(0,t)$ can be obtained by reversing the sign of h in $v_{r1}'(0,t)$ and $v_{r1}''(0,t)$, respectively.

Expression (3.32) is the exact solution for the linearly rising part of the lightning current.

A second contribution must be added to obtain the overall current waveshape, which corresponds to its tail part (constant-level or drooping tail). As shown in Figure 3.18, in the case of constant-level tail, the second contribution is a time-delayed ramp with a negative slope whose magnitude is equal to that of the positive slope; for a drooping tail of negative slope $-\alpha' = -I_0/(2 \cdot t_h)$, where $t_h = t_t - t_f$ is the time needed for current to fall from the peak value to the half peak value, the second contribution is a time delayed ramp of fictitious negative slope which is equal to

$$-\alpha^* = -\alpha - \alpha' = -\frac{I_0 \cdot (t_f + 2 \cdot t_h)}{2 \cdot t_f \cdot t_h}. \tag{3.33}$$

This expression can be easily derived by examining Figure 3.18. We note that, when $t_t = \infty$, $\alpha^* = \alpha$.

In the case of constant-level tail, the second contribution, denoted by $v_r'(0,t)$, can be written as

$$v_r'(0,t) = -[v_{r1}(0, t - t_f) - v_{r2}(0, t - t_f)]. \tag{3.34}$$

For the drooping tail, $v_r'(0,t)$ is computed as

$$v_r'(0,t) = -[v_{r1}^*(0, t - t_f) - v_{r2}^*(0, t - t_f)], \tag{3.35}$$

where $v_{r1}^*(0, t - t_f)$ and $v_{r2}^*(0, t - t_f)$ are obtained, respectively, by replacing the slope α in $v_{r1}(0, t - t_f)$ and $v_{r2}(0, t - t_f)$ with α^*.

In Figure 3.19(a), we show induced voltages computed for a linearly rising current with constant-level tail for different front times. We start with a very fast front time of 1 ns (not applicable to lightning, but shown for comparison with the step current case dealt with in the previous section) and then vary t_f from 0.1 to 1 μs, with a 0.1-μs step. In Figure 3.19(b), we show the results obtained for a linearly rising current with front times that range from 1 μs, which is typical for subsequent strokes, to 10 μs, which is typical for first strokes, with a step of 1 μs. One can see that a subsequent stroke, all other parameters being the same, can produce an induced voltage which is about 200% higher than the first-stroke one.

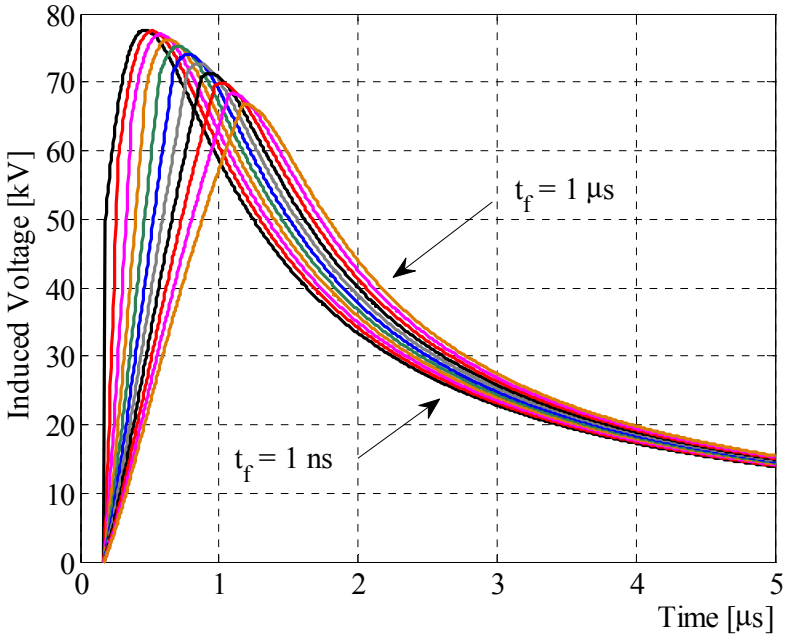

(a)

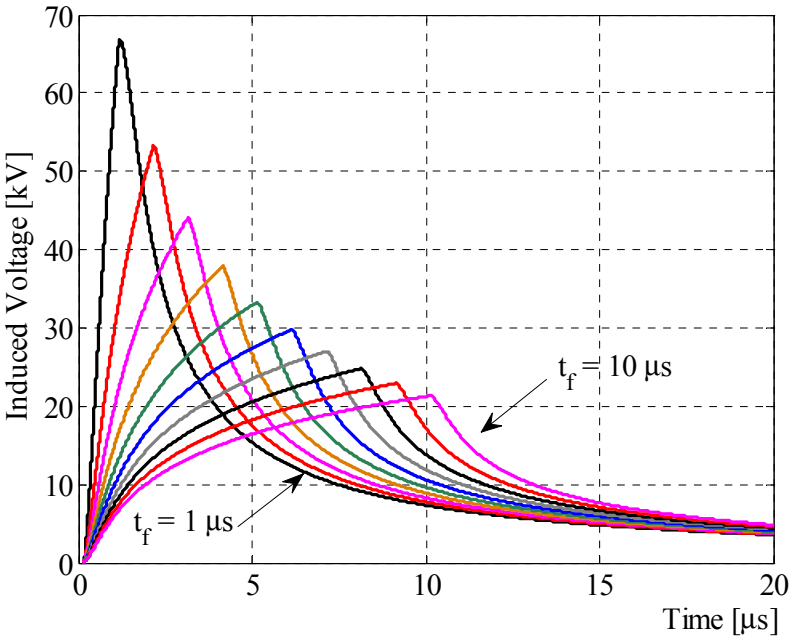

(b)

Figure 3.19 – Induced voltages obtained for different t_f at $x = 0$ (midpoint position of the line) with $h = 10$ m, $d = 50$ m, $I_0 = 10$ kA, $\beta = 0.4$.

We now consider the evaluation of the induced voltage at an arbitrary value of x along the line. We will separate vertical and horizontal-field contributions, and we will derive exactly only the first one. For the horizontal contribution, we will give an approximate expression.

Let us consider first the induced voltage contribution due to the vertical electric field component. In this case, the unit step response $s(t)$ in the convolution integral (3.30) is given by expression (3.4). The exact analytical solution, obtained using expression (A.1), in which δ_0 is replaced with δ, reads

$$v_r^z(x,t) = v_{r0}^z(x,t) + v_{r1}^z(x,t) - v_{r2}^z(x,t), \tag{3.36a}$$

where

$$v_{r0}^z(x,t) = \frac{\mu_0}{2\pi \cdot \beta}\alpha \cdot (c \cdot t - r_0) \cdot ln\left(\frac{h + r_0}{r}\right) \cdot u(t - t_0), \tag{3.36b}$$

and

$$v_{r1}^z(x,t) = \frac{\mu_0}{4\pi \cdot \beta^2 \cdot \gamma^2}\alpha \cdot \left[\lambda \cdot ln\left(\lambda + \sqrt{\lambda^2 + \delta^2}\right) - \lambda_0 \cdot ln\left(\lambda_0 + \sqrt{\lambda_0^2 + \delta^2}\right) - \sqrt{\lambda^2 + \delta^2} + \sqrt{\lambda_0^2 + \delta^2}\right] \cdot u(t - t_0), \tag{3.36c}$$

with $\lambda_0 = \beta \cdot \mathrm{c} \cdot t_0 - h$. The expression for $v_{r2}^z(x,t)$ is obtained from $v_{r1}^z(x,t)$ by reversing the sign of h.

As to the horizontal contribution, due to the complexity of the integrand in (3.5), we were not able to obtain a sufficiently compact expression. For this reason, an approximate solution will be presented here.

It is worth noting that an approximate solution for the evaluation of the induced voltage due to a linearly rising current has been obtained by Sekioka [23]. This solution was obtained by means of a convolution of the scalar and vector potentials calculated by Rusck [9] for the step current. Since Rusck's solution is the first-order approximation of the exact one, for the convolution product linearity, the Sekioka's solution can be considered as the first-order approximation of the exact one as well.

We here note that the advantage of the Rusck's coupling model compared to the one of Taylor *et al.* is that the evaluation is based on the scalar and vector potentials rather than on the electric field. This results in an easier evaluation of induced voltages, although the separation between horizontal and vertical contributions, as we have done previously, is not possible. For this reason, Sekioka gives the overall voltage expression, with no separation between vertical and horizontal contributions.

Based on the above, the "first-order" horizontal contribution can be obtained by subtracting from the "first-order" voltage obtained by Sekioka, the "first-order" vertical contribution, i.e.,

$$v_r^x(x,t) = v_{r,S}(x,t) - v_{r,R}^z(x,t), \tag{3.37}$$

where $v_{r,S}(x,t)$ is the solution obtained by Sekioka [23]:

$$v_{r,S}(x,t) = \frac{\mu_0 \cdot h}{4\pi \cdot \beta}\alpha \cdot \left\{ ln\left[1 + \left(\frac{\beta}{d} \cdot \frac{c^2 \cdot t^2 - r^2}{c \cdot t + \xi}\right)^2\right] + 2\beta \cdot ln\left[\frac{\beta \cdot c \cdot t + \xi}{r \cdot (1+\beta)}\right]\right\} \cdot u(t - \tilde{t}_0), \tag{3.38}$$

with $\xi = \sqrt{(\beta \cdot c \cdot t)^2 + \delta^2}$, $\tilde{t}_0 = r/c$, and where $v_{r,R}^z(x,t)$ is the "first-order" vertical contribution, obtained by convolving, according to (3.30), the following step response expression obtained by Rusck [9]:

$$v_{s,R}^z(x,t) = -\int_0^h e_z(x,d,z,t) \cdot u(t - t_0)dz \cong \frac{\zeta_0 \cdot I_0}{2\pi \cdot \beta} \cdot h \cdot \left(\frac{1}{r} - \frac{1-\beta^2}{\xi}\right) \cdot u(t - \tilde{t}_0). \tag{3.39}$$

We, therefore, obtain

$$v_{r,R}^z(x,t) = \frac{\mu_0 \cdot h}{2\pi \cdot r \cdot \beta^2}\alpha \cdot \left[\beta \cdot (c \cdot t - r_0) - \frac{\delta}{\gamma} \cdot ln\left(\frac{\beta \cdot c \cdot t + \xi}{\beta \cdot r_0 + \xi_0}\right)\right] \cdot u(t - \tilde{t}_0), \tag{3.40}$$

where $\xi_0 = \sqrt{(\beta \cdot c \cdot t_0)^2 + \delta^2}$.

Substituting (3.38) and (3.40) in (3.37), and making the appropriate simplifications, we obtain the following expression for the horizontal contribution:

$$v_r^x(x,t) = \frac{\mu_0 \cdot h}{4\pi \cdot \beta}\alpha \cdot \left\{ ln\left[1 + \left(\frac{\beta}{d} \cdot \frac{c^2 \cdot t^2 - r^2}{c \cdot t + \xi}\right)^2\right] + \frac{2}{\beta} \cdot ln\left(\frac{\beta \cdot c \cdot t + \xi}{\beta \cdot r_0 + \xi_0}\right) \right.$$
$$\left. + 2\beta \cdot ln\left[\frac{\beta \cdot r_0 + \sqrt{r^2 + \beta^2 \cdot h^2}}{r \cdot (1+\beta)}\right] - 2 \cdot \left(\frac{c \cdot t - r_0}{r}\right)\right\} \cdot u(t - \tilde{t}_0). \tag{3.41}$$

By adding expressions for the vertical contribution (3.36) and horizontal contribution (3.41), we finally obtain an approximate formula for the evaluation of the total induced voltage at an arbitrary position along the line:

$$v_r(x,t) = v_r^z(x,t) + v_r^x(x,t). \tag{3.42}$$

Note that this expression corresponds only to the linearly rising part of the lightning current. The contribution from the current tail that must be added to account for the overall current waveform can be obtained as described above for the closest point case.

The 3-D plot of the induced voltages computed using (3.42) for the case of linearly rising front and constant-level tail is shown in Figure 3.20.

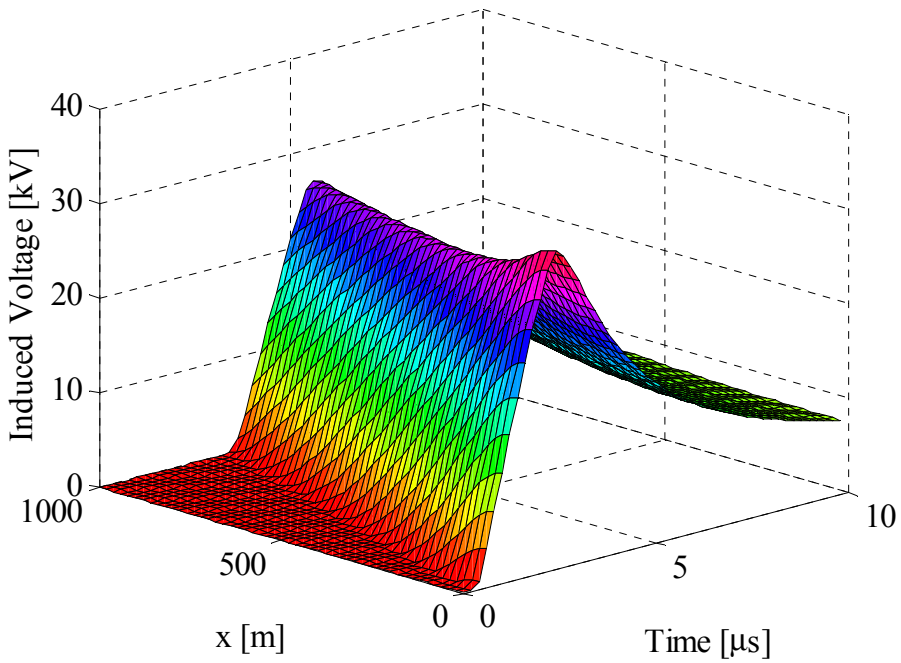

Figure 3.20 – 3-D plot of induced voltages obtained for h = 10 m, d = 100 m, I_0 = 10 kA, β = 0.4, and return-stroke current waveform characterized by t_f = 2 μs, t_t =∞.

3.2.2.2 Multi-conductor line

In this case we make reference to case (b) of Figure 3.10. We recall that for a power line equipped with a ground wire connected at only one grounding point, the SF (PR) is given by (3.26). In our case of exact formulation for the linearly rising current, the ratio v_b/v_a is the ratio between the expressions obtained by applying (3.32) to conductors a and b for the rising part and (3.34) or (3.35) for the constant or drooping tail, respectively. In this case, the SF (PR) depends on the line geometry through Z_{ba} and Z_{bb}, on the grounding

resistance R_b, and, through the ratio, it is also a function of time (due to the linearity of the convolution operator, we expect that it depends on the position of x_p, but we are not able to analyze this dependence since the exact solution was calculated only for $x_p = 0$). In the case of Sekioka's solution, the ratio v_b/v_a is obtained by applying (3.38) to conductors a and b, and this leads to an expression which is the same as the Rusck's one (3.27). As for the step current case, this approach greatly simplifies the problem, but we have to check its validity. In Figure 3.21, we show the time dependence of the ratio v'_a/v_a calculated applying (3.32) and (3.35) to conductors a and b for the typical distribution line geometry given in Figure 3.11. Here, we found that the approximation given by (3.27) which yields a value of 0.63538 is not accurate only in the very early period of time, where, however, the induced voltages are still very low without any isolation problem. The voltage peak is formed after 0.75 μs, when the SF is well established at its asymptotic value.

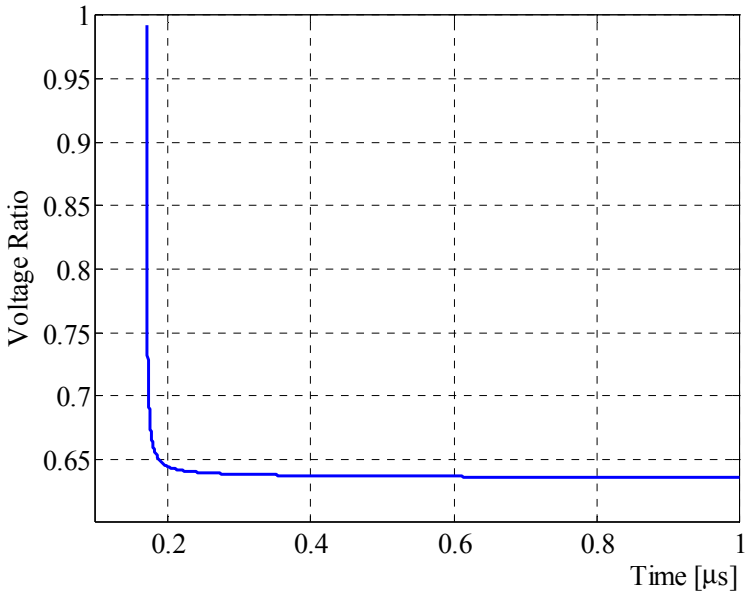

Figure 3.21 – Voltage ratio for the central phase conductor of Figure 3.11 (h_a= 10 m, h_b= 11 m, S_b= 16 mm^2, R_b = 0 Ω, d = 50 m, I_0 = 12 kA, β = 0.43, and return-stroke current waveform characterized by t_f = 0.5 μs, t_t = 20 μs).

We will now use the exact solution for a linearly rising current in the case of a multi-conductor line with a grounded conductor as a test bench for two numerical approaches; in particular, we have compared the results obtained by using formulas (3.32) and (3.35) combined with (3.27) with those obtained by Yokoyama [40] and by Paolone *et al.* [41] using numerical approaches for the same line configuration and return stroke current. In Figure 3.22(a), we show induced voltages on the inner phase conductor of a line like the

one shown in Figure 3.11 for different values of grounding resistance, to be compared which similar results from [40] and [41] (note that the model used in [41] is implemented in the LIOV-EMTP code [37]) shown in Figure 3.22(b) and (c), respectively. Parameters used for the comparison are the same as in [40] and [41] (that is: h_a= 10 m, h_b= 10.5 m, S_b= 50.3 mm^2, d = 100 m, I_0 = 100 kA, β = 0.1, t_f = 2 μs, t_t = 40 μs).To better display the comparison, in Figure 3.23, we have superimposed the induced voltages obtained by using the three different approaches for the case of an infinite grounding resistance. The numerical model proposed in [40] is seen to be very accurate; a good accuracy is also found for the model used in [41].

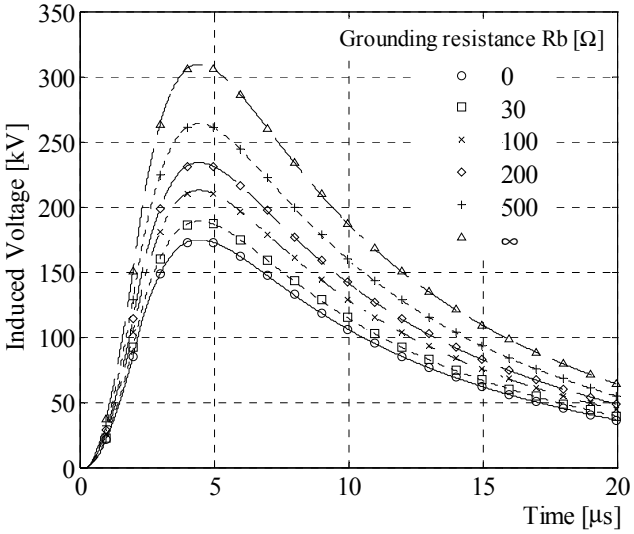

(a)

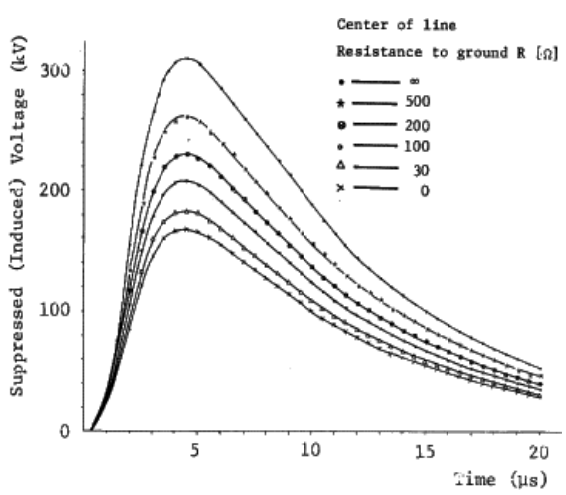

(b)

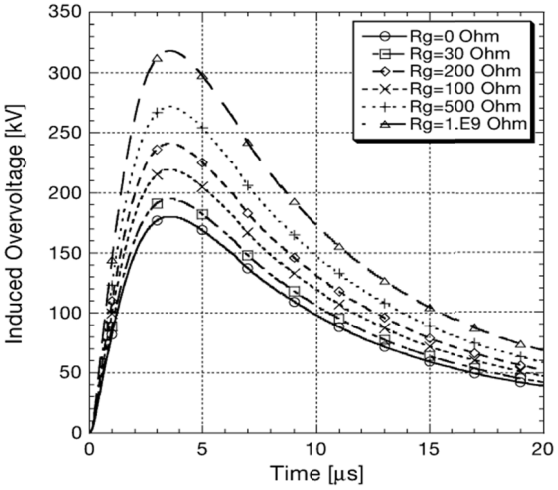

(c)

Figure 3.22 – Induced voltages on the inner phase conductor at the point closest to the lightning channel, for different values of grounding resistance: (a) computed using (3.32), (3.35) and (3.27), (b) adapted from [40], (c) adapted from [41]. Parameters used are the same as in [40] and [41].

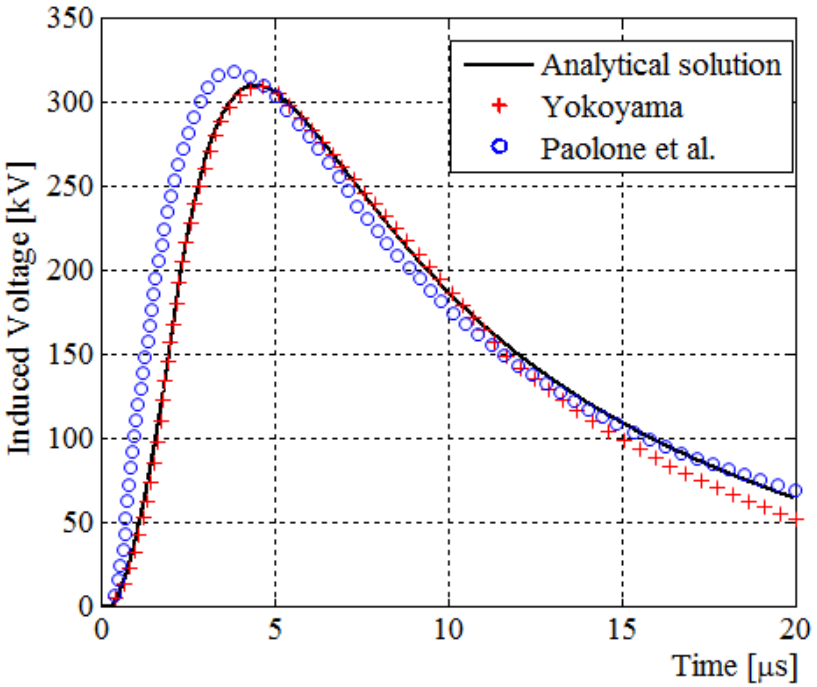

Figure 3.23 – Induced voltages on the inner phase conductor at the point closest to the lightning channel for $R_b = \infty$: comparison of calculations made by using (3.32), (3.35) and (3.27) with results from Yokoyama [40] and Paolone *et al.* [41]. Parameters used are the same as in [40] and [41].

3.2.2.3 Comparison with other models

As pointed out in the introduction, approximate analytical solutions for the evaluation of the lightning induced voltage on a lossless, infinitely long, single conductor located over an infinite-conductivity ground plane and excited by an external field due to a linearly rising current (followed by a constant or drooping tail) which move along a vertical lightning channel according to the TL model, that is the configuration depicted in case (b) of Figure 3.1, have been proposed by Chowdhuri-Gross [18], [19], Liew-Mar [20], Høidalen [10], and Sekioka [23].

In this paragraph, predictions of the exact analytical solution presented above for the evaluation of the voltages induced at the point of the line closest to the lightning channel will be compared to those obtained by using the approximate solutions found in the literature.

For the comparison purposes, we will assume a channel-base current with a peak value I_0 = 12 kA, a front time t_f = 0.5 μs, and a drooping tail with t_t = 20 μs. This specific channel base current was selected since it represents the best fit of a typical measured channel base current [10].

- *Chowdhuri-Gross's formula*

The solution proposed by Chowdhuri and Gross [18], [19], for a linearly current of constant slope $\alpha = I_0/t_f$, was obtained starting by a coupling model developed by the authors themselves and known as the "Chowdhuri-Gross model" (e.g., [38]). The original Chowdhuri-Gross's formula was first published in [18]. Afterwards, in [19], Chowdhuri modified it on the basis of the suggestions given by Cornfield [48], who found a mistake in the original expression. The final expression, for $x = 0$, reads:

$$v_{CG}(0,t) = \frac{\mu_0 \cdot h}{4\pi \cdot \beta}\alpha \cdot \left\{\frac{1}{\gamma^2}\cdot\left[ln\left(\frac{\gamma^4}{d^2}\cdot\left[\frac{d^2}{\gamma^2}+\beta^2\cdot c^2\cdot t^2\cdot(1+\beta^2)-2\beta^2\cdot c\cdot t\cdot\xi_1\right]\right)\right.\right.$$
$$\left.\left.-2ln\left(\frac{c\cdot t}{d}\right)\right]+ln\left(\frac{f_1\cdot f_3}{f_2\cdot f_4}\right)\right\}\cdot u(t-\tilde{t}_2), \tag{3.43}$$

where

- $f_1 = m + c^2\cdot t^2 - d^2$, $f_2 = m - c^2\cdot t^2 + d^2$;
- $f_3 = m_0 - c^2\cdot \tilde{t}_2^2 + d^2$, $f_4 = m_0 + c^2\cdot \tilde{t}_2^2 - d^2$;
- $m = \sqrt{(c^2\cdot t^2 + d^2)^2 + 4h_c^2\cdot c^2\cdot t^2}$;
- $m_0 = \sqrt{(c^2\cdot \tilde{t}_2^2 + d^2)^2 + 4h_c^2\cdot c^2\cdot \tilde{t}_2^2}$;
- h_c is the length of the lightning channel;
- $\xi_1 = \sqrt{(\beta\cdot c\cdot t)^2 + \delta_0^2}$;
- $\tilde{t}_2 = d/c$.

Expression (3.43) is the solution for the linearly rising part of the lightning current. A second contribution must be added to obtain the overall current waveshape, which corresponds to its tail (constant-level or drooping tail). This contribution can be obtained as described above for the exact analytical solution.

Now, we will compare the induced voltage waveform obtained by using the Chowdhuri-Gross's formula (3.43) with the one obtained by using the exact solution (3.32). In Figure 3.24(a), the comparison is shown for a 10 meters height line located at distance d = 50 m from the lightning channel; results have been obtained for I_0 = 12 kA, β = 0.4, t_f = 0.5 μs, and t_t = 20 μs. The same comparison, but with d increased to 100 meters, is shown in Figure 3.24(b). We point out that, since the Chowdhuri-Gross's formula refers to a finite lightning channel length, for comparison purposes we have considered, for both graphs, $h_c \to \infty$ in (3.43). Moreover, for the sake of completeness, we have also checked the finite

length channel case, assuming h_c = 3 km (see Figures 3.25(a) and (b)). The comparison clearly shows that the Chowdhuri-Gross's formula, as for the step current case analyzed in [8], cannot be considered correct. In fact, in all considered cases, it predicts significantly higher peak value and steeper front, and a too rapid decay of the current tail.

Furthermore, we notice a polarity inversion, particularly accentuated when h_c is finite, which cannot be justified for the voltage induced by a linearly rising current waveform in case of lossless ground.

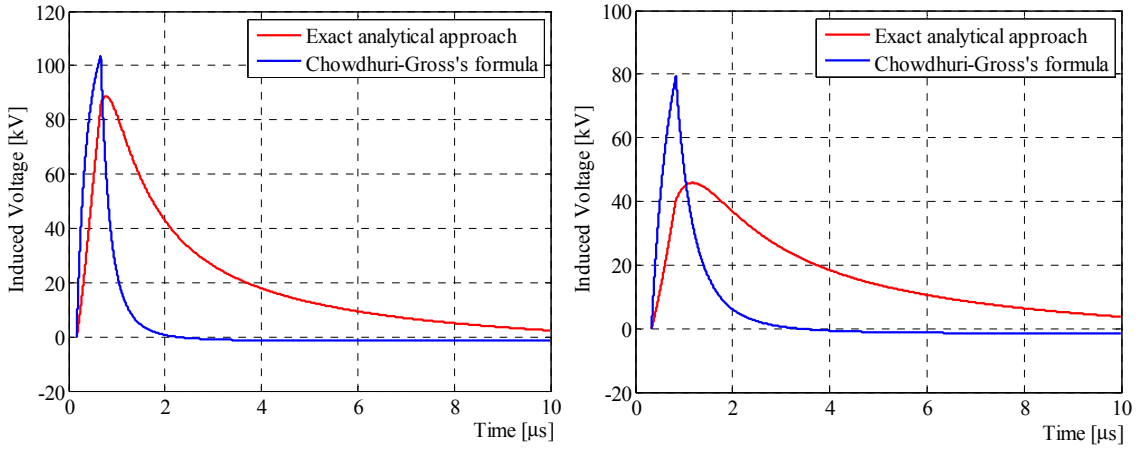

Figure 3.24 – Comparison between the induced voltage evaluated at x = 0 by means of Chowdhuri-Gross's formula and the proposed exact analytical approach (h = 10 m, I_0 = 12 kA, β = 0.4, t_f = 0.5 μs, t_t = 20 μs, h_c = ∞): (a) d = 50 m, (b) d = 100 m.

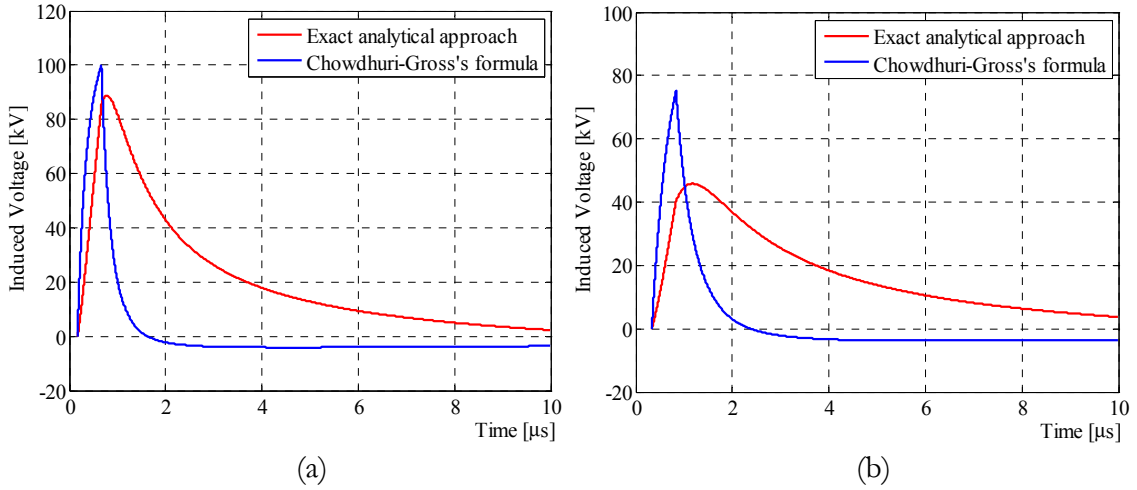

Figure 3.25 – Comparison between the induced voltage evaluated at x = 0 by means of Chowdhuri-Gross's formula and the proposed exact analytical approach (h = 10 m, I_0 = 12 kA, β = 0.4, t_f = 0.5 μs, t_t = 20 μs, h_c = 3 km): (a) d = 50 m, (b) d = 100 m.

- *Liew-Mar's formula*

The closed form solution proposed by Liew and Mar was first published in [20] and then revised by Liew and Haldar in the discussion of [19], since the original formula contained several typographical errors. It has been obtained starting from the Chowdhuri-Gross coupling model, as discussed in [8]. The final expression, specified for $x = 0$, reads

$$v_{LM}(0,t) = \frac{\mu_0 \cdot h}{4\pi \cdot \beta}\alpha \cdot \left\{\left[ln\left(\frac{\gamma^4}{d^2}\cdot\left[\frac{d^2}{\gamma^2} + \beta^2 \cdot c^2 \cdot t^2 \cdot (1+\beta^2) - 2\beta^2 \cdot c \cdot t \cdot \xi_1\right]\right)\right.\right.$$
$$\left. -2ln\left(\frac{c \cdot t}{d}\right)\right] - \left[arccosh\left(\frac{a+p}{s}\right) - arccosh\left(\frac{a_0+p}{s}\right)\right.$$
$$\left. - arccosh\left(\frac{b+p/q^2}{w}\right) + arccosh\left(\frac{b_0+p/q^2}{w}\right)\right] + 2\beta$$
$$\left. \cdot arcsinh\left(\frac{\beta \cdot \gamma \cdot c \cdot t}{d}\right) - arcsinh\left(\frac{\beta \cdot \gamma \cdot c \cdot \tilde{t}_2}{d}\right)\right\} \cdot u(t - \tilde{t}_2), \qquad (3.44)$$

where

- $a = (c \cdot t)^{-2}$;
- $a_0 = (c \cdot \tilde{t}_2)^{-2}$;
- $b = (c \cdot t)^2$;
- $b_0 = (c \cdot \tilde{t}_2)^2$;
- $p = (d^2 + 2h_c^2)/d^4$;
- $q = 1/d^2$;
- $s = \sqrt{p^2 - q^2}$;
- $w = \sqrt{p^2/q^4 - 1/q^2}$.

Also in this case, expression (3.44) refers to the linearly rising portion of the channel-base current. A second contribution must be added, as specified in the previous sections.

Now, we will compare results obtained by using the exact solution (3.32) and their counterparts obtained by using the Liew-Mar's formula (3.44). In Figure 3.26(a), the induced voltage waveforms obtained for h = 10 m, d = 50 m, I_0 = 12 kA, β = 0.4, t_f = 0.5 μs, and t_t = 20 μs are shown. In Figure 3.26(b), the same comparison is shown, but for d = 100 m. As for the Chowdhuri-Gross's formula, the Liew-Mar solution also refers to a lightning channel of finite length: for comparison purposes we have considered $h_c \to \infty$ in (3.44) for both graphs. We have also checked the finite length channel case, assuming h_c =

3 km (see Figures 3.27(a) and (b)). As one can see from the comparison, the Liew-Mar's formula predicts a lower peak value for d = 50 m, and a higher peak value for d = 100 m. In both cases, results obtained by (3.44) show a steeper front, a too rapid decay of the current tail, and a polarity inversion. The latter effect can be seen both for finite and infinite lengths of the lightning channel.

We conclude that the Liew-Mar solution cannot be considered correct.

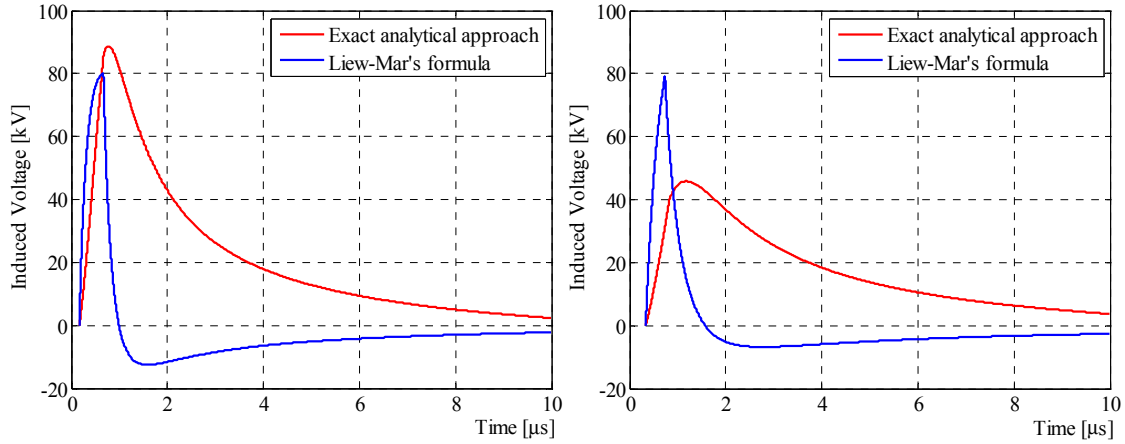

Figure 3.26 – Comparison between the induced voltage evaluated at x = 0 by means of Liew-Mar's formula and the proposed exact analytical approach (h = 10 m, I_0 = 12 kA, β = 0.4, t_f = 0.5 μs, t_t = 20 μs, h_c = ∞): (a) d = 50 m, (b) d = 100 m.

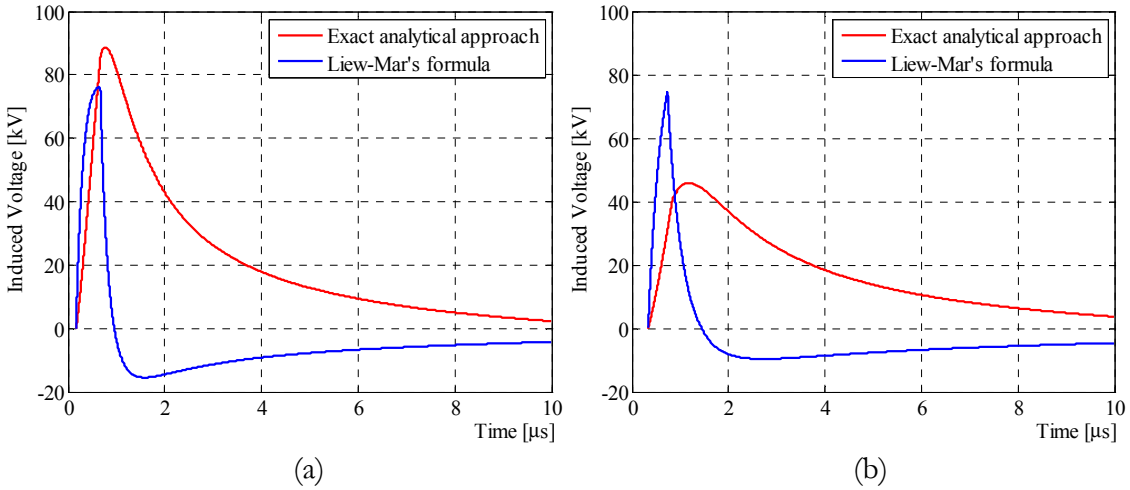

Figure 3.27 – Comparison between the induced voltage evaluated at x = 0 by means of Liew-Mar's formula and the proposed exact analytical approach (h = 10 m, I_0 = 12 kA, β = 0.4, t_f = 0.5 μs, t_t = 20 μs, h_c = 3 km): (a) d = 50 m, (b) d = 100 m.

- *Sekioka's formula*

As indicated in paragraph 3.2.2.1, an approximate solution for the evaluation of the induced voltage due to a linearly rising current has been proposed by Sekioka [23]. This solution was obtained by means of a convolution of the scalar and vector potentials calculated by Rusck [9] for the step current case, and was derived by using the so-called Rusck's coupling model [9]. The Sekioka's formula (3.38), for $x = 0$, can be rewritten as

$$v_S(0,t) = \frac{\mu_0 \cdot h}{4\pi \cdot \beta}\alpha \cdot \left\{ ln\left[1 + \left(\frac{\beta}{d} \cdot \frac{c^2 \cdot t^2 - d^2}{c \cdot t + \xi_1}\right)^2\right] + 2\beta \cdot ln\left[\frac{\beta \cdot c \cdot t + \xi_1}{d \cdot (1+\beta)}\right]\right\} \cdot u(t - \tilde{t}_2). \tag{3.45}$$

Also in this case, this formula refers only to the initial linearly rising portion of the current.

By comparing the results obtained by using the exact solution (3.32) and their counterparts obtained by using the Sekioka's formula (3.45), calculated for the same values of parameters proposed above (h = 10 m, d = 50, and 100 m, I_0 = 12 kA, β = 0.4, t_f = 0.5 μs, and t_t = 20 μs), one can observe that, on a 10-μs time-scale, the results are practically the same (the two induced voltage waveforms overlap each other). Some minor differences can be spotted by zooming in the graphs, as shown in Figure 3.28(a) for the case of d = 50 m.

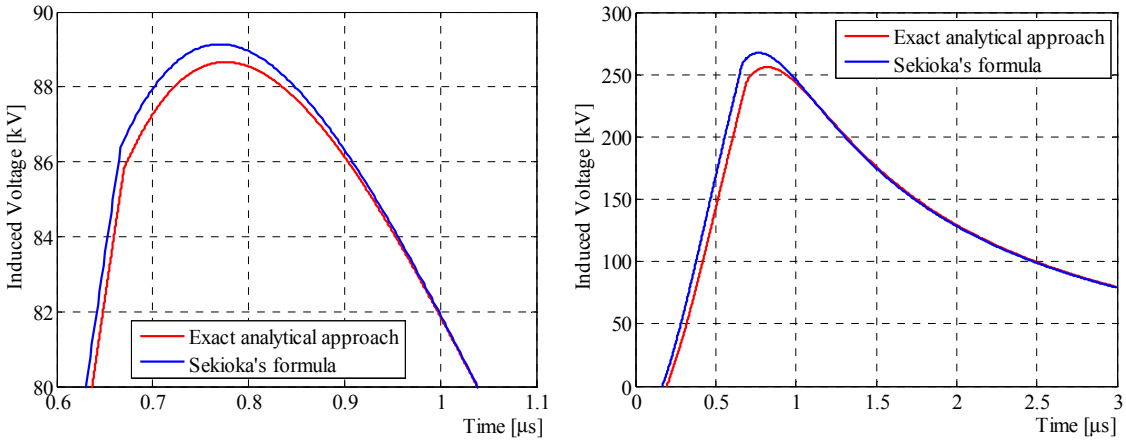

Figure 3.28 – Comparison between the induced voltage evaluated at x = 0 by means of Sekioka's formula and the proposed exact analytical approach (d = 50 m, I_0 = 12 kA, β = 0.4, t_f = 0.5 μs, t_t = 20 μs): (a) magnification of the 0.6÷1.1 μs time interval for h = 10 m, (b) h = 30 m.

We can therefore conclude that the Sekioka's formula is consistent with the exact solution and can be considered suitable for analyzing power distribution lines, for which the height is relatively small. For higher lines, such as transmission lines, small differences between predictions of (3.32) and (3.45) can be appreciated. However, the Sekioka's formula can still be considered a suitable tool for this kind of lines. In Figure 3.28(b), a 30-meter height line is considered.

- *Høidalen's formula*

Høidalen [10] also proposed an approximate formula which allows one to evaluate the induced voltage along the line. This solution has been obtained by a numerical convolution of Rusck's expression for the step current case.

As the expressions presented above, the Høidalen's solution is the sum of two contributions, which account for the linearly rising and the tail part of the current. At $x = 0$, the formula reads

$$v_H(0,t) \approx A(0,t) - b_H \cdot A\big(0, t - t_f\big), \tag{3.46}$$

with

$$A(0,t) = \frac{I_m \cdot \Delta t}{I_0 \cdot t_f} \cdot \left[\sum_{i=0}^{t/\Delta t - 1} v_H^s(0, i \cdot \Delta t) + \frac{1}{2} \cdot v_H^s(0,t) \right] \cdot u(t), \tag{3.47}$$

where

- $b_H = 1 + t_f / \big[2 \cdot (t_t - t_f)\big]$;
- I_m is the linearly rising current peak value;
- Δt is the time step used for the numerical integration.

The term $v_H^s(0,t)$ represents the voltage induced by a step current, whose expression is given in [10]. Note that the expression given in [10] refers to a finite-length line and to an arbitrary value of x. It can be easily extended to the case of an infinite-length line and the resulting expression, for $x = 0$, reads

$$v_H^s(0,t) = \frac{\zeta_0}{2\pi} \cdot I_0 \cdot \beta \cdot h \cdot \frac{c \cdot t}{d^2 + (\beta \cdot c \cdot t)^2} \cdot \left(1 + \frac{\beta^2 \cdot c \cdot t}{\xi_1} \right) \cdot u(t - \tilde{t}_2). \tag{3.48}$$

A comparison between predictions of the exact solution (3.32) and the results obtained by using the Høidalen's formula (3.46) is shown in Figures 3.29(a) and (b), respectively, for a 10-m-high line and a 30-m-high line. As in the case of Sekioka's expression, no practical differences are observed for a 10 m line (the graph was zoomed in to show some minor differences), whereas for the 30 m line, even if differences can be seen, Høidalen's formula can still be considered a suitable approximation of the exact solution.

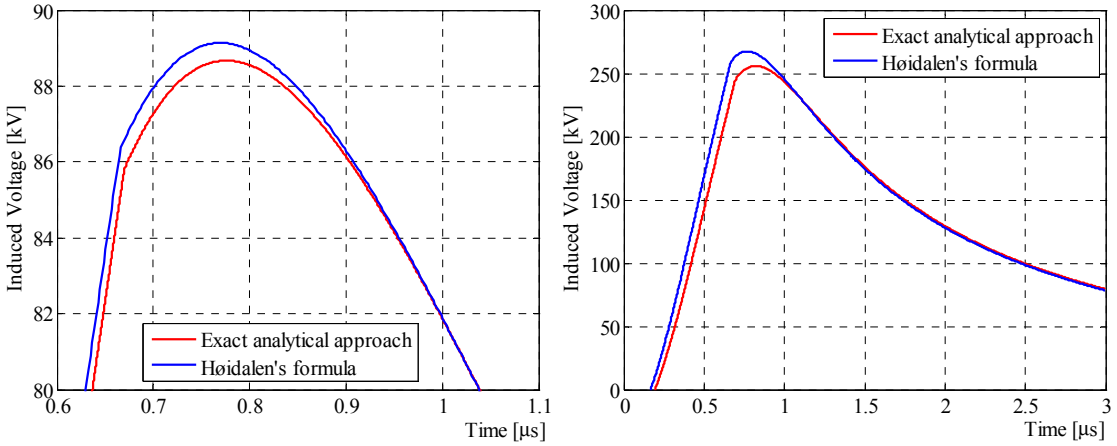

Figure 3.29 – Comparison between the induced voltage evaluated at $x = 0$ by means of Høidalen's formula and the proposed exact analytical approach ($d = 50$ m, $I_0 = 12$ kA, $\beta = 0.4$, $t_f = 0.5$ μs, $t_t = 20$ μs): (a) magnification of the 0.6÷1.1 μs time interval for $h = 10$ m, (b) $h = 30$ m.

Finally, in order to check also the proposed approximate equation for an arbitrary value of x along the line, we have compared the predictions of (3.42) with those of the approximate solutions proposed by Høidalen [10] and Sekioka [23]. Figure 3.30 shows the results obtained at a distance of 500 m from the center of the line (closest point of the line to the lightning channel). In both cases, an excellent correspondence can be seen. The maximum relative error was found to be 0.33% in the case of Høidalen's expression and 0.32% in the case of Sekioka.

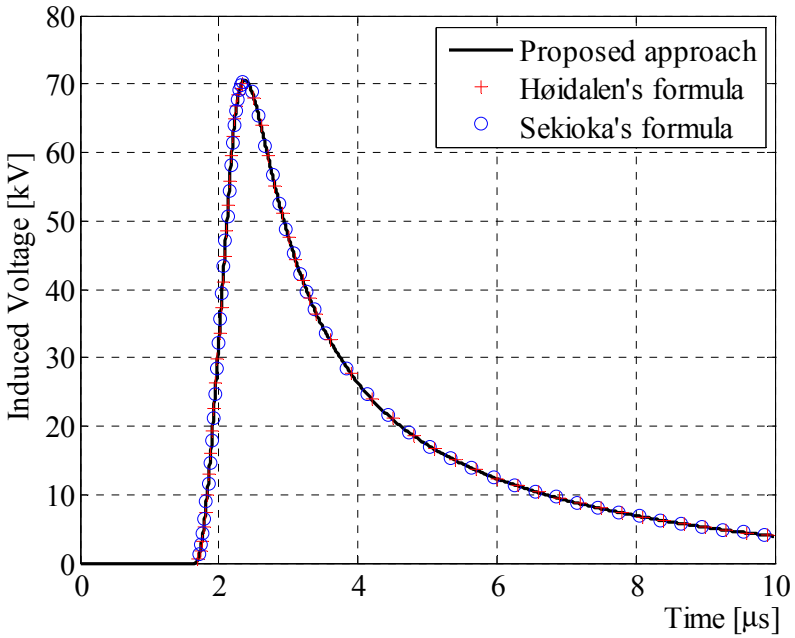

Figure 3.30 – Induced voltage on an infinitely long line at a distance of 500 m from the center: comparison between the results obtained using (3.42) and the Høidalen [10] and Sekioka [23] formulas. Parameters used are h = 10 m, d = 50 m, I_0 = 12 kA, β = 0.4, t_f = 0.5 μs, t_t = 20 μs.

3.3 Lossy ground case

In this section, the solutions presented above for the lossless ground case and both the step current and linearly rising current will be extended to take into account lossy ground effects. For this purpose, it is important to recall that lossy ground affects the lightning electromagnetic field, in particular, the horizontal electric field at line height (as detailed in [33] and in Chapter 2). The propagation of the induced voltage along the line is affected too. Nevertheless, in this thesis work, only the lossy-ground effects on the horizontal field at line height will be considered.

Finally, results obtained using the model developed below will be compared with those given by other formulas found in the literature.

3.3.1 General formulation

Let us consider a long, lossless, single conductor located over a finite-conductivity ground plane, and excited by an external field due to both a step channel-base current and a linearly rising channel-base current moving along a vertical lightning channel according to

the TL model. The configuration is the same as the one depicted in Figure 3.1, except for the soil conductivity.

In the ideal ground case, as described in section 3.2.1.1, the expression for the induced voltage along the line can be obtained by analytically solving equation (3.1), in which appear the vertical and the line axial components of the electric field produced by a step current if one is studying case (a) of Figure 3.1, or by a linearly rising current if one is studying case (b).

In the case of lossy ground, both $e_z(\cdot)$ and $e_x(\cdot)$ will be affected by finite ground conductivity effects, but since we are neglecting the lossy effects along the line, (3.1) still holds. Rigorously, $e_z(\cdot)$ and $e_x(\cdot)$ should be calculated by solving the Sommerfeld integrals [49], but in this case the integrals in (3.1) could not be closed analytically. However, since the vertical component $e_z(\cdot)$ is practically unaffected by the finite ground conductivity and the line axial component $e_x(\cdot)$ can be satisfactory represented by the Cooray-Rubinstein approximation (see Chapter 2 for a detailed discussion of the lossy ground effects), for which a time-domain representation has also been given [35], we will adopt this approximation in the following analysis. The validity of the Cooray-Rubinstein formula has been investigated by many authors (e.g., [34], [50], [51]). At close ranges, where the induced voltages are the most critical, the error associated with the Cooray-Rubinstein approach is significant only for very poorly conducting earth [52]. Therefore, σ = 0.001 S/m can be considered as a lower limit for ground conductivities. Down to this value, the errors can be considered negligible [52].

According to the Cooray-Rubinstein's approximation, the line axial field $e_x(\cdot)$ can be calculated by means of the following expression [35]:

$$e_x(x,y,z,t) = e_{xi}(x,y,z,t) - \sqrt{\frac{\mu_0}{\varepsilon}} \cdot h_{yi}(x,y,0,t) + h_{yi}(x,y,0,t) * K(t), \qquad (3.49)$$

where

- $e_{xi}(\cdot)$ is the ideal electric field line axial component (calculated as if the ground were a perfect conductor);
- $h_{yi}(\cdot)$ is the ideal azimuthal magnetic field line normal component (calculated as if the ground were a perfect conductor);
- ε is the ground permittivity.

The sign $*$ denotes a convolution, and $K(t)$ can be expressed by [53]

$$K(t) = \sqrt{\frac{\mu_0}{\varepsilon}} \cdot \frac{\sigma}{2\varepsilon} \cdot \left[J_0\left(\frac{\sigma}{2\varepsilon} \cdot t\right) - J_1\left(\frac{\sigma}{2\varepsilon} \cdot t\right) \right] \cdot e^{-\frac{\sigma}{2\varepsilon} \cdot t} = -\sqrt{\frac{\mu_0}{\varepsilon}} \cdot \frac{d}{dt} \left[J_0\left(\frac{\sigma}{2\varepsilon} \cdot t\right) \cdot e^{-\frac{\sigma}{2\varepsilon} \cdot t} \right], \tag{3.50}$$

where σ is the ground conductivity, $J_0(\cdot)$ is the modified Bessel function of the first type and order 0, $J_1(\cdot)$ is the modified Bessel function of the first type and order 1.

Therefore, (3.1) can be written as

$$\begin{aligned} v(x,t) = \Bigg\{ & -\int_0^h e_{zi}(x,d,z,t)dz \\ & -\frac{1}{2}\int_{-\infty}^{+\infty} e_{xi}\left(\eta,d,h,t-\frac{|\eta-x|}{c}\right)\cdot sign(\eta-x)d\eta \\ & +\frac{1}{2}\cdot\sqrt{\frac{\mu_0}{\varepsilon}}\cdot\int_{-\infty}^{+\infty} h_{yi}\left(\eta,d,0,t-\frac{|\eta-x|}{c}\right)\cdot sign(\eta-x)d\eta \\ & -\frac{1}{2}\cdot\int_{-\infty}^{+\infty}\left[h_{yi}\left(\eta,d,0,t-\frac{|\eta-x|}{c}\right)\cdot sign(\eta-x)\right] * K(t)d\eta \Bigg\} \cdot u(t-t_0). \end{aligned} \tag{3.51}$$

The first two terms on the right-hand side of (3.51) represent the induced voltage in case of perfectly conducting ground, whereas the remaining two terms represent the necessary corrections to account for lossy ground effects.

Let us consider two arbitrary time functions $f(t)$ and $g(t)$. It is well known that their convolution product is defined as

$$f(t) * g(t) = \int_0^t f(\tau) \cdot g(t-\tau)d\tau. \tag{3.52}$$

Hence, the last term on the right-hand side of (3.51), apart from the multiplying factor $-1/2$, can be written as

$$\int_{-\infty}^{+\infty}\left[\int_{0}^{t} h_{yi}\left(\eta, d, 0, \tau - \frac{|\eta - x|}{c}\right)\cdot sign(\eta - x)\cdot K(t-\tau)d\tau\right]d\eta. \tag{3.53}$$

For our purposes, we need to reverse the integration order in (3.53), so as to obtain

$$\int_{0}^{t}\left[\int_{-\infty}^{+\infty} h_{yi}\left(\eta, d, 0, \tau - \frac{|\eta - x|}{c}\right)\cdot sign(\eta - x)d\eta\right]\cdot K(t-\tau)d\tau. \tag{3.54}$$

If we set

$$w_h(x,t) = \int_{-\infty}^{+\infty} h_{yi}\left(\eta, d, 0, t - \frac{|\eta - x|}{c}\right)\cdot sign(\eta - x)\cdot u(t-t_0)d\eta, \tag{3.55}$$

and call $v_i(x,t)$ the induced voltage in the case of ideal ground, (3.51) can be rewritten as

$$v(x,t) = v_i(x,t) + \frac{1}{2}\cdot\sqrt{\frac{\mu_0}{\varepsilon}}\cdot w_h(x,t) - \frac{1}{2}\cdot\int_{0}^{t} w_h(x,\tau)\cdot K(t-\tau)d\tau\,. \tag{3.56}$$

Expressions for $v_i(x,t)$ have been presented above, both for the step current case (see paragraph 3.2.1) and the linearly rising current case (see paragraph 3.2.2)

In the next two sections, we will give the analytical expression of $w_h(\cdot)$ in an exact form (i.e., with no approximations) both for the step and the linearly rising channel-base current cases.

As for the evaluation of the convolution integral appearing in (3.56), we will use the approach proposed in [53] that will be briefly outlined here. Let us call the convolution shown in (3.56) as

$$CI(t) = \int_{0}^{t} w_h(x,\tau)\cdot K(t-\tau)d\tau\,. \tag{3.57}$$

If we consider N equally spaced time samples in the interval $[0,t]$, and assume that the function $w_h(x,\tau)$ is constant between the samples

$$w_h(x,\tau) \approx V_n \qquad \forall\, \tau \in [t_n, t_{n+1}), \tag{3.58}$$

with $t_n = \Delta t \cdot (n-1)$, $n = 1,2,\dots,N$ and $V_n = w_h(x,t_n)$, one can compute $CI(t)$ in an approximate way at each time sample between $t_1 = 0$ and t_N, implementing the following formula [53]:

$$\begin{cases} CI(t_1) = CI_1 = 0, \\ CI(t_n) = CI_n = \sum_{m=1}^{n-1} V_n \cdot IK_{n-m}, \qquad n = 2,\dots,N \end{cases} \tag{3.59}$$

where

- $IK_n = VIK_{n+1} - VIK_n$;
- $VIK_n = -J_0(\sigma/(2\varepsilon)\cdot t_n)\cdot e^{-\sigma/(2\varepsilon)\cdot t_n}$.

3.3.2 Step channel-base current

To evaluate the last two terms of (3.56), representing the lossy ground effects, we need to solve (3.55). First, we recall the exact analytical expression for the line normal component of the ideal azimuthal magnetic field (i.e., the field calculated as if the ground were a perfect conductor) evaluated at ground level ($z = 0$) for the step current case [8]

$$h_{yi}^s(x,d,0,t) = \frac{I_0}{2\pi\cdot r^2}\cdot\frac{\beta\cdot c\cdot t\cdot x}{\xi}\cdot u(t-t_0). \tag{3.60}$$

The integral in (3.55), with h_{yi} given by (3.60), is solved in the Appendix, and the solution reads

$$w_h^s(x,t) = w_s(x,t) + w_s(-x,t), \tag{3.61a}$$

with

$$w_s(x,t) = \frac{I_0}{2\pi}\cdot\left[ln\left(\frac{\beta\cdot c\cdot t+\xi}{\hat{\lambda}-\beta x_l+\xi_l}\right)+\beta\cdot ln\left(\frac{x-\beta\hat{\lambda}+\xi}{x_l-\beta\hat{\lambda}+\xi_l}\right)+ln\left(\frac{\delta_l}{\delta}\right)\right]\cdot u(t-t_0), \tag{3.61b}$$

where

- $\hat{\lambda} = \beta \cdot (c \cdot t + x)$;
- $\xi_l = \sqrt{\left(\beta x_l - \hat{\lambda}\right)^2 + \delta_l^2}$.

By using these results, we first show in Figure 3.31 the induced voltages at different points along the line (x = 0 m, 500 m, 1000 m, 1500 m, and 2000 m) both for perfect ground (Figure 3.31(a)) and lossy ground (Figures 3.31(b) and (c)) for two different ground conductivities (σ = 0.01 S/m and 0.001 S/m) assuming a relative permittivity, ε_r, of 10. The well-known polarity inversion effect is reproduced [3], [54]. Note also that all waveshapes do not start from zero due to the discontinuity produced by the step current. The lossy ground has also the effect of magnifying the induced voltage at the point closest to the lightning channel and reducing the positive polarity peaks for "off-the-center" positions. It should be noted also in Figures 3.31(b) and (c) that the negative polarity peak increases with increasing x.

For direct comparison purposes, we show in Figure 3.32 the induced voltages at x = 0 for perfectly conducting ground, σ = 0.01 S/m, and σ = 0.001 S/m. The peak increases by about 14% when σ = 0.01 S/m and by about 49% when σ = 0.001 S/m, compared to the perfect ground case.

For the off-the-center position (x = 500 m), a different behavior is seen in Figure 3.33: the positive polarity peaks decrease and negative polarity peaks increase with decreasing ground conductivity (note that waveforms for perfectly conducting ground do not exhibit negative polarity peaks).

3.3.3 Linearly rising channel-base current

For the case of a linearly rising current, we first need to calculate the line normal component of the ideal-ground azimuthal magnetic field at z =0. It can be obtained starting from (3.60) by means of the Duhamel's integral (3.30).

Let us consider the integral (3.30) when the input $f(t)$ is a ramp of constant slope $\alpha = I_0/t_f$, and where the unit-step response $s(t)$ is the one given by (3.60). This integral can be solved exactly and the solution reads

$$h_{yi}^r(x, d, 0, t) = \frac{I_0 \cdot x}{2\pi \cdot \beta \cdot c \cdot t_f \cdot r^2} \cdot (\xi - r) \cdot u(t - t_0). \tag{3.62}$$

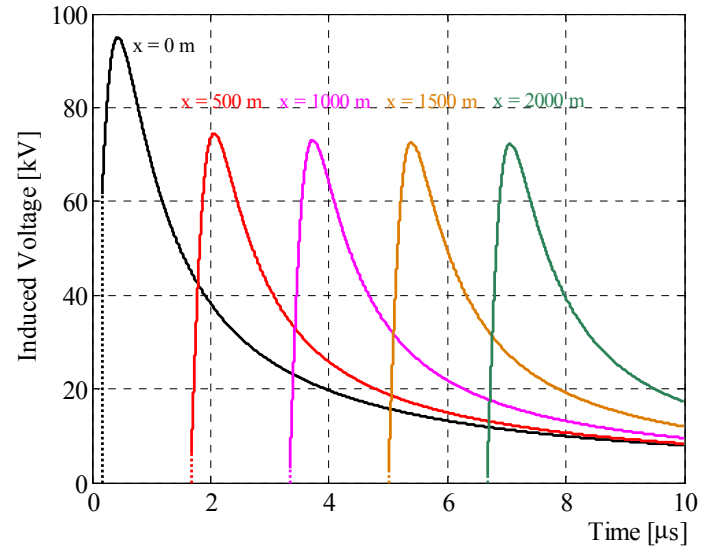

(a)

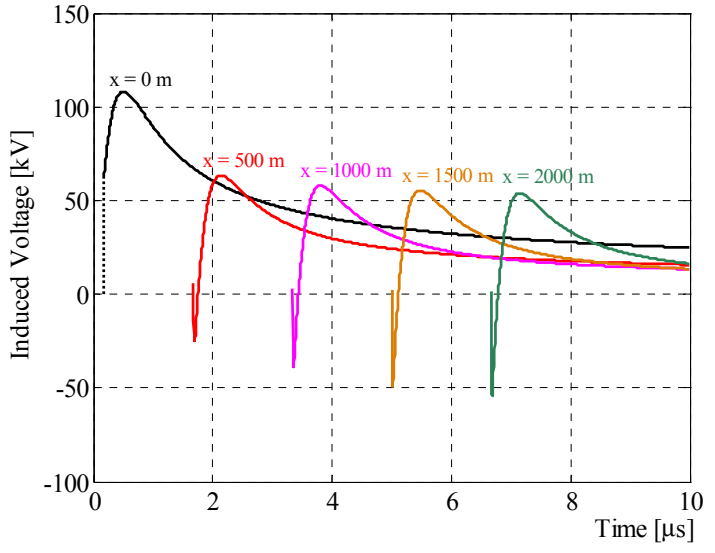

(b)

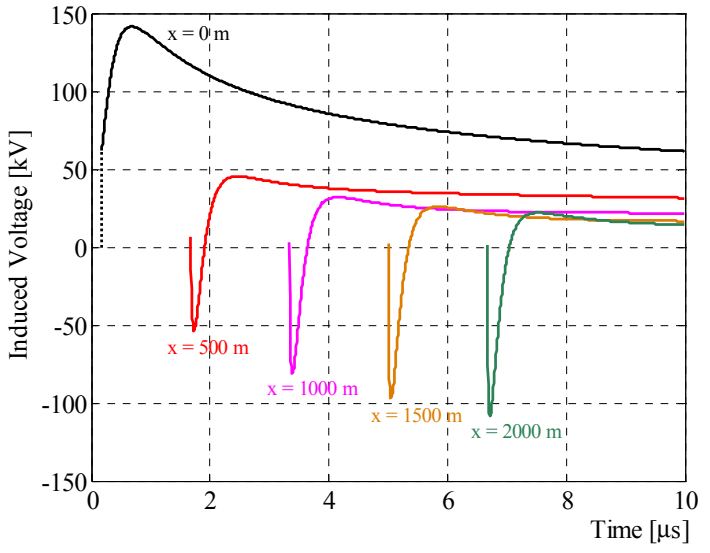

(c)

Figure 3.31 – Plots of the induced voltages at different positions along the line (h = 10 m, d = 50 m, I_0 = 12 kA, β = 0.43): (a) $\sigma = \infty$ and $\varepsilon_r = 1$, (b) σ = 0.01 S/m and ε_r = 10, (c) σ = 0.001 S/m and ε_r = 10.

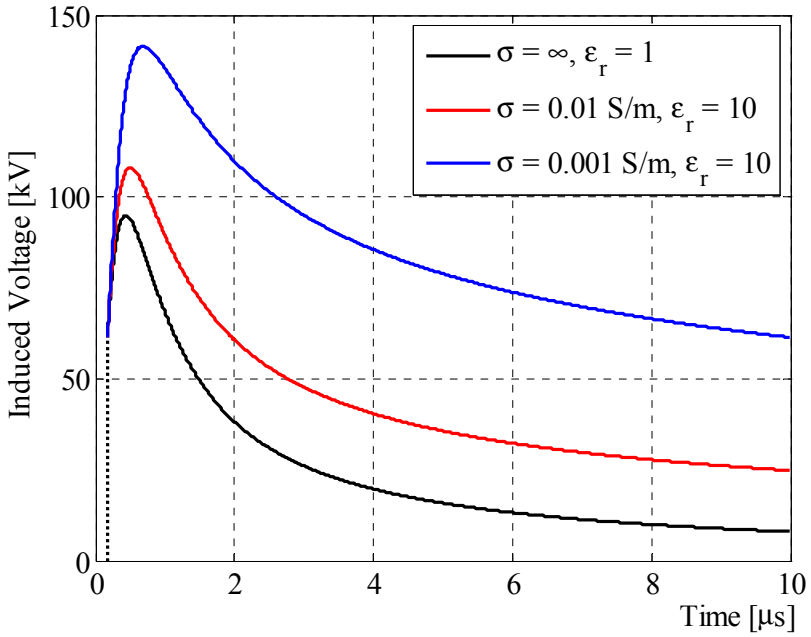

Figure 3.32 – Comparison of the induced voltages at $x = 0$ for perfectly conducting ground ($\sigma = \infty$ and $\varepsilon_r = 1$), $\sigma = 0.01$ S/m, and $\sigma = 0.001$ S/m ($\varepsilon_r = 10$). Plots are obtained for $h = 10$ m, $d = 50$ m, $I_0 = 12$ kA, $\beta = 0.43$.

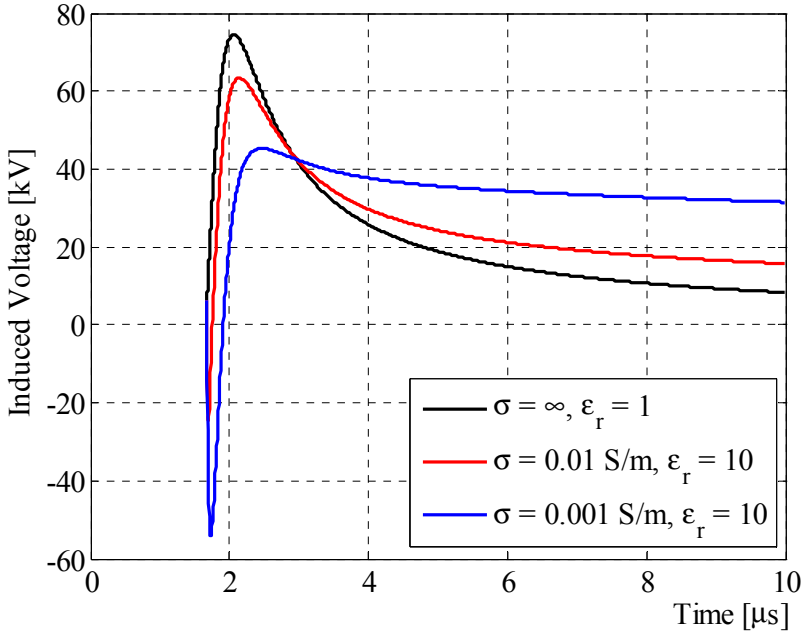

Figure 3.33 – Comparison of the induced voltages at $x = 500$ m for perfectly conducting ground ($\sigma = \infty$ and $\varepsilon_r = 1$), $\sigma = 0.01$ S/m, and $\sigma = 0.001$ S/m ($\varepsilon_r = 10$). Plots are obtained for $h = 10$ m, $d = 50$ m, $I_0 = 12$ kA, $\beta = 0.43$.

As for the case of a step current, by using (3.62), the integral in (3.55) can be solved exactly, as shown in the Appendix. The solution reads

$$w_h^r(x,t) = w_r(x,t) + w_r(-x,t), \tag{3.63a}$$

with

$$w_r(x,t) = \frac{I_0}{2\pi \cdot \beta \cdot c \cdot t_f} \cdot \left\{ \xi_l - \xi + \beta\hat{\lambda} \cdot ln\left(\frac{x - \beta\hat{\lambda} + \xi}{x_l - \beta\hat{\lambda} + \xi_l}\right) + \sqrt{x^2 + d^2} - \sqrt{x_l^2 + d^2} \right.$$
$$+ \frac{\beta^4}{\hat{\lambda}^2 \cdot P \cdot \sqrt{Q - T^2}} \cdot \left\{ R \cdot \left[arctanh\left(\frac{\sqrt{W^2(x) + Q}}{\sqrt{Q - T^2}}\right) - arctanh\left(\frac{\sqrt{W^2(x_l) + Q}}{\sqrt{Q - T^2}}\right)\right] \right.$$
$$\left.\left. + \frac{S}{T} \cdot \left[arctan\left(\frac{W(x_l) \cdot \sqrt{Q - T^2}}{T \cdot \sqrt{W^2(x_l) + Q}}\right) - arctan\left(\frac{W(x) \cdot \sqrt{Q - T^2}}{T \cdot \sqrt{W^2(x) + Q}}\right)\right]\right\}\right\} \cdot u(t - t_0), \tag{3.63b}$$

where

- $P = \sqrt{[(c \cdot t + x)^2 + d^2] \cdot (1 - \beta^2)}$;
- $Q = \left[d^2 + \hat{\lambda}^2\right]/[(c \cdot t + x)^2 \cdot (1 - \beta^2)]$;
- $R = (c \cdot t + x)^2 \cdot [(c \cdot t + x)^2 + d^2]$;
- $S = d^2 \cdot [(c \cdot t + x)^2 + d^2]$;
- $T = d/(c \cdot t + x)$;
- $W(\varphi) = [(c \cdot t + x) \cdot \varphi + d^2]/[(c \cdot t + x) \cdot (c \cdot t + x - \varphi)]$.

By using these results, Figure 3.34 shows the induced voltages computed at the point closest to the lightning channel (x = 0) for a linearly rising current with drooping tail (t_t = 20 μs) for different front times. We start with a very fast front time of 1 ns (not applicable to lightning, but shown for comparison with the step current case) and then vary t_f from 0.1 to 1 μs, with 0.1-μs step. Figure 3.34(a) refers to the perfectly conducting ground, whereas Figure 3.34(b) refers to a ground with σ = 0.001 S/m and ε_r = 10. We notice that finite conductivity ground significantly increases the voltage peaks for all front times. In Figure 3.35, we show the induced voltages at different points along the line (x = 0 m, 500 m, 1000 m, 1500 m, and 2000 m) both for perfect ground (Figure 3.35(a)) and lossy ground for σ = 0.001 S/m and ε_r = 10 (Figures 3.35(b)). The assumed current has a front time t_f = 0.5 μs and a drooping tail with tail time t_t = 20 μs. This specific channel-base current

was selected since it represents the best fit [10] of a current obtained using Heidler functions [54] which, in turn, reproduce a typical measured channel-base current [55] (see also the following paragraph "Model validation"). As for the step current case, we observe the inversion of polarity of the waveshapes; the lossy ground has also the effect of magnifying the induced voltage at the point closest to the lightning channel and reducing the positive polarity peaks for an "off-the-center" position. It should be also noted in Figure 3.35(b) that negative polarity peaks increase with increasing x.

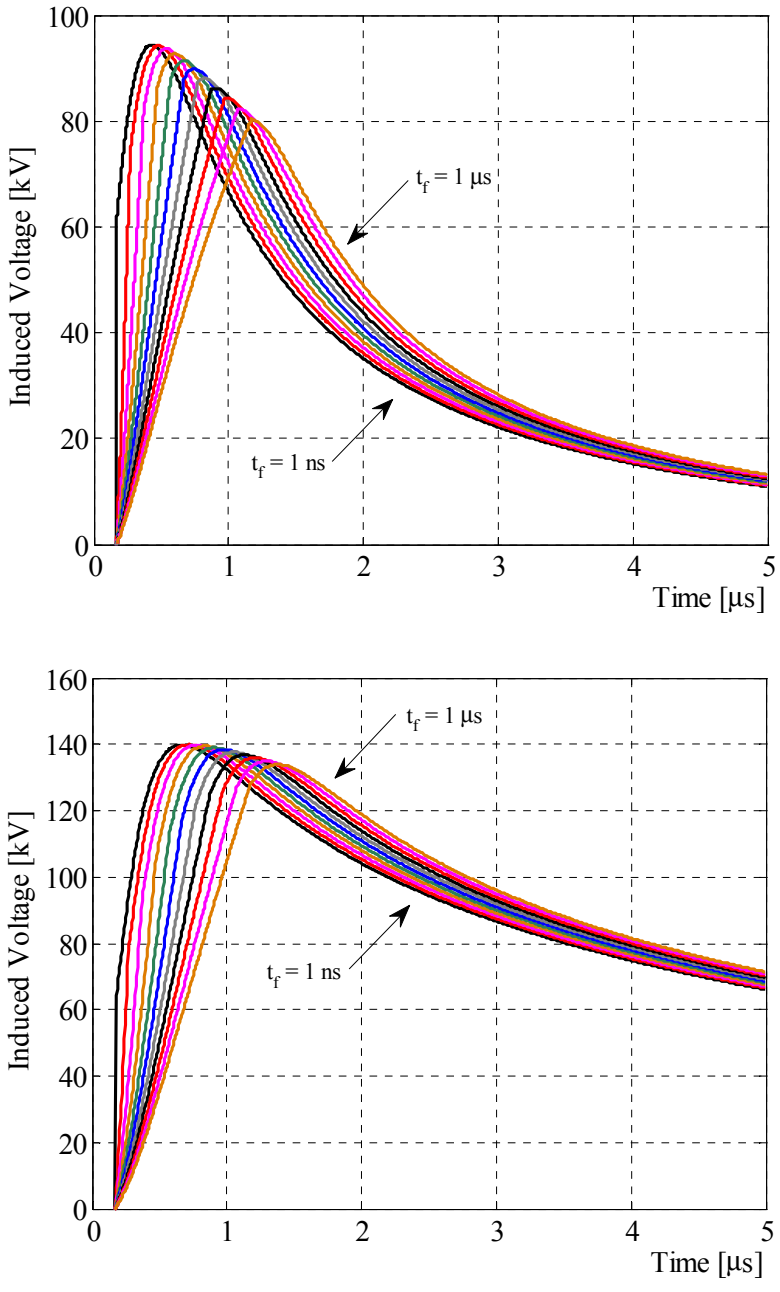

Figure 3.34 – Induced voltages obtained for different t_f at $x = 0$ by assuming $h = 10$ m, $d = 50$ m, $I_0 = 12$ kA, $\beta = 0.43$, $t_t = 20$ μs: (a) $\sigma = \infty$ and $\varepsilon_r = 1$, (b) $\sigma = 0.001$ S/m and $\varepsilon_r = 10$.

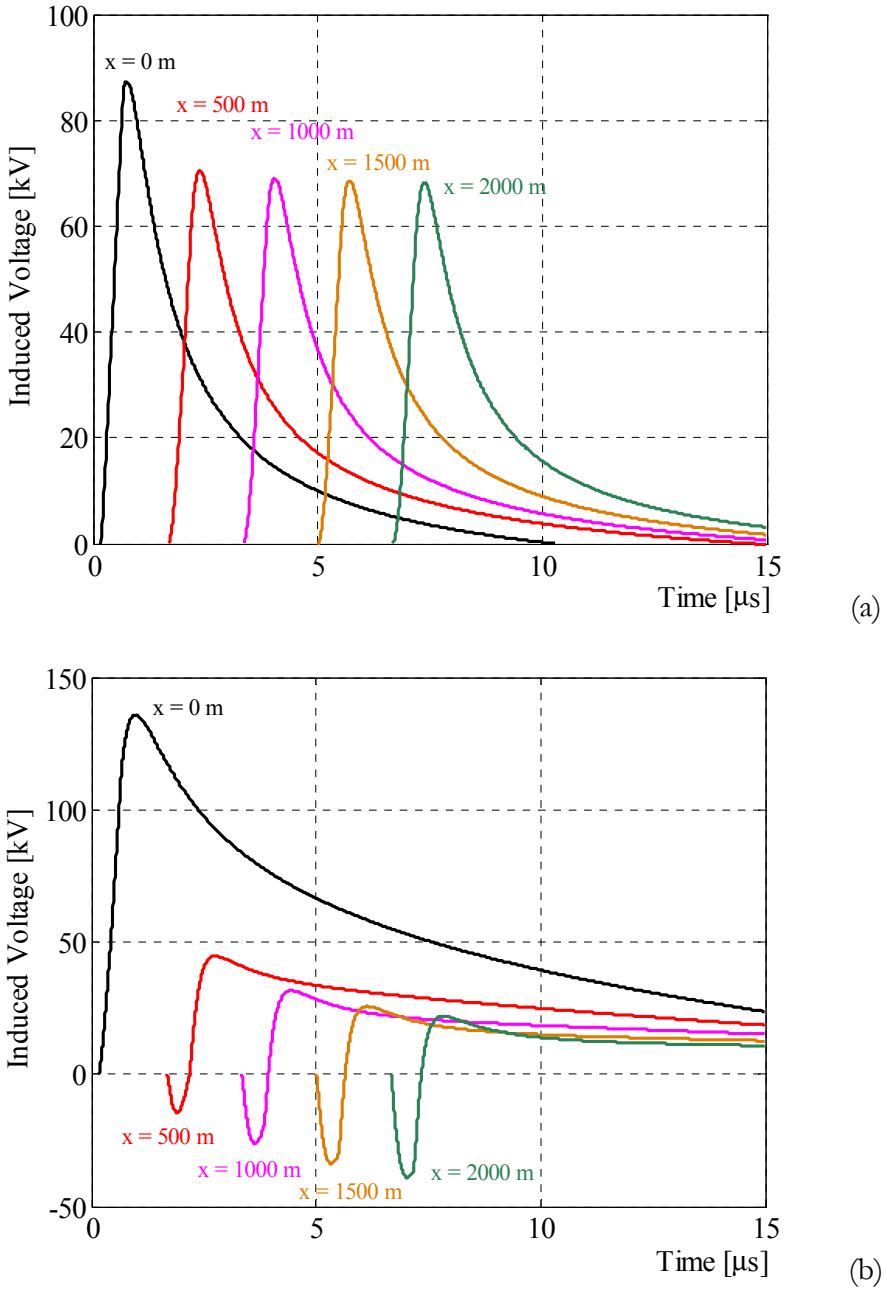

Figure 3.35 – Plots of the induced voltages at different positions along the line (h = 10 m, d = 50 m, I_0 = 12 kA, β = 0.43, t_f = 0.5 μs, t_t = 20 μs): (a) $\sigma = \infty$ and ε_r = 1, (b) σ = 0.001 S/m and ε_r = 10.

For direct comparison purposes, Figure 3.36 shows the induced voltages at x =0 for perfectly conducting ground, σ = 0.01 S/m, and σ = 0.001 S/m. The peak increases by about 16% when σ = 0.01 S/m and by about 54% when σ = 0.001 S/m, compared to the perfect ground case. For an "off-the-center" position x = 500 m, (see Figure 3.37), the different behavior noticed in the case of a step current is also noticed here: the positive polarity peaks decrease and negative polarity peaks increase with decreasing σ (note that for perfectly conducting ground there is no negative polarity peak).

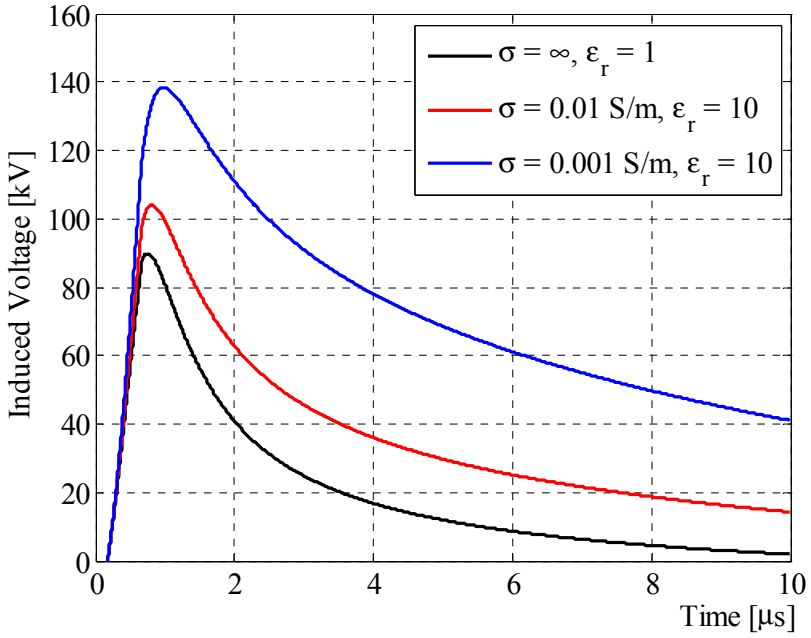

Figure 3.36 – Comparison of the induced voltages at $x = 0$ for perfectly conducting ground ($\sigma = \infty$ and $\varepsilon_r = 1$), $\sigma = 0.01$ S/m, and $\sigma = 0.001$ S/m ($\varepsilon_r = 10$). Plots are obtained for $h = 10$ m, $d = 50$ m, $I_0 = 12$ kA, $\beta = 0.43$, $t_f = 0.5$ μs, $t_t = 20$ μs.

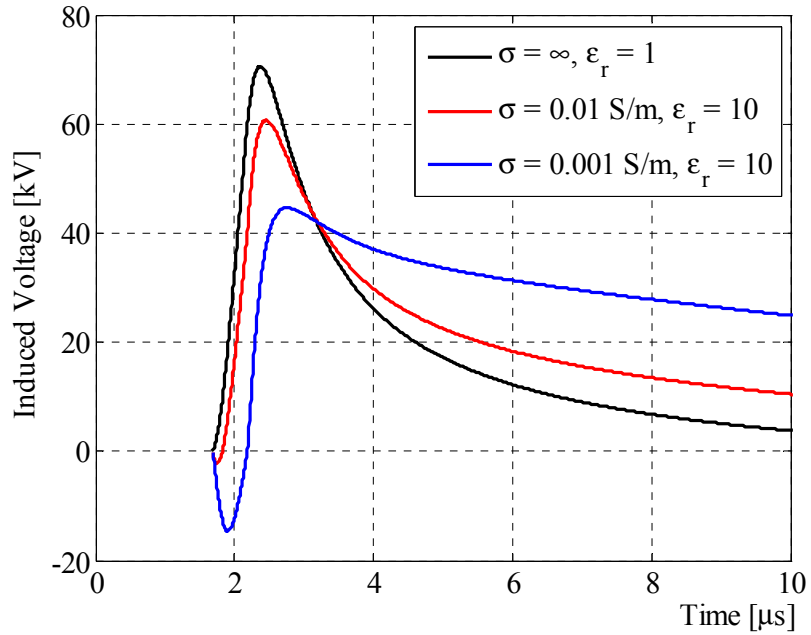

Figure 3.37 – Comparison of the induced voltages at $x = 500$ m for perfectly conducting ground ($\sigma = \infty$ and $\varepsilon_r = 1$), $\sigma = 0.01$ S/m, and $\sigma = 0.001$ S/m ($\varepsilon_r = 10$). Plots are obtained for $h = 10$ m, $d = 50$ m, $I_0 = 12$ kA, $\beta = 0.43$, $t_f = 0.5$ μs, $t_t = 20$ μs.

3.3.4 Model validation

In order to test the validity of the model, we compared predictions of the proposed approach and those of the LIOV (Lightning Induced OverVoltage) code [37], [54] based on solving telegrapher's equations generalized to include source terms and, similar to the proposed approach, employs the Cooray-Rubinstein approximation. Since simulations with the LIOV code for a single-conductor line in the presence of lossy ground are available, but for a channel-base current of the Heidler-function type (see Chapter 2), we have approximated the Heidler-function channel base-current with a linearly rising current with drooping tail, using the approximation proposed in [10]: the parameters used are I_0 = 12 kA, t_f = 0.5 μs, and t_t = 20 μs. Further, since simulations with the LIOV code are available only for a finite length line, we have adapted the new approach to the geometry considered in [54], which refers to a single-phase 1-km-long and 10-m-high line terminated in its characteristic impedance. The method used to consider the case of the finite length line is similar to the one developed in paragraph 3.2.1.2. The lightning channel is located 50 m from the overhead line center. In Figure 3.38, we show the induced voltages at the line terminal calculated with the proposed approach and with the LIOV code for both perfectly-conducting ($\sigma = \infty$, $\varepsilon_r = 1$) and lossy ground (σ = 0.001 S/m, $\varepsilon_r = 10$) cases (note a slight difference relative to the induced voltage calculated for an infinite length line in Figure 3.37). The results match well in the case of lossless ground, whereas a discrepancy up to about 14% in peak values is seen in the lossy ground case. Reasons for this relatively small discrepancy are presently unknown. In summary, the proposed formulation seems to perform well and can represent a useful test bench for numerical and analytical models.

3.3.5 Comparison with other models

As mentioned in the introduction, several authors have presented simple formulas or more complex analytical developments for the model described by both case (a) and case (b) of Figure 3.1 in presence of a lossy ground. For case (a), formulas have been proposed by Barker *et al.* [24], Darveniza [25], and Paulino *et al.* [26]. For case (b), solutions have been proposed by Paulino *et al.* [29], and Høidalen [10].

In this section, predictions of the new formulation proposed for the evaluation of the voltages induced on an overhead, lossless, single-conductor line located above a finitely conducting ground, and due to both a step and a linearly rising current will be compared to those based on the other approaches found in the literature.

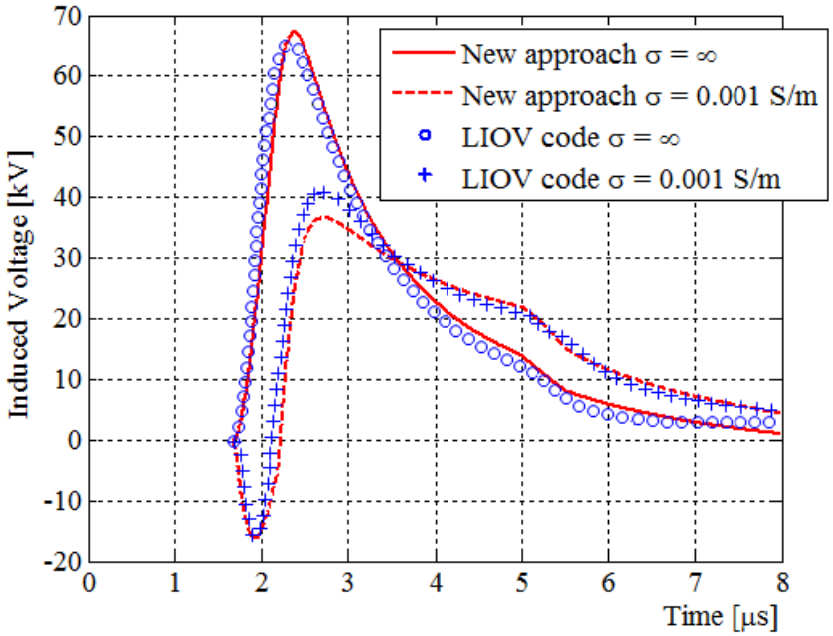

Figure 3.38 – Comparison of the induced voltages at the line terminal (x = 500 m) evaluated by means of LIOV code [37], [54] and the proposed approach (h = 10 m, d = 50 m, I_0 = 12 kA, β = 0.43, t_f = 0.5 μs, t_t = 20 μs).

3.3.5.1 Step current models

Comparison of different models will be performed for a single-conductor line above lossy ground, as the one shown in Figure 3.39, where the line conductor height h and ground conductivity σ will be variable parameters.

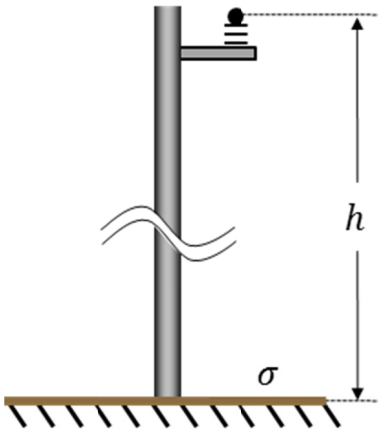

Figure 3.39 – Line geometry used for calculations.

- *Barker et al.'s formula*

In the approach proposed by Barker *et al.* [24], only the peak value of the induced voltage at the point of the line closest to the channel ($x = 0$) is estimated. They propose a correction factor to be applied to the corresponding Rusck's expression [9] (which was derived for a lossless ground), in order to bring model predictions closer to the experimental data. The correction factor serves to increase the induced voltage relative to the perfectly ground case. Note that, according to Barker *et al.*, this correction factor was needed to compensate for inaccuracies in the return-stroke model, however, as pointed out by Ishii in the discussion accompanying their paper [24], this correction was needed to account primarily for the lossy ground effects. Other studies confirm that lossy ground produces higher over-voltages compared to the lossless case (e.g., [5], [10], [54]).

The original Rusck's formula is

$$V_{R\_peak} = 30 \cdot \frac{I_0 \cdot h}{d} \cdot \left(1 + \frac{\beta}{\sqrt{2 - \beta^2}}\right), \tag{3.64}$$

which, for $\beta = 0.4$, the value adopted in the IEEE Standard 1410 [14], becomes

$$V_{R\_peak} = 38.8 \cdot \frac{I_0 \cdot h}{d}. \tag{3.65}$$

Barker *et al.*, on the basis of their analysis of experimental data obtained at Camp Blanding, FL, proposed the following modified formula:

$$V_{B\_peak} = 1.63 \cdot \left(38.8 \cdot \frac{I_0 \cdot h}{d}\right) \cong 63 \cdot \frac{I_0 \cdot h}{d}, \tag{3.66}$$

which, in their opinion, is able to better reproduce the experimental findings. Note that (3.66) does not include the value of the ground conductivity (corresponds to the ground conductivity at the Camp Blanding research facility) and, in addition, is limited to the case of $\beta = 0.4$.

We now compare the induced voltages obtained using (3.66) with the peak values of the voltage waveforms obtained by using (3.56) together with (3.3), (3.59), and (3.61), for $x = 0$.

In Figure 3.40(a), we compare the results obtained for different ground conductivities by using $I_0 = 10$ kA, $\beta = 0.4$, $\varepsilon_r = 10$, at a distance $d = 100$ m, for a 10-m high line. One

can see that the results match only when the ground conductivity is about 1.5 mS/m. Figure 3.40(b) shows the same simulation, but with the height of the line reduced to 7.5 m. In this second case (corresponding to the average conductor height in the experiment), the match is found for a ground conductivity of about 2.7 mS/m. This means that the results by Barker *et al.* are strongly affected by the line height. We also note that values of ground conductivity at the Camp Blanding site, either measured or inferred from low-frequency grounding resistance measurements, which are summarized by Thang *et al.* [56], range between 0.25 and 1.8 mS/m. The value of 2.7 mS/m is higher than these values.

In summary, (3.66) does not seem to provide an accurate solution in the finite conductivity ground case. However, we note, once again, that the correction factor was not directly proposed by Barker *et al.* to account for finite ground conductivity effects, but, as pointed out in the discussion section of the same paper [24], it primarily represented the direct consequence of these effects.

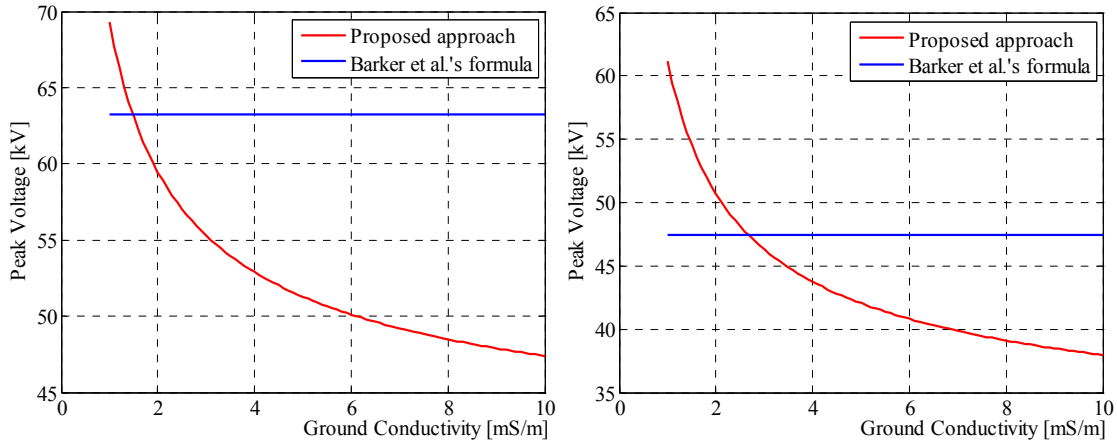

Figure 3.40 – Comparison between the induced voltage peak values computed at $x = 0$ by means of Barker *et al.*'s formula and the proposed approach ($d = 100$ m, $I_0 = 10$ kA, $\beta = 0.4$, and $\varepsilon_r = 10$): (a) $h = 10$ m, (b) $h = 7.5$ m.

- *Darveniza's formula*

Darveniza [25] presented an empirical formula for the calculation of the peak values of the induced voltages at $x = 0$, which was derived from experimental data, theoretical considerations, and values obtained from computational simulations. The Darveniza's formula, similar to that of Barker *et al.*, is an extension of Rusck's formula (3.64), but in this case, the actual height of the line is replaced by an "effective" value that accounts for the ground conductivity. This effective height is given by

$$h_{eff} = h + 0.15 \cdot \sqrt{1/\sigma}\,. \tag{3.67}$$

We first note that compared to Barker *et al.*'s formula, the Darveniza's one shows dependence on the ground conductivity.

We now compare the peak voltage values obtained by (3.64) with h replaced with h_{eff} and their counterparts obtained by using (3.56) together with (3.3), (3.59), and (3.61), for $x = 0$.

In Figure 3.41, we show the results obtained for different ground conductivities by using h = 10 m, d = 100 m, I_0 = 10 kA, β = 0.4, ε_r = 10. One can observe that the peak value estimated by using the Darveniza's formula is always lower than the one calculated by using the proposed analytical approach, but always within 20%. The percentage difference was computed as

$$\frac{V_{peak-new\ approach} - V_{peak-Darveniza}}{V_{peak-new\ approach}} \cdot 100. \tag{3.68}$$

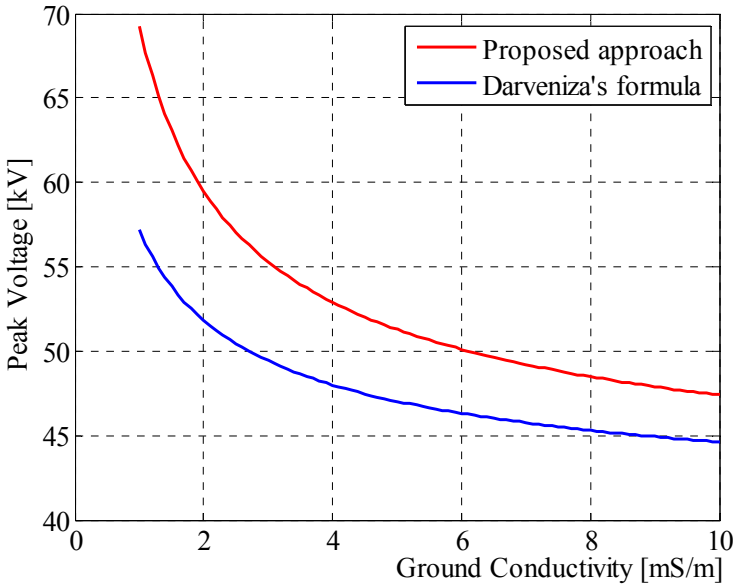

Figure 3.41 – Comparison between the induced voltage peak values evaluated at x = 0 by means of Darveniza's formula and the proposed approach (h = 10 m, d = 100 m, I_0 = 10 kA, β = 0.4, and ε_r = 10).

In Figure 3.42, we plot 3-D graphs showing the percentage difference between the results obtained by using the Darveniza's formula and the proposed approach as a function of the line height and the distance between the lightning channel and the line. Figure

3.42(a) is for σ = 0.01 S/m and ε_r = 10, Figure 3.42(b) for σ = 0.001 S/m and ε_r = 10. The difference is up to about 22% for σ = 0.01 S/m, and up to about 44% for σ = 0.001 S/m, increasing with the distance. The range 50÷250 m was selected because for shorter distances the lightning strike will be probably intercept the line, whereas for longer distances it will not be able to produce critical overvoltages.

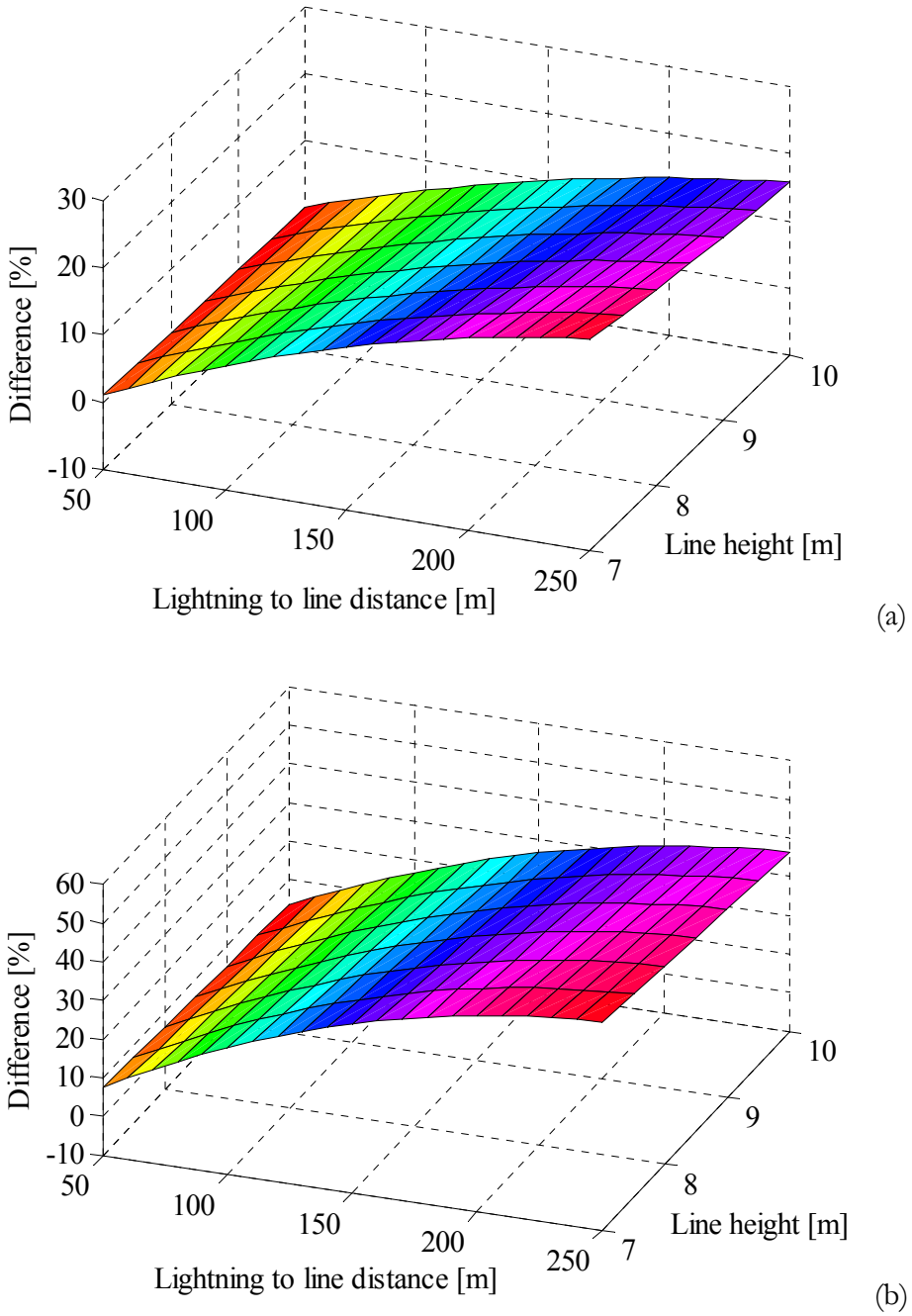

Figure 3.42 – 3-D plots of the differences between the induced voltage peak values at x = 0 computed by means of Darveniza's formula and the proposed approach (I_0 = 10 kA, β = 0.4, and ε_r = 10): (a) σ = 0.01 S/m, (b) σ = 0.001 S/m.

- *Paulino et al.'s formula*

Paulino *et al.* [26] derived a formula, based on a large number of numerical simulations, which, similar to other formulas discussed before, is an extension of the Rusck's formula. It is given by

$$V_{P\_peak} = k_c \cdot (V_R + V_S), \tag{3.69}$$

where V_R stands for the original Rusck's formula given by (3.64), and V_S is an additional term which accounts for the finite conductivity ground effects. This additional term is given by [26]

$$V_S = \sqrt{3} \cdot \beta^{\frac{1}{3}} \cdot I_0 \cdot \sqrt{1/(\sigma \cdot d)}\,. \tag{3.70}$$

The k_c factor in (3.69) is needed to compensate errors due to the delay between the voltage peaks associated with the two contribution V_R and V_S (see [26] for more details). For an overhead line above lossy ground ($\sigma \neq \infty$), the suggested value for k_c is 0.85 (in the lossless ground case, k_c = 1). Paulino *et al.* also give the expression for V_S for the case of β = 0.4, which reads

$$V_S = 1.28 \cdot I_0 \cdot \sqrt{1/(\sigma \cdot d)}. \tag{3.71}$$

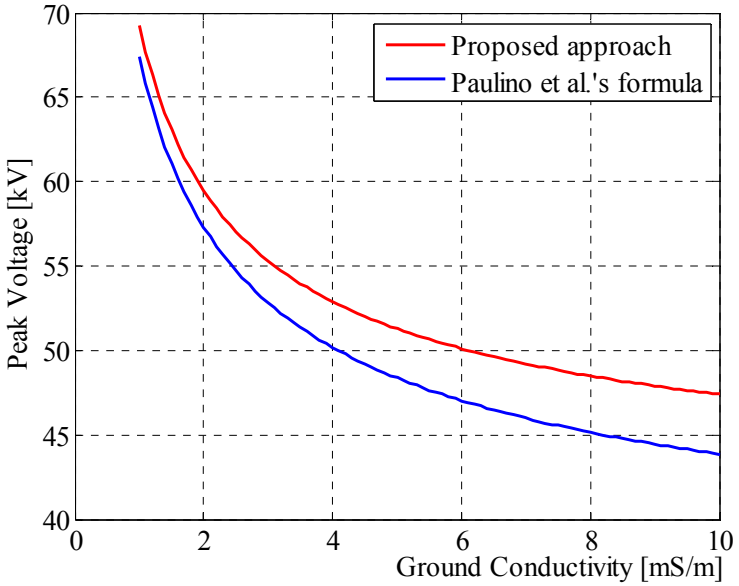

Figure 3.43 – Comparison between the induced voltage peak values evaluated at x = 0 by means of Paulino *et al.*'s formula and the proposed approach (h = 10 m, d = 100 m, I_0 = 10 kA, β = 0.4, and ε_r = 10).

In Figure 3.43, we compare the values obtained by (3.69) with their counterparts obtained by using (3.56) together with (3.3), (3.59), and (3.61), for $x = 0$. In particular we compare the results obtained for different ground conductivities by using h = 10 m, d = 100 m, I_0 = 10 kA, β = 0.4, ε_r = 10. One can see that predictions of Paulino *et al.*'s formula are reasonably close to the ones obtained by using the proposed approach. The maximum difference is about 3.5 kV (7.5%).

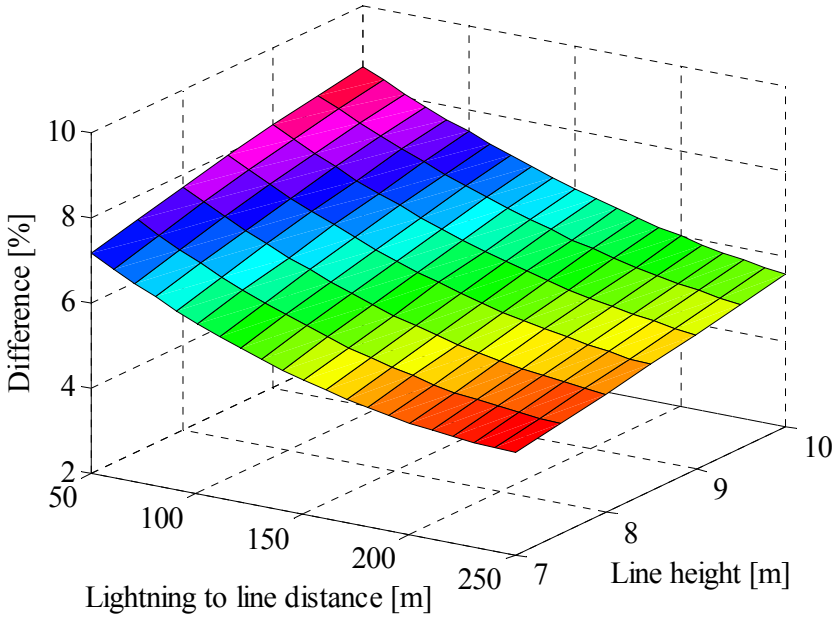

(a)

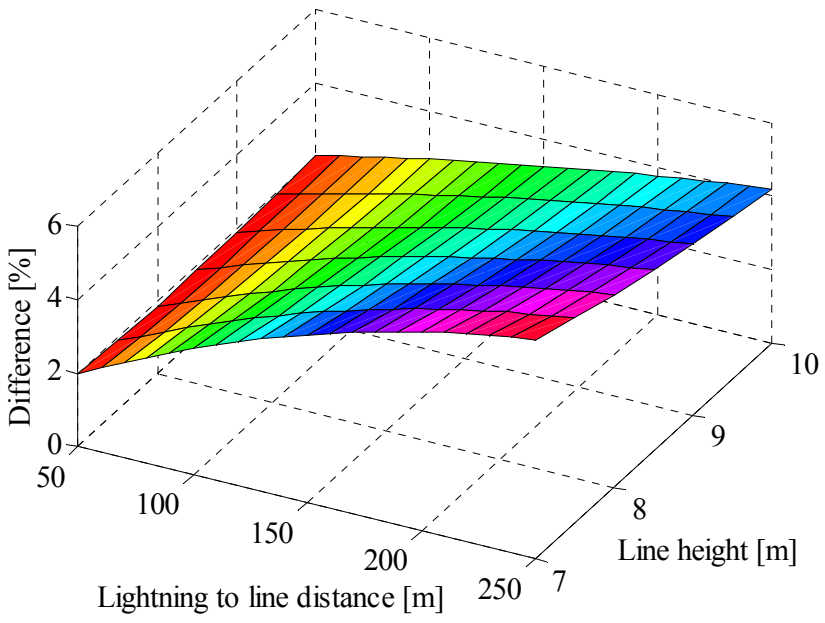

(b)

Figure 3.44 – 3-D plots of the differences between the induced voltage peak values at $x = 0$ computed by means of Paulino *et al.*'s formula and the proposed approach (I_0 = 10 kA, β = 0.4, and ε_r = 10): (a) σ = 0.01 S/m, (b) σ = 0.001 S/m.

In Figure 3.44, we plot 3-D graphs showing the differences between the results obtained by using the Paulino *et al.*'s formula and the proposed method as a function of the line height and the distance between the lightning channel and the line. Figure 3.44(a) is for σ = 0.01 S/m and ε_r = 10, Figure 3.44(b) for σ = 0.001 S/m and ε_r = 10. One can see a maximum difference of 8.6% in Figure 3.44(a), and a maximum difference of 6.0% in Figure 3.44(b).

3.3.5.2 Linearly rising current models

Also in this case, comparison of different models will be performed for a single-conductor line above lossy ground. We will use again the line geometry shown in Figure 3.39.

- *Paulino et al.'s formula*

For the linearly rising current, Paulino *et al.* [29] proposed a formula which, similar to (3.69), is made up of two contributions

$$V_{P\_peak} = k_c \cdot (V_R + V_S), \tag{3.72}$$

where V_S is the same as in (3.70). As for the V_R, they make a numerical convolution of the Rusck's expression (3.64), written for a return-stroke velocity of 120 m/μs (i.e., β = 0.4), and for a front time t_f = 3.8 μs, which is the median value suggested by CIGRÉ for negative first strokes [57]. They found that [29]

$$V_R = 8.5 \cdot I_0 \cdot \frac{h}{\sqrt[4]{d^3}}\,. \tag{3.73}$$

For the correction factor k_c, they suggest the values k_c = 0.90 for $\sigma \neq \infty$, and k_c = 1 for lossless case.

In Figure 3.45, as we have done for the step current case, we compare, for different ground conductivities, induced peak voltages obtained by using (3.72) with their counterparts obtained by using (3.56) together with (3.32), (3.59), and (3.63), for x = 0. A trapezoidal channel base current (i.e., a linearly rising current followed by a constant tail) with I_0 = 10 kA and t_f = 3.8 μs has been considered for calculations; other parameters used are h = 10 m, d = 100 m, β = 0.4, and ε_r = 10. One can see that the results given

by Paulino *et al.*'s formula are reasonably close to the ones obtained by the proposed approach. The maximum difference is about 2.8 kV (4.4%).

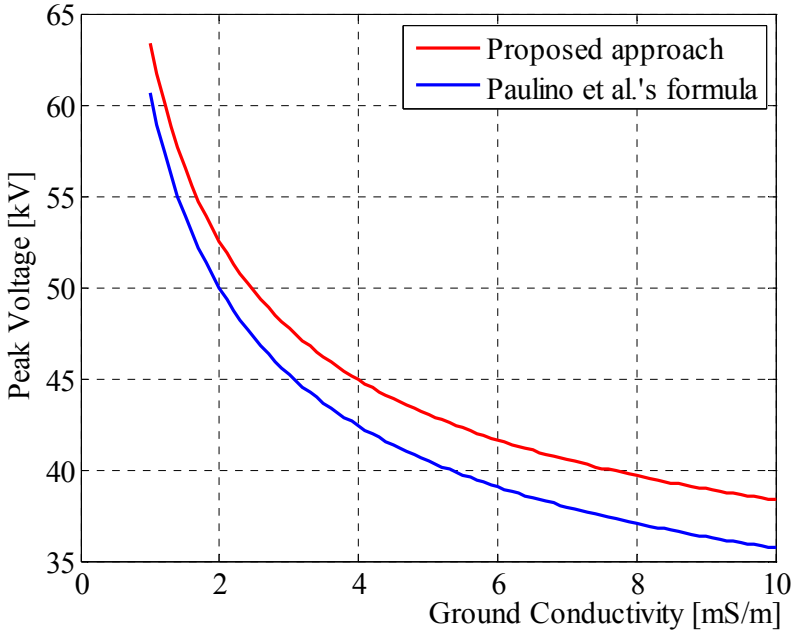

Figure 3.45 – Comparison between the induced voltage peak values evaluated at $x = 0$ by means of Paulino *et al.*'s formula and the proposed approach (h = 10 m, d = 100 m, I_0 = 10 kA, β = 0.4, t_f = 3.8 μs, $t_t = \infty$, and ε_r = 10).

In Figure 3.46, as we have done for the step current case, we plot 3-D graphs showing the percentage differences between the results obtained by using the Paulino *et al.*'s formula and the proposed method as a function of both the line height and distance between the lightning channel and the line. Figure 3.46(a) is for σ = 0.01 S/m and ε_r = 10, Figure 3.46(b) for σ = 0.001 S/m and ε_r = 10. One can see a maximum difference of 7.8% in Figure 3.46(a), and a maximum difference of 5.2.% in Figure 3.46(b).

- *Høidalen's formula*

Høidalen [10], unlike the other analytical expressions discussed before, proposed a formula which evaluates the overall voltage waveshape for a general position x along the line. Høidalen considered the sum of two contributions: one for the lossless case (V_i), and the other to account for the lossy ground effects (V_σ) [10]

$$V_H(x,t) = V_i(x,t) + V_\sigma(x,t), \tag{3.74a}$$

with $V_i(x,t)$ and $V_\sigma(x,t)$ given, respectively, by

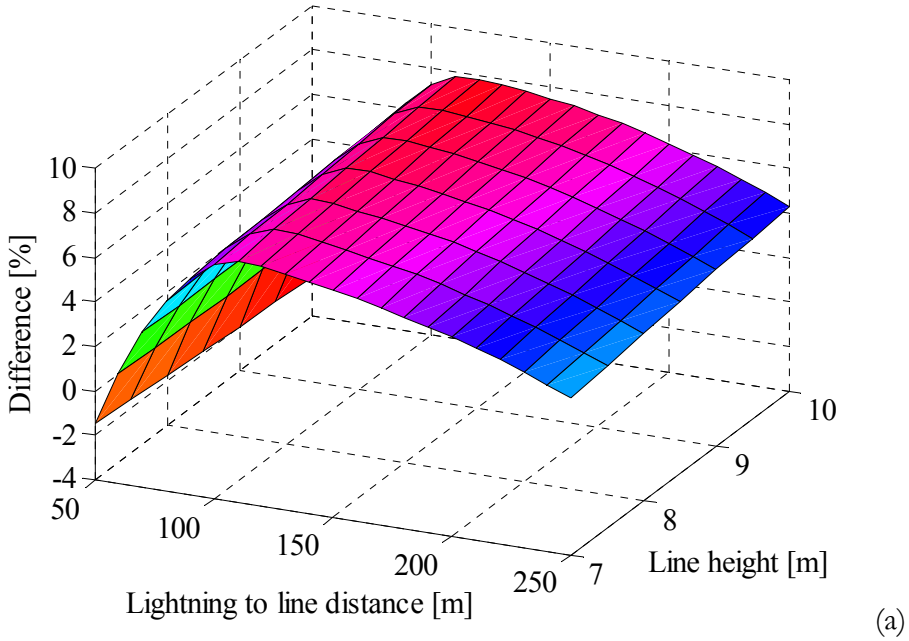

(a)

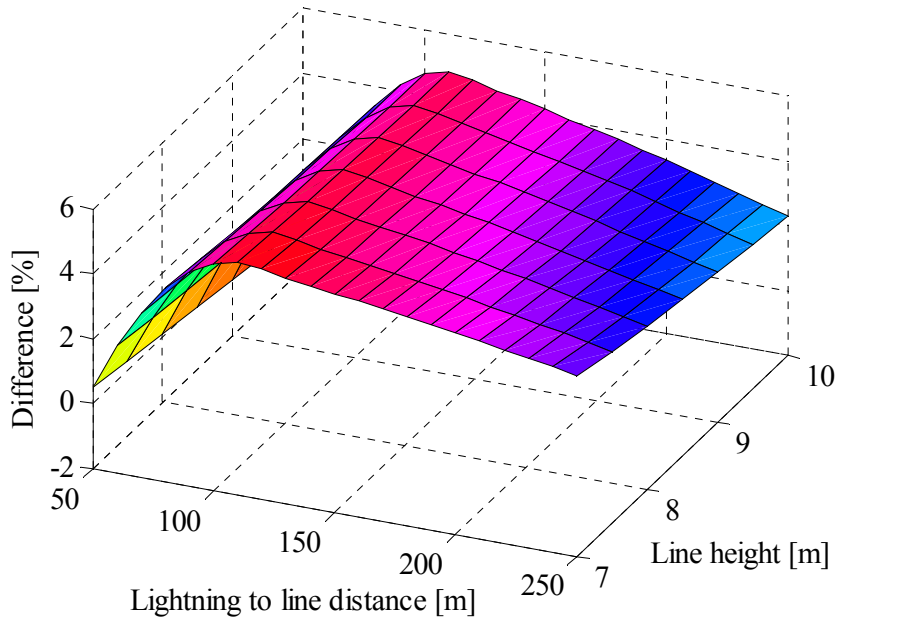

(b)

Figure 3.46 – 3-D plots of the differences between the induced voltage peak values at $x = 0$ computed by means of Paulino *et al.*'s formula and the proposed approach ($I_0 = 10$ kA, $\beta = 0.4$, $t_f = 3.8$ μs, $t_t = \infty$, and $\varepsilon_r = 10$): (a) $\sigma = 0.01$ S/m, (b) $\sigma = 0.001$ S/m.

$$V_i(x,t) \approx A_i(x,t) - b_H \cdot A_i\left(x, t - t_f\right), \tag{3.74b}$$

and

$$V_\sigma(x,t) \approx A_\sigma(x,t) - b_H \cdot A_\sigma\left(x, t - t_f\right), \tag{3.74c}$$

where

$$A_i(x,t) = \frac{I_m \cdot \Delta t}{I_0 \cdot t_f} \cdot \left[\sum_{i=0}^{t/\Delta t-1} v_H^s(x, i \cdot \Delta t) + \frac{1}{2} \cdot v_H^s(x,t) \right] \cdot u(t), \tag{3.75}$$

$$A_\sigma(x,t) = -\frac{I_m}{I_0 \cdot t_f} \cdot \sqrt{\frac{\varepsilon_0 \cdot \Delta t}{\pi \cdot \sigma}} \cdot \left[\sum_{i=0}^{t/\Delta t-1} \frac{w_H(x, i \cdot \Delta t)}{\sqrt{t/\Delta t - i}} + \left(-0.22 \cdot \kappa^3 + \frac{1}{6}\right) \cdot w_H(x, t-\Delta t) + \left(-1.07 \cdot \kappa + 0.22 \cdot \kappa^3 + \frac{4}{3}\right) \cdot w_H(x,t) \right] \cdot u(t), \tag{3.76}$$

with $\kappa = \sqrt{\varepsilon_r \cdot \varepsilon_0/(\pi \cdot \sigma \cdot \Delta t)}$. The term $v_H^s(x,t)$ represents the voltage induced by a step current in case of ideal ground, and $w_H(x,t)$ is an expression obtained integrating the horizontal magnetic field, whose expressions are [10]

$$v_H^s(x,t) = \frac{\zeta_0}{2\pi} \cdot I_0 \cdot \beta \cdot h \cdot \frac{c \cdot t - x}{d^2 + \beta^2 (c \cdot t - x)^2} \cdot \left[1 + \frac{x + \beta^2 (c \cdot t - x)}{\xi} \right] \cdot u(t - \tilde{t}_0), \tag{3.77}$$

$$w_H(x,t) = \frac{\zeta_0}{2\pi} \cdot I_0 \cdot \beta \cdot \left[ln\left(\frac{c \cdot t - x}{d^2 + \beta^2 (c \cdot t - x)^2} \cdot [x + \beta^2 (c \cdot t - x) + \xi] \right) - \frac{1}{\beta} \cdot ln\left(\frac{\beta \cdot c \cdot t + \xi}{(1-\beta) \cdot r} \right) \right] \cdot u(t - \tilde{t}_0). \tag{3.78}$$

Since Høidalen proposed a solution for the calculation of the overall waveshape, we first make a comparison in Figure 3.47, where the waveshapes for an infinitely long line are evaluated at the point closest to the lightning channel (x = 0) by using the Høidalen's equation (3.74) and the proposed approach (i.e., by using (3.56) together with (3.32), (3.59), and (3.63)). Waveforms are given for three different values of ground conductivity (σ = ∞, σ = 0.01 S/m, and σ = 0.001 S/m), and have been obtained for a trapezoidal channel-base current with I_0 = 10 kA, t_f = 1 μs, and t_t = ∞; other parameters used are h = 10 m, d = 100 m, β = 0.4. From the comparison, one can observe that the results given by Høidalen's method match the ones predicted by the proposed approach both for the perfectly conducting ground and for σ = 0.01 S/m. Some differences between the results are seen for σ = 0.001 S/m.

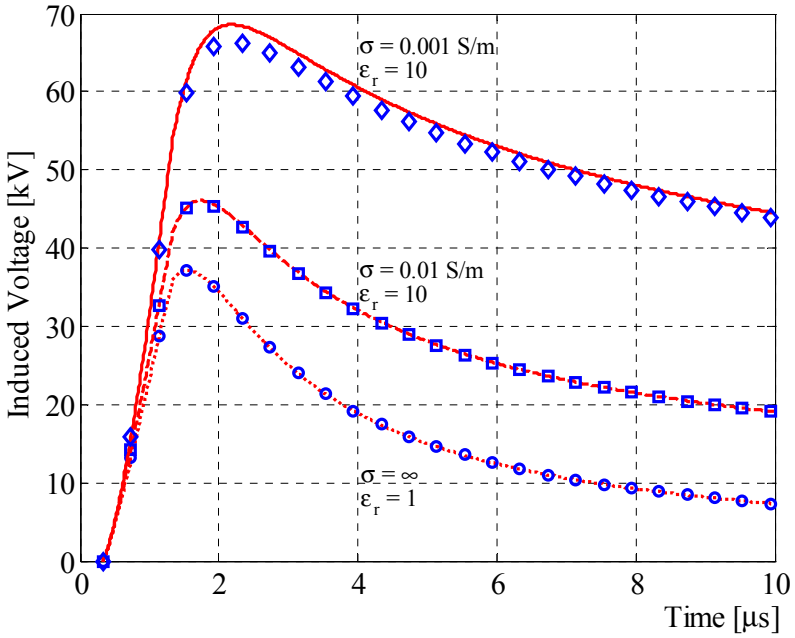

Figure 3.47 – Comparison between the induced voltages evaluated at $x = 0$ using Høidalen's approach and the proposed method ($h = 10$ m, $d = 100$ m, $I_0 = 10$ kA, $\beta = 0.4$, $t_f = 1$ μs, $t_t = \infty$). Høidalen: ◊,□,○.

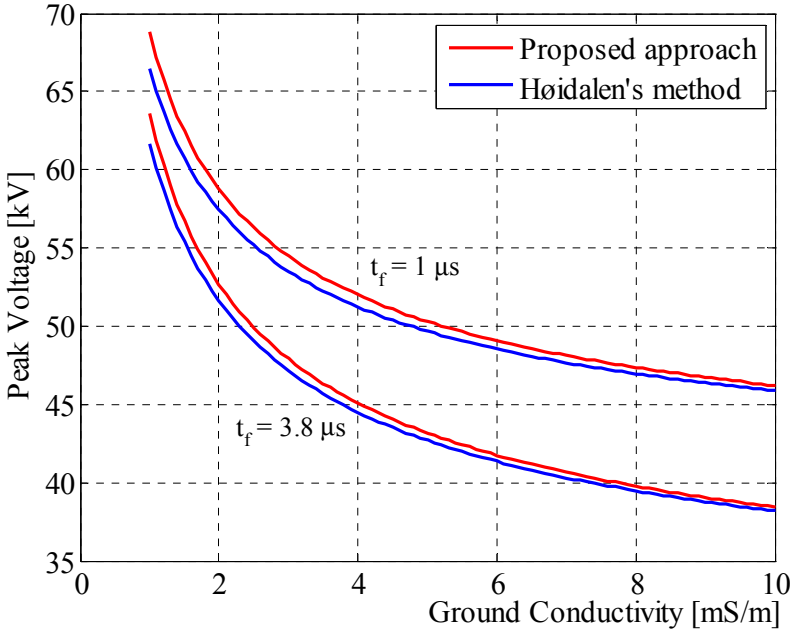

Figure 3.48 – Comparison between the induced voltage peak values evaluated at $x = 0$ by means of Høidalen's approach and the proposed method ($h = 10$ m, $d = 100$ m, $I_0 = 10$ kA, $\beta = 0.4$, $t_t = \infty$, and $\varepsilon_r = 10$).

In Figure 3.48, we compare, for different ground conductivities, peak values of the induced voltages evaluated at $x = 0$ by means of Høidalen's formula (3.74) and by using (3.56) together with (3.32), (3.59), and (3.63). The parameters used are the same as in Figure 3.47, but this time, two different front times are analyzed: the first one, $t_f = 1$ μs, is representative of subsequent strokes, and the second one, $t_f = 3.8$ μs, is representative of first strokes. One can see that the results given by Høidalen are very close to the ones predicted by the proposed method. One can also observe that the difference decreases as the front time grows: the maximum difference is about 2.3 kV (3.4%) for $t_f = 1$ μs, and about 1.9 kV (3%) for $t_f = 3.8$ μs.

Finally, in Figure 3.49, we plot 3-D graphs showing the percentage differences between the Høidalen's formula and the proposed approach as a function of the line height and distance between the lightning channel and the line. Figure 3.49(a) is for $\sigma = 0.01$ S/m and $\varepsilon_r = 10$, and Figure 3.49(b) is for $\sigma = 0.001$ S/m and $\varepsilon_r = 10$. One can see a maximum difference of 0.9% in Figure 3.49(a), and a maximum difference of 2.8% in Figure 3.49(b). These very small differences between the two methods confirm the conclusion drawn for the lossless ground case (see [8] and paragraph 3.2.2.3): the two approaches lead to practically identical results for typical distribution lines ($h \approx 10$ m), but differences are expected in the analysis of typical transmission lines ($h \approx 30$ m).

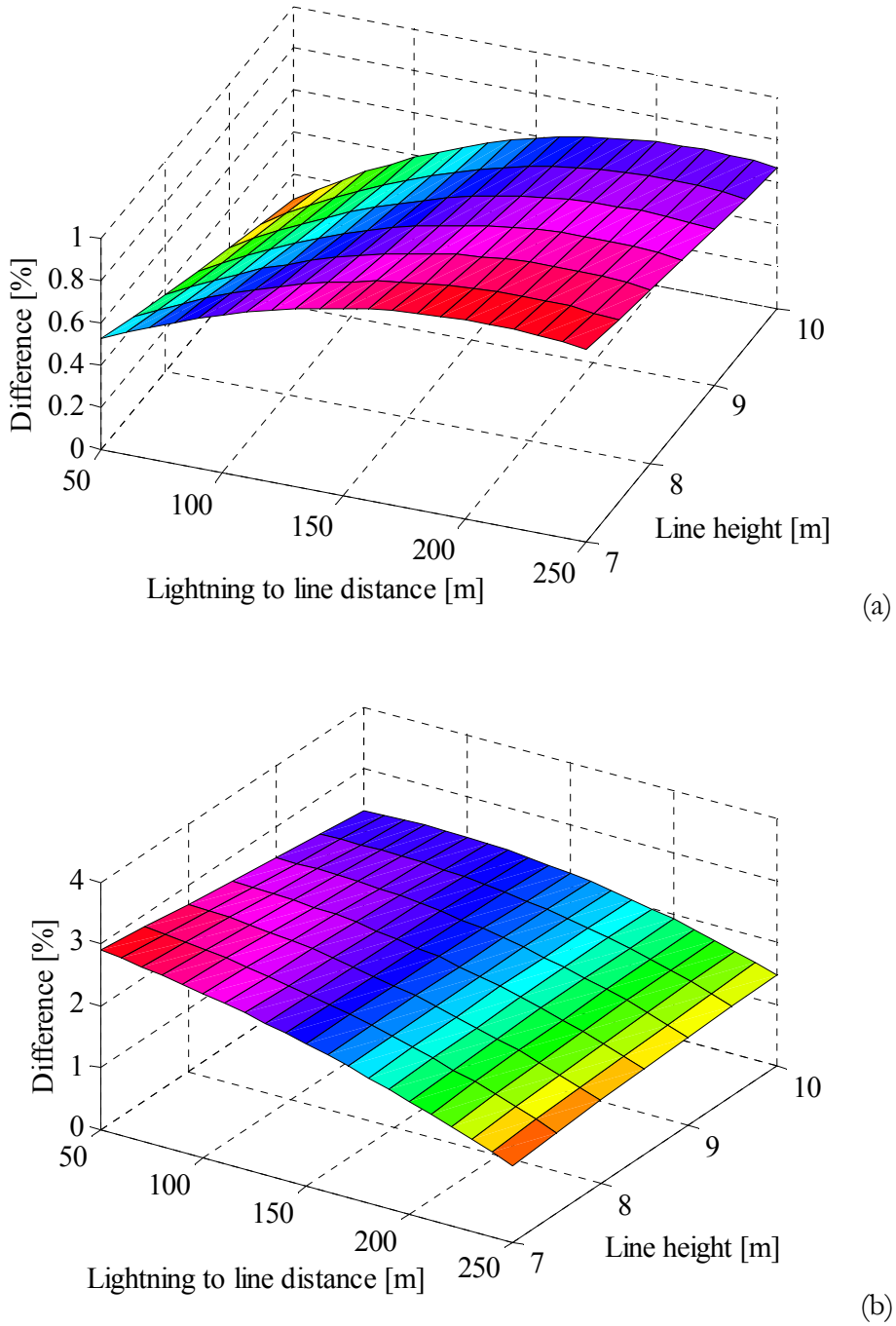

Figure 3.49 – 3-D plots of the differences between the induced voltage peak values at $x = 0$ computed by means of Høidalen's approach and the proposed method ($I_0 = 10$ kA, $\beta = 0.4$, $t_f = 3.8$ μs, $t_t = \infty$, and $\varepsilon_r = 10$): (a) $\sigma = 0.01$ S/m, (b) $\sigma = 0.001$ S/m.

References

[1] F. Vance, *Coupling to Shielded Cables*. New York: Wiley, 1978.

[2] F. M. Tesche, M. Ianoz and T. Karlsson, *EMC Analysis Methods and Computational Models,* New York: Wiley Interscience, 1997.

[3] F. Rachidi, C. A. Nucci, and M. Ianoz, "Transient analysis of multiconductor lines above a lossy ground," *IEEE Trans. Power Del.,* vol. 14, no. 1, pp. 294–302, Jan. 1999.

[4] G. Diendorfer, "Induced voltage on an overhead line due to nearby lightning", *IEEE Trans. Electromagn. Compat.*, vol. 32, no. 4, pp. 292–299, Nov. 1990.

[5] H. K. Høidalen, J. Slebtak, and T. Henriksen, "Ground effects on induced voltages from nearby lightning," *IEEE Trans. Electromagn. Compat.*, vol. 39, no. 4, pp. 269–278, Nov. 1997.

[6] A. Andreotti, U. De Martinis, A. Maffucci, and G. Miano, "A Mixed Frequency and Time Domain Approach for Accurate Evaluation of the Dynamics of LEMP Excited Lossy Multiconductor Power Lines," *Electrical Engineering*, Springer publisher, vol. 83, no. 3, pp. 147-155, May 2001.

[7] A. Andreotti, U. De Martinis, and L. Verolino, "A Spice simulation of lightning induced overvoltages on power transmission lines", *Advances in Engineering Software*, vol. 31, no. 10, pp. 757 – 762, Oct. 2000.

[8] A. Andreotti, D. Assante, F. Mottola, and L. Verolino, "An exact closed-form solution for lightning-induced overvoltages calculations," *IEEE Trans. Power Del.*, vol. 24, no. 3, pp. 1328-1343, Jul. 2009.

[9] S. Rusck, "Induced lightning over-voltages on power transmission lines with special reference to the overvoltage protection of low voltage networks," *Trans. Royal Inst. Technol.*, no. 120, Stockholm, Sweden, pp. 1-118, Jan. 1958.

[10] H. K. Høidalen, "Analytical formulation of lightning-induced voltages on multiconductor overhead lines above lossy ground," *IEEE Trans. Electromagn. Compat.*, vol. 45, no. 1, pp. 92-100, Feb. 2003.

[11] J. O. S. Paulino, C. F. Barbosa, and W. C. Boaventura, "Effect of the Surface Impedance on the Induced Voltages in Overhead Lines From Nearby Lightning," *IEEE Trans. Electromagn. Compat.*, vol. 53, n. 3, pp. 749-754, Aug. 2011.

[12] F. Napolitano, "An analytical formulation of the electromagnetic field generated by lightning return strokes," *IEEE Trans. Electromagn. Compat.*, vol. 53, n. 1, pp. 108-113, Feb. 2011.

[13] C. F. Barbosa and J. O. S. Paulino, "A time-domain formula for the horizontal electric field at the earth surface in the vicinity of lightning," *IEEE Trans. Electromagn. Compat.*, vol. 52, n. 3, pp. 640-645, Aug. 2010.

[14] IEEE *Guide for Improving the Lightning Performance of Electric Power Overhead Distribution Lines*, IEEE Stdandard. 1410, 2010.

[15] P. Chowdhuri, "Parametric effects on the induced voltages on overhead lines by lightning strokes to nearby ground," *IEEE Trans. Power Del.,* vol. 4, no. 2, pp. 1185-1194, Apr. 1989.

[16] H. K. Høidalen, "Calculation of lightning-induced overvoltages using MODELS," in *Proc. Int. Conf. Power Systems Transients,* Budapest, Hungary, Jun. 20-24, 2003, pp. 7-12.

[17] N. J. Higham, *Accuracy and Stability of Numerical Algorithms*. 2nd ed., Philadelphia, PA: SIAM, 2002.

[18] P. Chowdhuri and E. T. B. Gross, "Voltage surges induced on overhead lines by lightning strokes," in *Proc. Inst. Elect. Eng.*, vol. 114, no. 12, Dec. 1967, pp. 1899-1907.

[19] P. Chowdhuri, "Analysis of lightning-induced voltages on overhead lines," *IEEE Trans. Power Del.*, vol. 4, no. 1, pp. 479–492, Jan. 1989.

[20] A. C. Liew and S. C. Mar, "Extension of the Chowdhuri-Gross model for lightning induced voltage on overhead lines," *IEEE Trans. Power Syst.*, vol. 1, no. 2, pp. 240–247, May 1986.

[21] A. Agrawal, A. H. Price, and S. Gurbaxani, "Transient response of multiconductor transmission lines excited by a nonuniform electromagnetic field," *IEEE Trans. Electromagn. Compat.*, vol. 22, no. 2, pp. 119–129, May. 1980.

[22] C. A. Nucci, F. Rachidi, M. Ianoz, and C. Mazzetti, "Comparison of two coupling models for lightning-induced overvoltage calculations," *IEEE Trans. Power Del.*, vol. 10, no. 1, pp. 330–339, Jan. 1995.

[23] S. Sekioka, "An equivalent circuit for analysis of lightning-induced voltages on multiconductor system using an analytical expression," in *Proc. Int. Conf. Power Syst. Trans.*, Montreal, Canada, Jun. 2005, pp. 1-6.

[24] P. P. Barker, T. A. Short, A. Eybert-Berard, and J. B. Berlandis, "Induced voltage measurements on an experimental distribution line during nearby rocket triggered lightning flashes", *IEEE Trans. Power Del.*, vol. 11, no. 2, pp. 980-995, Apr. 1996.

[25] M. Darveniza, "A practical extension of Rusck's formula for maximum lightning-induced voltages that accounts for ground resistivity," *IEEE Trans. Power Del.*, vol. 22, no. 1, pp. 605–612, Jan. 2007.

[26] J. O. S. Paulino, C. F. Barbosa , I. J. S. Lopes, and W. C. Boaventura, "An approximate formula for the peak value of lightning-induced voltages in overhead lines," *IEEE Trans. Power Del.*, vol. 25, no. 2, pp. 843-851 Apr. 2010.

[27] C. F. Barbosa and J. O. S. Paulino, "An approximate time domain formula for the calculation of the horizontal electric field from lightning," *IEEE Trans. Electromagn. Compat.*, vol. 49, no. 3, pp. 593–601, Aug. 2007.

[28] C. F. Barbosa, J. O. S. Paulino, G. C. Miranda, W. C. Boaventura, F. E. Nallin, S. Person, and A. Zeddam, "Measured and modeled horizontal electric field from rocket-triggered lightning," *IEEE Trans. Electromagn. Compat.*, vol. 50, no. 4, pp. 913–920, Nov. 2008.

[29] J. O. S. Paulino, C. F. Barbosa, I. J. S. Lopes, and W. C. Bonaventura, "The peak value of lightning-induced voltages in overhead lines considering the ground resistivity and typical return stroke parameters," *IEEE Trans. Power Del.*, vol. 26, no. 2, pp. 920–926, Apr. 2011.

[30] E. D. Sunde, *Earth Conduction Effects in Transmission Systems*, New York: Dover, 1968.

[31] B. Djebari, J. Hamelin, C. Leteinturier, and J. Fontaine, "Comparison between experimental measurements of the electromagnetic field emitted by lightning and different theoretical models. Influence of the upward velocity of the return stroke," in *Proc. 4th Int. Symp. Tech. Exhib. Electromagn. Compat.*, Zürich, Switzerland, Mar 10-12, 1981.

[32] M. Rubinstein, "Voltages induced on a test power line from artificially initiated lightning: Theory and experiment," *Ph.D. thesis dissertation*, University of Florida, Gianesville, 1991.

[33] V. Cooray and V. Scuka, "Lightning-induced overvoltages in power lines: Validity of various approximations made in overvoltage calculations," *IEEE Trans. Electromagn. Compat.*, vol. 40, no. 4, pp. 355-363, Nov. 1998.

[34] M. Rubinstein, "An approximate formula for the calculation of the horizontal electric field from lightning at close, intermediate, and long range," *IEEE Trans. Electromagn. Compat.*, vol. 38, no. 3, pp. 531-535, Aug. 1996.

[35] C. Caligaris, F. Delfino, and R. Procopio, "Cooray–Rubinstein formula for the evaluation of lightning radial electric fields: Derivation and implementation in the time domain," *IEEE Trans. Electromagn. Compat.*, vol. 50, no. 1, pp. 194-197, Feb. 2008.

[36] C. R. Paul, *Analysis of Multiconductor Transmission Lines*, NewYork: Wiley, 1994.

[37] C. A. Nucci, V. Bardazzi, R. Iorio, A. Mansoldo, and A. Porrino, "A code for the calculation of lightning-induced overvoltages and its interface with the electromagnetic transient program," in *Proc. 22nd Int. Conf. Lightning Protection*, Budapest, Hungary, Sep. 19–23, 1994, pp. 19–23.

[38] V. Cooray, "Calculating lightning-induced overvoltages in power lines. A comparison of two coupling models*," IEEE Trans. Electromagn. Compat.*, vol. 36, no. 3, pp. 179–182, Aug. 1994.

[39] F. Rachidi, C. A. Nucci, M. Ianoz, and C. Mazzetti, "Response of multiconductor power lines to nearby lightning return stroke electromagnetic fields," *IEEE Trans. Power Del.*, vol. 12, no. 3, pp. 1404–1411, Jul. 1997.

[40] S. Yokoyama, "Calculation of lightning-induced voltages on overhead multiconductor systems," *IEEE Trans. Power App. Syst.*, vol. 103, no. 1, pp. 100–108, Jan. 1984.

[41] M. Paolone, C. A. Nucci, E. Petrache, and F. Rachidi, "Mitigation of lightning-induced overvoltages in medium voltage distribution lines by means of periodical grounding of shielding wires and of surge arresters: Modeling and experimental validation," *IEEE Trans. Power Del.*, vol. 19, no. 1, pp. 423–431, Jan. 2004.

[42] S. Yokoyama, "Distribution surge arrester behavior due to lightning induced voltages," *IEEE Trans. Power Del.*, vol. 1, no. 1, pp. 171–178, Jan. 1986.

[43] P. Chowdhuri, "Lightning-induced voltages on multiconductor overhead lines," *IEEE Trans. Power Del.*, vol. 5, no. 2, pp. 658–667, Apr. 1990.

[44] S. Yokoyama, "Experimental analysis of earth wires for induced lightning surges," in *Proc. Inst. Elect. Eng., Gener., Trans. Distrib.*, Jan. 1980, vol. 127, no. 1, pp. 33–40.

[45] A. Piantini, "Lightning protection of low-voltage networks," in *Lightning Protection*, V. Cooray, Ed. U.K.: The Institution of Engineering and Technology, 2010, pp. 553–634.

[46] S. Matsuura, T. Noda, A. Asakawa, and S. Yokoyama, "EMTP modeling of a distribution line for lightning overvoltage studies," in *Proc. Int. Conf. Power Systems Trans.*, Lyon, France, Jun. 4–7, 2007, pp. 1–6.

[47] R. B. Anderson and A. J. Eriksson, "Lightning parameters for engineering application," *Electra*, vol. 69, pp. 65–102, 1980.

[48] G. Cornfield, "Voltage surges induced on overhead lines by lightning strokes", in *Proc. Inst. Elect. Eng.*, vol. 119, no.7, Jul. 1972, pp. 893–894.

[49] A. Sommerfeld, "On the propagation of waves in wireless telegraphy," *Ann. Phys.*, vol. 81, no.25, pp. 1135-1153, Dec. 1926.

[50] J. R. Wait, "Concerning the horizontal electric field of lightning," *IEEE Trans. Electromagn. Compat.*, vol. 39, no. 2, p. 186, May 1997.

[51] V. Cooray, "Horizontal electric field above- and underground produced by lightning flashes," *IEEE Trans. Electromagn. Compat.*, vol. 52, no. 4, pp. 936–943, Nov. 2010.

[52] C. F. Barbosa, J. O. S. Paulino, and W. C. Bonaventura, "Induced voltages on overhead lines in the vicinity of lightning," presented at the *30th Int. Conf. Light. Protect.*, Cagliari, Italy, Sep. 13–14, 2010.

[53] F. Delfino, P. Girdinio, R. Procopio, M. Rossi, and F. Rachidi, "Time-domain implementation of Cooray-Rubinstein formula via convolution integral and rational approximation," *IEEE Trans. Electromagn. Compat.*, vol. 53, no. 3, pp. 755–763, Aug. 2011.

[54] F. Rachidi, C. A. Nucci, M. Ianoz, and C. Mazzetti, "Influence of a lossy ground on lightning-induced voltages on overhead lines," *IEEE Trans. Electromagn. Compat.*, vol. 38, no. 3, pp. 250–264, Aug. 1996.

[55] C. A. Nucci, "Lightning-induced voltages on overhead power lines. Part I: Return-stroke current models with specified channel-base current for the evaluation of return stroke electromagnetic fields," *Electra*, vol. 161, pp. 74-102, Aug. 1995.

[56] T. H. Thang, Y. Baba, N. Nagaoka, A. Ametani, J. Takami, S. Okabe, and V. A. Rakov, "FDTD simulation of lightning surges on overhead wires in the presence of corona discharge," *IEEE Trans. Electromagn. Compat.*, vol. 54, no. 6, pp. 1234–1243, Dec. 2012.

[57] *Guide to Procedures for Estimating the Lightning Performance of Transmission Lines*, CIGRÉ Working Group 01 of SC 33, 1991, CIGRÉ, ref. no. 63.

Chapter 4

Conclusions

The aim of this thesis is to present *new analytical approaches* to the evaluation of lightning induced voltages on overhead power lines, that allow to overcome errors and/or approximations present in the solutions available in the literature. An accurate evaluation of lightning induced voltages is indeed essential in order to reduce the effects of lightning flashes and improve the Power Quality of the system.

In *Chapter 1,* the main aspects of the lightning phenomenon have been resumed.

In *Chapter 2,* the models proposed in the literature for the evaluation of the lightning induced voltages have been presented. In particular, the most used lightning return stroke models, the techniques for the calculation of the electromagnetic fields generated by the lightning current, and the most important field-to-line coupling models have been presented.

In *Chapter 3*, new analytical approaches to the evaluation of lightning induced voltages on overhead power lines have been presented, and predictions of the proposed solutions have been compared to those based on the other approaches found in the literature in order to check their validity and accuracy.

As shown in this chapter, the most basic case for lightning induced voltage calculations, which consists in a lossless, single-conductor line located over an infinite-conductivity ground plane and excited by an external field due to a step current moving at constant speed, unattenuated and without distortion, along a vertical lightning channel, has been solved in an *exact* way, i.e., without approximations, only recently by Andreotti *et al.* [1]. The work started in [1] has been extended here to more practical line configurations.

Specifically, still for the case of an external field due to a step current and perfectly conducting ground, the cases of terminated single-conductor and multi-conductor lines (including grounded conductors) have been studied. Further, single-conductor and multi-

conductor lines (including grounded conductors) excited by an external field due to a linearly rising current have been examined and a new analytical approach for the calculation of induced voltages has been proposed. Predictions of this new formulation have been compared to those given by other analytical (approximate) solutions proposed in the literature. In particular, the solutions proposed by Chowdhuri and Gross, Liew and Mar, Sekioka, and Høidalen have been considered. The comparison showed that both the Chowdhuri-Gross's and the Liew-Mar's formula predict results which are in disagreement with the proposed method, and hence cannot be considered correct. Conversely, both the Sekioka's solution and the Høidalen's formula are consistent with the proposed analytical solution, and can be considered suitable for lightning induced overvoltages analysis.

Afterwards, the exact model for the evaluation of voltages induced on a overhead line in presence of an infinite-conductivity ground plane has been extended to account for the lossy ground effects. Also in this case, predictions of the new proposed model have been compared to those based on other formulations found in the literature. In particular, the solutions proposed by Barker *et al.*, Darveniza, and Paulino *et al.*, for the step current case, and the solutions proposed by Paulino *et al.* and Høidalen, for the linearly rising current case, have been considered. The results of this comparison show that Paulino *et al.*'s approach yields voltage peaks that differ by less than 10% from results obtained using the proposed approach, for both step and linearly rising currents. Predictions of Høidalen's approach are within a few percent of those based on the new method. Darveniza's formula is less accurate, with errors of some tens of percent. Barker *et al.*'s formula does not account for variation of induced voltage with ground conductivity. For the height of the line used in the Camp Blanding experiment, it yields results consistent with the proposed approach for ground conductivity equal to 2.7 mS/m, which is higher than values measured or inferred from measured low-frequency grounding resistances and geometry of grounding rods at the Camp Blanding site. In summary, Barker *et al.*'s formula does not seem to provide an accurate solution in the finite conductivity ground case. Finally, we note that this new approach can result in a shorter computation time compared with methods that use numerical field integration (e.g., 2-D-FDTD), and can be particularly useful in the evaluation of indirect lightning performance of distribution lines. We have tested the procedure by computer simulations in MathWorks Matlab 7.12.0 (R2011a) environment, on a 3.4-GHz Intel CoreTM i7 processor with 6 GB of RAM. The computation time for a total of 1000 time points was about 3 s.

Some of the results showed in Chapter 3 are also published in the articles [2]-[4].

Future studies will be devoted to obtaining analytical solutions for:

- different return-stroke models, such as the Modified Transmission Line model with Linear current decay with height, MTLL, the Modified Transmission Line model with Exponential current decay with height, MTLE, and the Travelling Current Source model, TCS.
- different channel-base current models, such as the Heidler model, the Diendorfer and Uman model, and the Nucci *et al.* model;
- lightning channels with different inclinations.

References

[1] A. Andreotti, D. Assante, F. Mottola, and L. Verolino, "An exact closed-form solution for lightning-induced overvoltages calculations," *IEEE Trans. Power Del.*, vol. 24, no. 3, pp. 1328-1343, Jul. 2009.

[2] A. Andreotti, A. Pierno, V. A. Rakov, L. Verolino, "Analytical formulations for lightning-induced voltage calculations," *IEEE Trans. Electromagn. Compat.*, vol. 55, no. 1, pp. 109-123, Feb. 2013.

[3] A. Andreotti, A. Pierno, V. A. Rakov, "An analytical approach to calculation of lightning induced voltages on overhead lines in case of lossy ground – Part I: Model development," *IEEE Trans. Power Del.*, vol. 28, no. 2, pp. 1213-1223, Apr. 2013.

[4] A. Andreotti, A. Pierno, V. A. Rakov, "An analytical approach to calculation of lightning induced voltages on overhead lines in case of lossy ground – Part II: Comparison with other models," *IEEE Trans. Power Del.*, vol. 28, no. 2, pp. 1224-1230, Apr. 2013.

Appendix A

Solution of Some Integrals of Chapter 3

In this appendix, we provide the closed-form solution for the integrals (3.32b), (3.32c), and (3.55) of Chapter 3.

A.1 Integrals (3.32b) and (3.32c)

The following integration formulas are used to derive the analytical expressions for lightning induced voltages due to a linearly rising current in presence of a perfectly conducting ground.

The integrals in (3.32b) and (3.32c) can be divided into two parts. For the first logarithm (the first integrand) on the right-hand side of both (3.32b) and (3.32c), the solution reads [1]

$$\int ln\left(\vartheta + \sqrt{\vartheta^2 + \delta_0^2}\right) d\vartheta = \vartheta \cdot ln\left(\vartheta + \sqrt{\vartheta^2 + \delta_0^2}\right) - \sqrt{\vartheta^2 + \delta_0^2}. \tag{A.1}$$

The solution for the second logarithm (the second integrand), by means of simple algebraic manipulations, can also be brought to a standard form [1]:

$$\int ln\left(-\beta\vartheta + \sqrt{\vartheta^2 + \delta_0^2}\right) d\vartheta = \vartheta \cdot \left[ln\left(-\beta\vartheta + \sqrt{\vartheta^2 + \delta_0^2}\right) - 1\right] + d \cdot \left[arctan\left(\frac{\vartheta}{d}\right) - arctan\left(\frac{\beta \cdot d}{\sqrt{\vartheta^2 + \delta_0^2}}\right)\right]. \tag{A.2}$$

A.2 Integral (3.55)

In this paragraph details are given for the solution of integral (3.55) for the step current case and the case of a linearly rising current.

Integral (3.55) can be divided into two integrals

$$\int_{-\infty}^{+\infty} h_{yi}\left(\eta, d, 0, t - \frac{|\eta - x|}{c}\right) \cdot sign(\eta - x) d\eta$$

$$= \int_{x}^{+\infty} h_{yi}\left(\eta, d, 0, t - \frac{\eta - x}{c}\right) d\eta - \int_{-\infty}^{x} h_{yi}\left(\eta, d, 0, t + \frac{\eta - x}{c}\right) d\eta\,. \quad \text{(A.3)}$$

The two integrals in (A.3) can be rewritten as

$$\int_{x}^{+\infty} h_{yi}\left(\eta, d, 0, t - \frac{\eta - x}{c}\right) d\eta = \int_{x}^{x_l} h_{yi}\left(\eta, d, 0, t - \frac{\eta - x}{c}\right) d\eta\,, \quad \text{(A.4)}$$

$$\int_{-\infty}^{x} h_{yi}\left(\eta, d, 0, t + \frac{\eta - x}{c}\right) d\eta = \int_{x_l'}^{x} h_{yi}\left(\eta, d, 0, t + \frac{\eta - x}{c}\right) d\eta\,. \quad \text{(A.5)}$$

The integration limit x_l in (A.4) is given by

$$x_l = \frac{1}{2} \cdot \frac{(c \cdot t + x)^2 - h^2 - d^2}{(c \cdot t + x)}, \quad \text{(A.6)}$$

and is the solution of the following equation representing the delay due to the propagation of the electromagnetic field and due to the propagation effects along the line:

$$t - \frac{\sqrt{d^2 + h^2 + x_l^2}}{c} - \frac{x_l - x}{c} = 0. \quad \text{(A.7)}$$

The same applies to the integration limit x_l' in (A.5), but this time with a different choice of the time delay along the line

$$x_l' = -\frac{1}{2} \cdot \frac{(c \cdot t - x)^2 - h^2 - d^2}{(c \cdot t - x)}. \quad \text{(A.8)}$$

By considering the field expression (3.60), we can rewrite the integrals (A.4) and (A.5), respectively, as

$$\frac{I_0}{2\pi}\cdot\int_{x}^{x_l}\frac{\beta\cdot(c\cdot t+x-\eta)}{\sqrt{[\beta\cdot(c\cdot t+x-\eta)]^2+(\eta^2+d^2)/\gamma^2}}\cdot\frac{\eta}{\eta^2+d^2}\cdot u(t-t_0)d\eta, \tag{A.9}$$

$$\frac{I_0}{2\pi}\cdot\int_{x_l'}^{x}\frac{\beta\cdot(c\cdot t-x+\eta)}{\sqrt{[\beta\cdot(c\cdot t-x+\eta)]^2+(\eta^2+d^2)/\gamma^2}}\cdot\frac{\eta}{\eta^2+d^2}\cdot u(t-t_0)d\eta. \tag{A.10}$$

Integral (A.9) can be brought to a standard form [1], and the solution reads

$$\frac{I_0}{2\pi}\cdot\int_{x}^{x_l}\frac{\beta\cdot(c\cdot t+x-\eta)}{\sqrt{[\beta\cdot(c\cdot t+x-\eta)]^2+(\eta^2+d^2)/\gamma^2}}\cdot\frac{\eta}{\eta^2+d^2}\cdot u(t-t_0)d\eta$$

$$=\frac{I_0}{2\pi}\cdot\left[ln\left(\frac{\beta\cdot c\cdot t+\xi}{\hat{\lambda}-\beta x_l+\xi_l}\right)+\beta\cdot ln\left(\frac{x-\beta\hat{\lambda}+\xi}{x_l-\beta\hat{\lambda}+\xi_l}\right)+ln\left(\frac{\delta_l}{\delta}\right)\right]\cdot u(t-t_0). \tag{A.11}$$

In order to solve integral (A.10), first we change the sign of η, obtaining, by using the technique of integration by substitution, the integral

$$\frac{I_0}{2\pi}\cdot\int_{-x_l'}^{-x}\frac{\beta\cdot(c\cdot t-x-\eta)}{\sqrt{[\beta\cdot(c\cdot t-x-\eta)]^2+(\eta^2+d^2)/\gamma^2}}\cdot\frac{\eta}{\eta^2+d^2}\cdot u(t-t_0)d\eta, \tag{A.12}$$

and then we change the sign of x. By observing that

$$-x_l'(-x)=\frac{1}{2}\cdot\frac{(c\cdot t+x)^2-h^2-d^2}{(c\cdot t+x)}=x_l, \tag{A.13}$$

integral (A.12) becomes

$$-\frac{I_0}{2\pi}\cdot\int_{x}^{x_l}\frac{\beta\cdot(c\cdot t+x-\eta)}{\sqrt{[\beta\cdot(c\cdot t+x-\eta)]^2+(\eta^2+d^2)/\gamma^2}}\cdot\frac{\eta}{\eta^2+d^2}\cdot u(t-t_0)d\eta. \tag{A.14}$$

Then, the solution of (A.10) can be obtained from (A.11) by replacing x with $-x$ and negating the whole expression.

If we consider instead the field expression (3.62), the integral (A.4) can be rewritten as

$$\frac{I_0}{2\pi\cdot\beta\cdot c\cdot t_f}\cdot\int_x^{x_l}\left[\sqrt{[\beta\cdot(c\cdot t+x-\eta)]^2+\frac{\eta^2+d^2}{\gamma^2}}-\sqrt{\eta^2+d^2}\right]\cdot\frac{\eta}{\eta^2+d^2}\cdot u(t-t_0)d\eta. \quad \text{(A.15)}$$

We can split this integral into two parts

$$\frac{I_0}{2\pi\cdot\beta\cdot c\cdot t_f}\cdot\int_x^{x_l}\sqrt{[\beta\cdot(c\cdot t+x-\eta)]^2+\frac{\eta^2+d^2}{\gamma^2}}\cdot\frac{\eta}{\eta^2+d^2}\cdot u(t-t_0)d\eta, \quad \text{(A.16)}$$

$$\frac{I_0}{2\pi\cdot\beta\cdot c\cdot t_f}\cdot\int_x^{x_l}\frac{-\eta}{\sqrt{\eta^2+d^2}}\cdot u(t-t_0)d\eta. \quad \text{(A.17)}$$

Now, the integral (A.16) can be rewritten as

$$\frac{I_0}{2\pi\cdot\beta\cdot c\cdot t_f}\cdot\int_x^{x_l}\frac{[\beta\cdot(c\cdot t+x-\eta)]^2+(\eta^2+d^2)/\gamma^2}{\sqrt{[\beta\cdot(c\cdot t+x-\eta)]^2+(\eta^2+d^2)/\gamma^2}}\cdot\frac{\eta}{\eta^2+d^2}\cdot u(t-t_0)d\eta. \quad \text{(A.18)}$$

Making the appropriate simplifications for the numerator of the integrand, and performing a polynomial division (by the divisor η^2+d^2), the integral (A.18), in turn, can be rewritten as

$$\frac{I_0}{2\pi\cdot\beta\cdot c\cdot t_f}\cdot\left[\int_x^{x_l}\frac{\eta-2\beta^2\cdot(c\cdot t+x)}{\sqrt{[\beta\cdot(c\cdot t+x-\eta)]^2+(\eta^2+d^2)/\gamma^2}}\cdot u(t-t_0)d\eta+\beta^2\cdot\int_x^{x_l}\frac{[(c\cdot t+x)^2-d^2]\cdot\eta-2d^2\cdot(c\cdot t+x)}{(\eta^2+d^2)\cdot\sqrt{[\beta\cdot(c\cdot t+x-\eta)]^2+(\eta^2+d^2)/\gamma^2}}\cdot u(t-t_0)d\eta\right]. \quad \text{(A.19)}$$

The first integral in (A.19) can be brought to a standard form [1], and the solution reads

$$\frac{I_0}{2\pi\cdot\beta\cdot c\cdot t_f}\cdot\int_{x}^{x_l}\frac{\eta-2\beta^2\cdot(c\cdot t+x)}{\sqrt{[\beta\cdot(c\cdot t+x-\eta)]^2+(\eta^2+d^2)/\gamma^2}}\cdot u(t-t_0)d\eta$$

$$=\frac{I_0}{2\pi\cdot\beta\cdot c\cdot t_f}\cdot\left[\xi_l-\xi+\beta\hat{\lambda}\cdot ln\left(\frac{x-\beta\hat{\lambda}+\xi}{x_l-\beta\hat{\lambda}+\xi_l}\right)\right]\cdot u(t-t_0). \quad \text{(A.20)}$$

As for the second integral that appears in (A.19), it can also be closed analytically. In particular, it is easy to verify that this integral can be rewritten as

$$\frac{I_0\cdot\beta}{2\pi\cdot c\cdot t_f}\cdot\int_{x}^{x_l}\frac{M\cdot\eta+N}{(A+B\cdot\eta+\eta^2)^m\cdot\sqrt{C\cdot(A_1+B_1\cdot\eta+\eta^2)}}\cdot u(t-t_0)d\eta, \quad \text{(A.21)}$$

where

- $M=(c\cdot t+x)^2-d^2$;
- $N=2d^2\cdot(c\cdot t+x)$;
- $A=d^2,\ B=0,\ C=1$;
- $A_1=\beta^2\cdot(c\cdot t+x)^2+(d/\gamma)^2$;
- $B_1=-2\beta^2\cdot(c\cdot t+x)$;
- $m=1$.

Integral (A.21) can be solved by using the technique of integration by substitution [1], and the solution reads

$$\frac{I_0\cdot\beta}{2\pi\cdot c\cdot t_f}\cdot\int_{x}^{x_l}\frac{M\cdot\eta+N}{(A+B\cdot\eta+\eta^2)^m\cdot\sqrt{C\cdot(A_1+B_1\cdot\eta+\eta^2)}}\cdot u(t-t_0)d\eta$$

$$=\frac{I_0\cdot\beta^3}{2\pi\cdot c\cdot t_f}\cdot\frac{1}{\hat{\lambda}^2\cdot P\cdot\sqrt{Q-T^2}}$$

$$\cdot\left\{R\cdot\left[arctanh\left(\frac{\sqrt{W^2(x)+Q}}{\sqrt{Q-T^2}}\right)-arctanh\left(\frac{\sqrt{W^2(x_l)+Q}}{\sqrt{Q-T^2}}\right)\right]\right.$$

$$\left.+\frac{S}{T}\cdot\left[arctan\left(\frac{W(x_l)\cdot\sqrt{Q-T^2}}{T\cdot\sqrt{W^2(x_l)+Q}}\right)-arctan\left(\frac{W(x)\cdot\sqrt{Q-T^2}}{T\cdot\sqrt{W^2(x)+Q}}\right)\right]\right\}\cdot u(t-t_0), \quad \text{(A.22)}$$

where

- $P = \sqrt{[(c \cdot t + x)^2 + d^2] \cdot (1 - \beta^2)}$;
- $Q = \left[d^2 + \hat{\lambda}^2\right]/[(c \cdot t + x)^2 \cdot (1 - \beta^2)]$;
- $R = (c \cdot t + x)^2 \cdot [(c \cdot t + x)^2 + d^2]$;
- $S = d^2 \cdot [(c \cdot t + x)^2 + d^2]$;
- $T = d/(c \cdot t + x)$;
- $W(\varphi) = [(c \cdot t + x) \cdot \varphi + d^2]/[(c \cdot t + x) \cdot (c \cdot t + x - \varphi)]$.

Finally, it is straightforward to evaluate the integral (A.17), and the solution reads

$$\frac{I_0}{2\pi \cdot \beta \cdot c \cdot t_f} \cdot \int_{x}^{x_l} \frac{-\eta}{\sqrt{\eta^2 + d^2}} \cdot u(t - t_0) d\eta$$

$$= \frac{I_0}{2\pi \cdot \beta \cdot c \cdot t_f} \cdot \left(\sqrt{x^2 + d^2} - \sqrt{x_l^2 + d^2}\right) \cdot u(t - t_0). \qquad \text{(A.23)}$$

By assuming the expressions (A.20), (A.22), and (A.23) we obtain the analytical solution of the integral (A.15).

The solution of the integral (A.5) with the field expression (3.61) can be obtained from the solution of the integral (A.15) by replacing x with $-x$ and negating the entire expression.

References

[1] I. S. Gradshteyn, and I. W. Ryzhik, *Table of Integrals, Series, and Products*, New York: Academic, 1980.